Dynamics of Liquid Metal Drops Influenced by Electromagnetic Fields

von Dipl.-Ing. Michael Conrath

Zusammenfassung

Diese Arbeit ist den Effekten gewidmet, die an der Oberfläche von Flüssigmetall im Magnetfeld auftreten können. Im Prinzip erlauben Magnetfelder, Lorentzkräfte auf flüssiges Metall auszuüben und in seinem Innern Induktionswärme zu generieren. Es ist aber auch bekannt, dass Flüssigmetall-Oberflächen durch Magnetfelder dramatische Formänderungen oder Schwingungen erfahren können. Ein Verständnis dieser Phänomene ist wichtig für sämtliche metallurgische Anwendungen, bei denen freie Oberflächen vorkommen.

Als repräsentatives Problem untersuchen wir einen Tropfen aus Flüssigmetall, der eine freie Oberfläche mit einem endlichen Volumen verbindet. Wir schliessen Temperatureffekte aus und konzentrieren uns auf die Wirkung der Lorentzkraft. Wir erarbeiten ein Schema zur Klassifikation von Tropfen-Magnetfeld-Problemen basierend auf der Frequenz des Magnetfeldes und dem Shielding-Parameter des Tropfens in diesem Feld. Anhand dieses Schemas wählen wir fünf Fallstudien aus und studieren das Tropfenverhalten im i) transienten, ii) hochfrequenten und iii) mittelfrequenten Magnetfeld. Die Untersuchungen sind vorwiegend analytischer Art, nur die Mittelfrequenz-Studie ist experimentell. Die beiden wichtigsten Probleme, welche die vorliegende Arbeit zum Gegenstand hat, sind das symmetrische Zusammendrücken oder Halten von Flüssigmetalltropfen einerseits und deren azimutale Verformungen andererseits. Für das transiente Magnetfeld werden zwei Studien präsentiert, jede zu einem der beiden Hauptprobleme. Eine Verbindung zwischen transientem und hochfrequentem Feld besteht darin, das mit beiden Feldtypen stationäre Kräfte im Metall erzeugt werden können. Ein wichtiger Unterschied ist jedoch, dass transiente Felder das Metall durchdringen können, während hochfrequente Felder vom Metall abgeschirmt werden, wodurch eine Kopplung zwischen Tropfenform und Magnetfeld entsteht. Die Effekte im hochfrequenten Feld sind daher schwieriger zu modellieren. Wir präsentieren eine Hochfrequenz-Studie, in der es um das Zusammendrücken und Halten von Tropfen in einem gegebenen Magnetfeld geht. Eine zweite Hochfrequenz-Studie beschäftigt sich mit longitudinaler Levitation. Dort geben wir als einfache Tropfenform einen Flüssigmetall-Zylinder vor und ermitteln das Magnetfeld, welches die vorausgesetzte Tropfenform tatsächlich ermöglichen würde. Im mittelfrequenten Feld bieten sich für theoretische Betrachtungen die grössten Schwierigkeiten, da das Magnetfeld den Tropfen nun partiell durchdringt und kaum noch vereinfacht werden kann. Dieser Bereich wurde daher durch die fünfte Studie experimentell erkundet. Dabei wurde eine Flüssigmetall-Scheibe verwendet, welche nur zweidimensionale Verformungen ausführen kann.

Die Ergebnisse der Arbeit zeigen, dass insbesondere transiente Magnetfelder gangbare Wege der analytischen Modellierung bieten. Ebenso wie hochfrequente Magnetfelder eignen sie sich zum Formen und Stützen freier Flüssigmetall-Oberflächen. Für das Studium der azimutalen Verformungen hat sich die Scheiben-Geometrie als günstig erwiesen, sowohl analytisch als auch experimentell. Insgesamt zeigt sich, dass eine Fortführung der Arbeit auf dem Gebiet der Wechselwirkung zwischen Magnetfeldern und Flüssigmetall-Oberflächen lohnenswert ist.

Abstract

This work is devoted to the free surface effects that occur when liquid metal is placed in a magnetic field. Principally, magnetic fields allow to exert Lorentz forces on liquid metal and to generate induction heat inside it. But it is also known that liquid metal surfaces in magnetic fields can undergo dramatic shape changes or experience oscillations. An understanding of these phenomena is crucial to all metallurgical applications showing free surfaces. As a representative problem we examine a liquid metal drop that combines a free surface with a finite volume. We exclude heat effects and focus on the consequences of the Lorentz force. To this end, we elaborate a classification scheme for liquid metal drop - magnetic field problems comprising the frequency of the magnetic field and the Shielding parameter of the drop in this field. On that basis we select five case studies involving i) transient, ii) middle-frequency and iii) high-frequency magnetic field to explore the behavior of liquid metal drops in it. We mainly use analytical means - only the middle-frequency study is experimental. The major problems we tackle concern the symmetric squeezing and supporting of drops and its azimuthal deformations, respectively. Two studies are presented for the transient magnetic field, each accounting for one of the two problems. A connection between transient and high frequency magnetic field is the possibility to exert a steady force on the liquid metal. An important difference is that transient fields can penetrate the metal while high-frequent fields are shielded by the metal resulting in a coupling between surface shape and magnetic field distribution. Therefore, the effects of high frequency magnetic fields are more difficult to model. We present one high frequency study where we presuppose the magnetic field and ask for the resulting drop shape (forward problem) and another one where we presuppose a simple surface shape and ask for the best suited magnetic field to obtain it (reverse problem). The most difficulties arise in middle-frequent magnetic fields. Here we have partial shielding which makes it necessary to solve the magnetic diffusion equation and to account for the coupling between magnetic field and drop surface at the same time. In this field, the fifth study reports experimental results on the azimuthal deformations of a liquid metal disc in an inhomogeneous inductor field.

The results of the work show that especially the transient fields provide feasible ways for analytical modeling. Like high frequency fields they are suited to shape and to support liquid metal surfaces. To study azimuthal deformations, the disc geometry has proven useful - both analytically and experimentally. Overall, it still seems worthwhile to further investigate the behavior liquid metal surfaces in magnetic fields.

Contents

List of Figures

Chapter 1

Introduction

1.1 Historical background and motivation

Metallic materials are indispensable in our daily life. Their properties gave birth to a variety of modern achievements that we take for granted nowadays.

However, the history of metals in the service of mankind is already over ten thousand years old. Earliest evidences of worked on metal tools were found in Anatoly, dating from the 9th millennium before Christ. They consist of copper which in places, here and there, occurs in pure metallic form in that region [1]. All advanced civilizations of the ancient world knew several metals. For example the Egyptians, around 3000 BC, knew about gold, silver, copper, lead and iron. Antique bronze, the alloy of copper and tin which is harder than its components, was first produced in Mesopotamia at the end of the 3rd millennium BC. Iron, the hardest material in the antique, was first harvested from meteorites before, around 1500 BC, the Indians were able to produce it in huge amounts. Aided by the most important trading nation of their time, the Phoenicians, this iron was exported across the whole world known at that time, until other nations mastered the iron smelting process themselves. In the course of time the role of trade grew and eventually all nations participated on each others knowledge about metals. Nevertheless, when the times changed from BC to AD even the Romans, technologically advanced and rulers of a vast empire, had additional knowledge only of quicksilver and brass [2].

Thousand years later in the middle ages, it were especially the alchemists in their seek for the "Philosophers stone", the "Homunculus" or synthetical gold that found new chemical elements and compounds. But only the publication of the periodical system of elements by Mendelejew and Meyer in 1869 [3] paved the way for systematic research to find new materials, amongst them also metals.

Meanwhile, the number of pure metals and alloys seems unlimited. Todays world production of metals is about 1000 million tons per year[1] or 4 cubic meters per second. During their production and processing they often are in liquid state. The melting temperatures of metals range from $-39°C$ (mercury) to $3380°C$ (wolfram). In numerous cases the liquid metal is not only very hot but also chemically aggressive. Therefore, the wear of all parts submerged in liquid metal remains a big problem. Either those parts, as for instance the crucible walls, have to be regularly renewed to compensate for erosion. Or they are intensively cooled to keep the metal solidified at the contact surfaces and prevent direct contact with the aggressive melt. But none of these solutions is satisfying. While the renovation strategy means inconvenience, maintenance expenses

---

[1] According to "Rohstoffwirtschaftliche Steckbriefe für Metall- und Nichtmetallrohstoffe" from the Bundesanstalt für Geowissenschaften und Rohstoffe

and a continuous contamination of the melt, the wall cooling consumes enormous amounts of energy, due to the high thermal conductivity of most metals, thus considerably reducing the efficiency.

In principle, a solution without these handicaps can be achieved by applying magnetic fields. Since the extensive experiments of Michael Faraday in the 1830's it is known that magnetic fields of time-dependent strength can induce eddy currents in metals and other electrically conducting materials. Inside the metal, these eddy currents cause thermal losses, named induction heat. At the same time, the so-called Lorentz force arises in the metal which is based on the interaction between the inducing magnetic field and the magnetic field originating from the eddy currents. Exploiting these two fundamental effects, magnetic fields are today successfully used to heat and to stir molten metals, to calm down convective motion or to influence the melt flow in other ways. The free surface of the melt can also be shaped by the Lorentz force which is done for example in cold crucible applications [4]. Here, the magnetic field repels the hot melt from the crucible walls which results in a dome of liquid metal in the crucible center. Beside such a semi-levitation process, where the melt still rests on a solid base, small liquid metal volumes can also completely be levitated. In solid metals only the Lorentz net force is important which makes it easy to levitate even heavy loads. A well known example is the magnetic train Transrapid. However, for liquid metal an additional demand is a distribution of the Lorentz force without any "magnetic hole". Otherwise the melt will leak right there.

Both, the distribution of the magnetic field and thus of the Lorentz force as well depend on the melt surface shape that can move freely. Vice versa, the free surface shape depends on the magnetic field distribution - which makes a coupled problem. This coupling between free metal surface and magnetic field can provoke surface instabilities manifesting itself in frozen, oscillating and irregular deformations where symmetries break. Although the phenomenon was continuously investigated over the past decades, the achieved insights are far from exhaustive.

It is the aim of the present work to expand the understanding in this research field further. On the basis of a liquid metal drop whose surface encloses a finite volume, the behavior of liquid metal surfaces in magnetic fields shall be further clarified. The focus is laid on analytical methods to explore the subject.
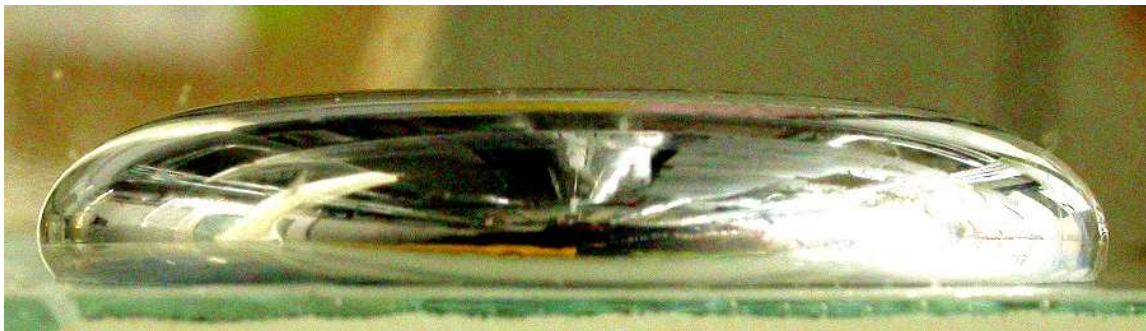
Figure 1.1: Liquid metal drop from aside in absence of a magnetic field

1.2 Preliminary works

Considering a liquid metal drop in magnetic fields, we face a capillary magnetohydrodynamic problem. It involves the solution of hydrodynamic, capillary and electromagnetic equations, respectively. Next, each aspect of the problem shall be introduced separately before focussing on the coupled problem.

Capillary Hydrodynamics

As for example Simonyi [5] points out, already the Greeks had remarkable knowledge in hydrodynamics[2]. Qualitative observations of the capillary rise of water in hair-thin tubes[3] were, according Bakker [6], already reported in the scientific diaries of Leonardo da Vinci dating back to 1490. It was in the first place his interest in anatomy that led him to conduct experiments on the human vascular system, especially the very thin veins called capillaries, too. Da Vincis insights survived only on handwritten manuscripts since he lived before the book press was invented. A review of the early history of observations of the capillary phenomenon and attempts to explain it can be found in the Zedler[7] which is the oldest german encyclopedia, dating back to about 1730. Among others, the encyclopedic entry praises Honoratus Fabri who knew the da Vinci manuscripts as well as Hauksbee. In 1712, Taylor [8] and Hauksbee [9] were the first to publish a study on a capillary phenomenon in a scientific journal. They had observed the hyperbolically shaped meniscus[4] due to the capillary rise of water between two glass planes forming a vertical wedge. In 1751, Segner introduced the concept of surface tension [10]. Independently, in 1805 Young [11] who refers to Segner and Laplace [12] proposed that the pressure jump caused by a soap film or by the tensed skin of a fluid drop corresponds to the product of surface tension and surface curvature. Owing to that fundamental discovery, the pressure balance at a free fluid surface is today called the Young-Laplace equation. A pioneer in its application was Poisson who in 1831 published a book with some of its analytical solutions [13] including the contour of an infinite long sessile drop. Delauney in 1841 succeeded in solving the Young-Laplace equation for axially symmetric menisci of constant curvature [14]. His results, the Delauney curves - nodoid, catenoid and undoloid - have negative, zero and positive curvature, respectively and account for the menisci of liquid bridges and suspended drops between plates in zero gravity. Many intriguing experiments were carried out by Plateau from the 1840's on in which he created a zero-gravity environment to reveal capillary action in pure form. The so-called Plateau tank consisted of a transparent container, filled with a water-alcohol mixture and equally buoyant oil immersed in it. In this artificial weightlessness the oil, for example, formed to drops that were governed by surface tension alone and hence floated as ideal spheres in the tank no matter how big the drop was. With his tank Plateau studied liquid bridges, drop oscillations, ring formation due to drop rotation, jet instabilities, breakup behavior and lots more. He published his experimental and theoretical insights in 1873 [15]. In 1879, Rayleigh [16] investigated the jet behavior theoretically by means of linear stability analysis. He found a relation between the growth rate of instabilities and their wavelength along the jet. According to this theory, the most critical perturbations of the jet are about 9 times its radius which was excellently confirmed by experiments. The modern name for this phenomenon is therefore Rayleigh-Plateau instability. A comprehensive review on its further history is given by Eggers [17]. At that time, around 1880, another important capillary problem of direct concern for the present work had shown resistent

---

[2]Greek: $\upsilon\delta\omega\rho$ = water, $\delta\upsilon\nu\alpha\mu\eta$ = force.

[3]Latin: capillus = hair.

[4]Greek: $\mu\eta\nu'\iota\sigma\kappa\sigma\sigma$ = shape of the new moon. Today "meniscus" is the common term for any capillary surface.

against every attack: What is the shape of a simple drop of water sessile to the ground? A first solution was found by Kelvin [18] (only published in 1891) who applied a graphical by hand shooting method. Bashforth and Adams also applied a shooting method to solve the problem but in a way numerically. They expanded the axisymmetric Young-Laplace equation into orders of spherical harmonics which allowed them to calculate the new positions during the shot in dependence of two shape factors. The result of their diligent work was published in 1883 [19] in form of extensive tables covering sessile and pendent drop profiles of a wide parameter range. Almost 80 years later, in a review article on the theory of capillarity, Buff [20] still claims that the Young-Laplace equation for the circular sessile drop cannot be solved analytically. And in 1971, Padday [21] extends the Bashforth/Adams tables essentially applying the same technique but aided by a computer. Thanks to the Personal Computer, the Padday tables have lost their importance today since the shots can be done by everybody himself. But still there exists no analytical solution to the problem.

Another problem of interest for the present work are the drop oscillations. Kelvin in 1863 [22] derived a relation for the oscillations of an inviscid liquid globe. Included in Rayleighs theory on jet instability 1879 [16] one finds a relation for the perimeter oscillations of a liquid disc. Both assume linear oscillations with infinitesimal amplitude. Only much later, in 1983, Tsamopoulos et al. [23] considered nonlinear oscillations of inviscid drops and found that their frequency decreases with increasing amplitude. An impressive study on three-dimensional drop oscillations of polyhedral type was conducted by Azuma et al. in 1999 [24].

Also of concern for the drop are rivulets on an inclined plane. They have a contact line, a free surface and internal flow and can be considered as a mirror-symmetric drop. A survey on the problem is given by Kern [25], [26] around 1970 who describes the typical flow behavior of rivulets due to an increase of the flow rate and tilt angle. He finds that a static straight rivulet is successively replaced by a static meandering rivulet, a slowly undulating pendulum rivulet with breakup and finally an uninterrupted rivulet again that slips slightly oscillating down the plane. Only the two static rivulet states were subject to theoretical investigations, too. So Allen and Biggin in 1974 [27] present analytical results for the shape and the flow field of a straight static rivulet. Davis in 1980 [28] tackles the effect of a moving contact line onto the rivulet and resulting instabilities. Nakagawa and Scott in 1984 [29] as well as Kim et al. in 2004 [30] focus on the meander flow regime. And finally Perazzo and Gratton [31] solve analytically the coupled problem of surface shape and flow field in a straight static rivulet and provide results for different contact angles.

For the effect of heat (which is neglected in this work) on the drop shape the work of Ehrhard in 1991 [32] can serve as a starting point. Recommended overview literature on the capillary subject is provided by Bakker [6], deGennes [33], Myshkis [34] and Langbein [35].

Electromagnetics and Magnetohydrodynamics

Exactly in 1800, Alessandro Volta presented the first chemical battery, the Volta pile [36], which was the first device to produce a steady electric current. Before that time, only static magnetism[5] and electricity[6] were open to investigations. Soon after, the theoretical and experimental works

---

[5]Named after "Magnesia", a town in Asia Minor at the time of the Trojan War which was founded by the tribe Magnets. Close to it magnetic stones were found in the Antique that attract each other as well as iron (there is a natural deposit of the iron mineral Magnetite: Fe_3O_4).

[6]Derived from greek: $\eta\lambda\epsilon\kappa\tau\rho\text{o}\nu\text{io}$ = amber. In the Antique it was found that amber can attract for example hair and cause tiny lightnings since it can easily be electrostatically charged due to its extremely low electrical conductivity.

of Ampere, Ohm, Joule, Biot, Savart, Helmholtz, Kirchhoff and many others pushed ahead the new science. A detailed history of Electromagnetism can be found in [5] and [37]. Outstanding were the experiments of Michael Faraday starting in the 1830's who systematically scrutinized all kinds of electric, magnetic and electromagnetic effects as well. Overall, he conducted 30 experimental series [38] each focussing on one effect and containing dozens of single experiments. Although his work as a whole is important simply for its extend and completeness, the discovery of the magnetic induction law surely was eminent. 30 years later, Maxwell derived his famous equations [39], having carefully read every note of Faraday and transforming his view to a mathematical model. Intuitively, Faraday had grasped the actions of electricity and magnetism as fields filling the space around interacting bodies and penetrating the bodies itself. Maxwells life's work was published posthumous in 1881 [40], comprehending the theoretical basis for electromagnetic studies as we still do today.

However, practical application of electromagnetic fields was restricted at that time since it still depended mainly on chemical batteries. That had only changed in 1867 when Werner Siemens built the first dynamoelectric machine [41]. There had been other generators before, but the dynamo was far superior. Because the induced current was also used to feed the magnetic field from which it was induced, the dynamo did no longer depend on weak permanent magnets. In the years to come the electric power generated by these machines exploded. Another breakthrough was the emergence of the three-phase system invented by Nikola Tesla in 1883, spreading from about 1890 in America and from about 1910 in Europe [37]. By allowing higher voltages it prompted another jump in the electric power generation and facilitated long distance distribution from central power stations as well.

Melting furnaces, welding and other electrical applications could prosper now and triggered an interest in Magnetohydrodynamics. For example, as early as 1907, Hering [42] reported observations of a pinch when direct current was applied along a liquid metal channel with a free surface. As he pointed out, the pinch posed a serious limitation to the power consumption inside the metal. From the 1920s on, efforts were made to use the magnetic forces on which electric machines rely for levitation devices [43]. But Hartmann is the one who is often considered to be the father of magnetohydrodynamics. Around 1937, he conducted experimental as well as theoretical studies on laminar mercury flow in a direct magnetic field [44] what is today called a Hartmann flow. Another MHD pioneer was Alfven who in the 1940s thought about solar physics and MHD of plasmas. His ideas inspired the research of geodynamos and nuclear fusion as well. In connection with the advent of computers the evaluation of complex analytical solutions became feasible. That is why, from the 1960s on, many solutions were elaborated for 2D eddy current problems, i.e. the distribution of time-dependent magnetic fields in metallic bodies [45, 46, 47, 48, 49, 50, 51]. An overview on solvable eddy current problems is provided by Tegopoulos and Kriezis in 1985 [52]. For a more complete view on MHD the books of Moreau [53] and Davidson [4] are recommended.

1.3 State of the art

Spherical liquid metal drops in magnetic fields

Spherical drops occur in zero and micro-gravity, free fall and also in electromagnetic levitation devices when surface tension dominates, i.e. for small droplets. Zambran in 1966 [54] theoretically investigates liquid metal drop behavior in a static magnetic field. Based on Kelvins theory he focusses on small axisymmetrical oscillations of inviscid spherical drops. In the very same journal, Gailitis [55] presents an extension of this analysis which accounts also for azimuthal oscillations and finite amplitudes. He identifies four types of oscillations depending on axisymmetric and azimuthal wave number conditions: i) purely capillary uninfluenced by the magnetic field, ii) damped in weak fields, aperiodic in strong fields, iii) always damped and iv) always aperiodic. For all types he offers an expression for the oscillation frequency and the damping rate as well.

Kirko et al. in 1970 [56] and Dobychin in 1973 [57] conduct experiments with a liquid mercury drop immersed in electrolyte and observe its behavior 1.5 seconds long in free fall. They record the height of the capillary jump and the oscillations i) purely hydrodynamic, ii) in an electric field, iii) in a magnetic field and iv) in crossed electric and magnetic field. In the latter case, a Lorentz force arises that can promote or brake the jump and remarkably damp the oscillations. Podoltsev in 1996 studies the behavior of spherical drops in a pulse magnetic field [58]. He uses an inhomogeneous field, decomposes the pulses in their cosine compartments, calculates the force and acceleration caused by each one and adds them afterwards. He shows that the skin depth in relation to the drop radius should be in the range $0.4 - 0.5$ for optimal force effect. A survey on pulsed magnetic fields is given by Knoeppel [59].

Priede and Gerbeth [60] in 2000 elucidate the origin of the spontaneous rotation that is sometimes observed at levitated loads. They consider a solid sphere and decompose the oscillating magnetic field in two counter-rotating components. The mechanical rotation speed adds or subtracts, respectively, to the magnetic rotation speed of the two components why one of them is shielded stronger. With a linear stability analysis they show that weak initial rotation thus can lead to a spin-up after a threshold of the magnetic field frequency. Moreover, they derive how the spin-up can be avoided. If the levitated load is liquid, internal flow will occur inside it. Song and Li[61] in 2001 study numerically the oscillations of a melt drop in micro-gravity. Applying a magnetic field of 427kHz to heat and center the melt drop, they take into account the coupling between temperature distribution, surface tension and internal flow and predict the drop oscillations. Furthermore, Shatrov et al. in 2001 and 2003 present a stability analysis for the flow in levitated drops [62],[63].

Another article of Priede and Gerbeth [64] is devoted to the spontaneous oscillations that is often observed on levitated load. Again, they consider a solid sphere and apply similar methods to find that above a critical frequency oscillations can set in. There is a maximum growth rate for these oscillations at some frequency, for high frequencies it approaches zero. Yasuda et al. in 2005 [65] present experimental results on such oscillations. In their experiment they superimpose a strong static magnetic field to the alternating one and by that suppress the oscillations.

Levitation melting of non-spherical drops

Cummings and Blackburn [66] in 1991 investigate how the deviation from sphericity affects the oscillation of liquid metal drops in levitation. They can show that the fundamental mode splits into three or five bands depending on the deformation.

Sneyd and Moffatt [67] in 1982 contribute an interesting work on levitation melting by suggesting

a new approach. To avoid the magnetic hole that occurs at the lowest point of the levitated blob in conical conductors they propose a toroidal geometry. Here, an initially solid torus of metal floats above two concentric ring wires that carry a high-frequent current in the same direction. They perform an analytical parameter study where they calculate the inductor current to generate the necessary lift force, the film flow at the onset of melting and, by a variational approach, the shape of the free surface in completely molten state.

Shaping of liquid metal

Beside complete electromagnetic levitation, liquid metal volumes can experience lateral support by a Lorentz force while still resting on a solid base. More general, we can speak of electromagnetic shaping. A classical application is the floating zone process where polycrystal silicon is remelted to obtain a single crystal. Here, for example, Riahi and Walker in 1989 [68] investigate the free liquid metal surface behavior under the action of a filamentary 3 MHz induction coil. They apply body adapted coordinates and a fourth-order Runge - Kutta method to calculate the resulting shapes for different inductor parameters and find out that for most practical parameter sets a critical value of the magnetic field exists where the float zone is pinched. They find the most effective position of the inductor coil to be around 45 degrees below the neck.

Many other electromagnetic shaping problems are collected in the book on "Continuous Casting" by Ehrke [69] from 2000. Additionally, an overview article from Durand [70] in 2005 focuses on "Cold Crucible" applications.

Stability and oscillation of liquid metal drops and interfaces

In 1968, Schaffer [71] presents a both experimental and theoretical analysis of surface waves on liquid metals in high frequency magnetic fields. For the experiment he uses an eutectic alloy of sodium and potassium in an evacuated 12cm long and 2cm wide channel. The surrounding wall of the channel acts as a secondary coil for the inductor to produce the magnetic field along the NaK surface. Astonishingly, there is no optical access to the liquid metal but all deformations of the liquid NaK are monitored by the frequency shift in the inductor. Performing a finite skin depth linear analysis for this geometry he derives a dispersion relation for various geometrical and magnetical parameters. He finds that the magnetic field only affects a shallow layer of about one half skin depth thickness. Although his experiment yields no very reproducible results, qualitative agreement to the theoretical predictions are found.

An extended theoretical study of free surface instability in alternating magnetic fields is performed by Fautrelle and Sneyd [72] in 1998. They include magnetic diffusion and do not average the magnetic pressure in time. They show that resonances to capillary oscillations play an important role and that ohmic damping is much more effective than viscous damping.

Perrier et al. [73] in 2003 experimentally and theoretically study a gallium pool with a free surface in a modulated magnetic field, i.e. consisting of a high-frequent and a low-frequent part. The main results are standing waves on the pool corresponding to capillary resonance to the low frequency.

In the low frequency regime settles also the "Starfish" experiment, from which Fautrelle [74] and Sneyd [75] report. In this experiment, a circular puddle of mercury in a conical dish was submitted to low-frequent magnetic fields. Depending on the field parameters, the observed oscillations range from axisymmetric over very regular azimuthal oscillations to completely chaotic flow patterns. Especially the azimuthal oscillations show a strong resonance to capillary eigenfrequencies

The stability of liquid metal surfaces in a middle frequency magnetic field was studied by Karcher

and Mohring [76],[77] both theoretically and experimentally. In the experiment they use Galinstan and restrict the melt to the annular gap between two concentric glass cylinders which allows only two-dimensional motion. Aided by a high-speed camera system, they observe in succession on increasing the field strength i) short gravity-capillary waves, ii) frozen wave patterns and iii) a pinch. Their theoretical model is based on skin-depth approximation as well as Hele-Shaw approximation and allows some qualitative insights.

Kocourek et al. [78],[79] study a sessile Galinstan drop in a middle frequency magnetic field. They use a spherically curved glass dish as substrate and vary drop volume, inductor current and frequency. Below a critical inductor current the drops are squeezed without deformations. Above the critical current azimuthal oscillations occur.

Interestingly, Perrier et al. [80] conduct a similar experiment using a mercury drop in a conical glass dish. But in contrast to the former experiment, only frozen azimuthal deformations are observed here.

An overview on the behavior of free liquid metal surfaces in different magnetic fields is also given by the review article of Fautrelle et al. [81]. In it they classify the magnetic field action by two dimensionless parameters, namely the shielding parameter to account for the field distribution and the interaction parameter to account for the strength of the field.

Magnetic energy and liquid metal

Linked to the current in the inductor as well as to induced eddy currents is a magnetic energy, proportional to the product of current and generated magnetic flux. Every deformation of a liquid metal surface in a magnetic field has an impact on the current distribution. As a consequence, magnetic energy and inductance, respectively, change, too.

This effect is exploited in the experiment of Bardet [82] who examines levitated drops in high frequency magnetic fields. By modulating the high frequency with low-frequent pulses he induces oscillations. After being excited and without further modulation, the oscillations decays. Hereby, the inductance of the inductor changes in the rhythm of the oscillation resulting in a oscillating frequency shift, too. Therefore, just by monitoring the frequency shift of the inductor current, the drop oscillations are detected. This is also similar to the above mentioned older experiment of Schaffer [71].

Hinaje, Vinsard et al. [83], [84] study experimentally, analytically and numerically a thin liquid metal layer in a beaker submitted to a middle frequency magnetic field. In their experiment, the layer pinches from the outside above a critical inductor current and retains a U-shape. Both analytically and numerically they prove that this new equilibrium state corresponds to a minimum of the magnetic energy.

1.4 Liquid metal drop - magnetic field interaction

1.4.1 General effects

Magnetic fields acting on liquid metal Time-dependent magnetic fields or movement in a time-independent field induce eddy currents in liquid metal. As one result, Lorentz forces arise, possibly leading to flow excitation (electromagnetic stirring) or surface deformations and movements. As a second result, Joule heat losses are generated (induction heat) which for example allow to melt the metal in the first place.

Counteraction of the liquid metal on magnetic fields The induced eddy currents build up a magnetic field of their own. Hence, the inducing magnetic field is disturbed. In its strongest markedness (skin effect) this leads to a complete deflection of the magnetic field which then flows around the metal body. What's also due to the field deformation is a change of the magnetic energy to which the metal is subjected. Moreover, the inductance of the whole metal load plus inductor arrangement changes which has an influence on the magnetic field frequency as well.

1.4.2 Magnetic field types

Spatial distribution and time dependence of a magnetic field have a great impact on its effect. Magnetic fields can be

- homogeneous or inhomogeneous with different orientation
- direct or time-dependent
- harmonically oscillating, pulsed, otherwise periodic or transient
- low-, middle- or high-frequent corresponding to no, partial and complete skin effect
- fixed in space or traveling, either translatory or rotationally
- crossed with an applied current density field
- composed of two or more of the above
- modulated, either in amplitude or in frequency
- unclassifiable as could be the result of a control circuit

Within this work we focus on space-fixed and time-dependent magnetic fields of individual type. We include i)transient, ii) middle-frequent and iii) high-frequent magnetic fields that are homogeneous in some cases, but inhomogeneous in others.

1.4.3 Modeling the magnetic field

To calculate the magnetic field distribution in space and time, we need the Maxwell equations:

$$\text{Solenoidy constraint} \qquad \nabla \cdot \mathbf{B} = 0 \; , \tag{1.1}$$

$$\text{Ampere's law} \qquad \nabla \times \mathbf{B} = \mu \mathbf{J} \; , \tag{1.2}$$

13

and

$$\text{Faraday's law} \qquad \nabla \times \mathbf{J} = -\sigma \frac{\partial \mathbf{B}}{\partial t} \ . \tag{1.3}$$

Combining Ampere and Faraday gives the diffusion equation

$$\nabla^2 \mathbf{B} = \mu\sigma \frac{\partial \mathbf{B}}{\partial t} \ . \tag{1.4}$$

1.4.4 Lorentz force

In general, the Lorentz force is

$$\mathbf{f}_L = \mathbf{J} \times \mathbf{B} \ , \tag{1.5}$$

$$\mathbf{f}_L = \frac{1}{\mu}(\mathbf{B}\nabla) \cdot \mathbf{B} - \nabla \frac{B^2}{2\mu} \ . \tag{1.6}$$

However, the application on different field types yields different results as we will clarify in the following. For simplicity, lets assume a magnetic field at the free surface in x-direction parallel to the surface as shown in Figure 1.2.

Low frequency   Here, the magnetic field $\mathbf{B} = B_0 \cos \omega t \cdot \mathbf{e}_x$ completely penetrates the metal in z-direction and is essentially not altered by the induced eddy currents. With Eqs. 1.3 and 1.5 we quickly find the eddy currents to be $J = -\frac{1}{2}\sigma\omega B_0^2 z \sin \omega t \cdot \mathbf{e}_y$ and the Lorentz force becomes

$$\mathbf{f}_L = \frac{1}{2}\sigma\omega B_0^2 z \cdot \sin 2\omega t \cdot \mathbf{e}_z \tag{1.7}$$

Obviously, in low-frequent fields the Lorentz force only consists of an oscillating component which has double frequency compared to the exciting magnetic field.

Middle frequency   Commonly, the magnetic field partially enters the metal and the magnetic diffusion equation 1.4 has to be solved. An important parameter is the equivalent skin depth defined by

$$\delta = \sqrt{\frac{2}{\omega\mu\sigma}} \tag{1.8}$$

where ω, μ, σ are the field frequency, the magnetic permeability and the electrical conductivity, respectively. It is found that

$$B_x(z,t) = B_{x0} \cdot \exp\left[-\frac{z}{\delta}\right] \cdot \cos\left(\omega t - \frac{z}{\delta}\right) \ . \tag{1.9}$$
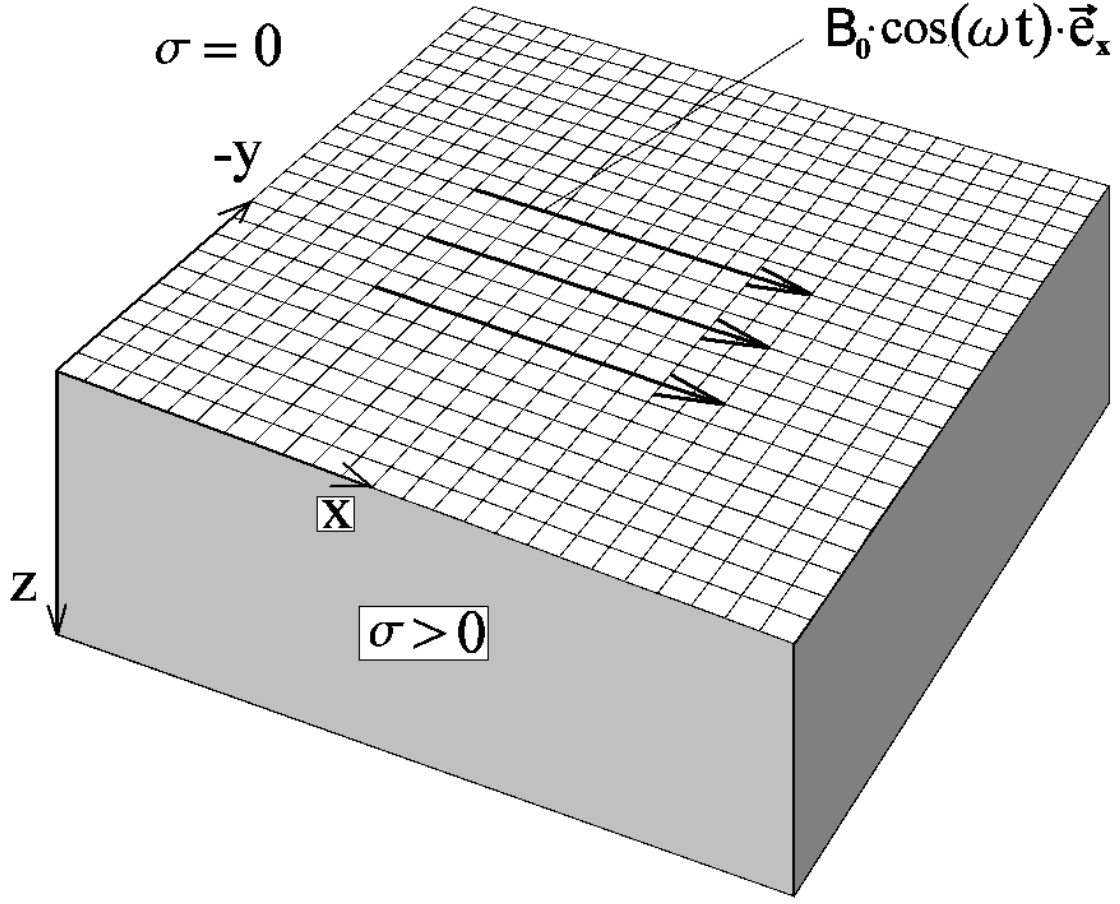
Figure 1.2: Semi-infinite space with a magnetic field at the interface

Apparently, the magnetic field exponentially decays as it penetrates the metal. At a distance of about 5δ from the surface the field is practically zero. Aided by Faraday's law, i.e. Eq. 1.3, we find the eddy currents to be distributed as

$$J_y(z,t) = -\frac{\sqrt{2}}{\delta\mu} \cdot B_{x0} \cdot \exp\left[-\frac{z}{\delta}\right] \cdot \cos\left(\omega t - \frac{z}{\delta} + \frac{\pi}{4}\right) \ . \tag{1.10}$$

Finally, the Lorentz force becomes

$$f_{Lz}(z,t) = \frac{1}{\delta\mu} \cdot B_{x0}^2 \cdot \exp\left[-\frac{2z}{\delta}\right] \cdot \left[1 + \sqrt{2} \cdot \cos\left(2\omega t - \frac{2z}{\delta} + \frac{\pi}{4}\right)\right] \ . \tag{1.11}$$

Again, it acts with double magnetic field frequency on the metal. Besides, it decays in half the distance. An important difference to low-frequent fields is the existence of a steady part in the Lorentz force which allows to squeeze, support or even to levitate liquid metals. Since the amplitude of the oscillating part is higher than the steady part, the metal surface is also pulled frequently.

15

High frequency As the skin depth of the magnetic field goes to zero, the Lorentz force is restricted to the surface. Therefore it is more appropriate to integrate Eq.1.11 along the depth and to use the Lorentz force per surface area. This corresponds to a magnetic pressure

$$p_m(t) = \frac{B_{x0}^2}{2\mu} \cdot [1 + \cos(2\omega t)] \ .$$
(1.12)

This so-called skin depth approximation spares the look at the bulk of the liquid metal and reduces the effect of the Lorentz forces to a pressure balance at the free surface. It should be noted that the field normally is neither parallel nor of constant value along the surface. This is accompanied by shear stresses, the so-called Maxwell stresses, that drive inner flow. However, in the frame of this work they are not needed which is why we will not go into detail here.

1.4.5 Capillary equation (Young-Laplace)

Basically, the Young-Laplace equation is the pressure equilibrium at a capillary surface $\Gamma = \{x_\Gamma, z_\Gamma\}$. For our purpose, it includes a constant pressure difference between ambient pressure p_∞ and the reference pressure p_0 at $\{x = 0, z = 0\}$ inside the liquid, furthermore the hydrostatic pressure $p_{hs} = \rho g z_\Gamma$, the magnetic pressure $p_M = \int \mathbf{f}_L d\mathbf{l}$ and the surface pressure p_γ which is the crucial term. Into p_γ goes the tension of the surface together with its curvature $C_\Gamma(x_\Gamma, z_\Gamma)$ which is usually a nonlinear term. It is $p_\gamma = \gamma \cdot C_\Gamma(x_\Gamma, z_\Gamma)$ and

$$p_0 - \rho g z_\Gamma - \int \mathbf{f}_L d\mathbf{l} + \gamma \cdot C_\Gamma(x_\Gamma, z_\Gamma) = p_\infty \ .$$
(1.13)

Here, the Lorentz force is defined to point inward the metal, the curvature is negative.

1.4.6 Hydrodynamic equation (Navier-Stokes)

In case the drop oscillates or an inner flow is driven by shear forces, the Navier-Stokes equations have to be solved. In our case, it is the Lorentz force that in general consists of a gradient and a whirling component as well. While the gradient part just adds to the pressure, the whirling part possibly excites a flow. In the form given here, the terms of the Navier-Stokes equation account for time dependence, inertia, pressure, viscosity and Lorentz force, respectively. It is

$$\frac{\partial \mathbf{u}}{\partial t} + (\mathbf{u}\nabla)\mathbf{u} = -\frac{\nabla p}{\rho} + \nu \nabla^2 \mathbf{u} - gz + \frac{\mathbf{f}_L}{\rho} \ .$$
(1.14)

In this connection we want to point out that in absence of flow and gravity and with a purely gradient Lorentz force, ref. Eq. 1.6, the Navier-Stokes equation becomes

$$\nabla p = -\nabla \frac{B^2}{2\mu} = -\nabla p_{mag} \ .$$
(1.15)

1.4.7 Dimensionless parameters

To categorize the problems that arise when liquid metal drops interact with different species of magnetic fields we briefly introduce some dimensionless parameters.

Magnetic Reynolds number R_M

If liquid metal in a domain of size L flows while submitted to a magnetic field then the magnetic Reynolds number R_M indicates whether the flow can distort the magnetic field. We have a flow speed U and a diffusion speed $U_d = 1/(\mu\sigma L)$. R_M is defined as the ratio of both giving

$$R_M = \mu\sigma U L \ . \tag{1.16}$$

If the flow is not imposed but excited by the magnetic field, the typical flow velocity derives from the balance of magnetic energy $W_{mag} = L^3 \cdot B^2/\mu$ and inertial energy $W_{kin} = L^3 \cdot \rho U^2$. The result is the Alfven velocity $U_A = B/\sqrt{\mu\rho}$. Inserting U_A in Equation (1.16) yields

$$R_M = B \cdot \ \sigma L \sqrt{\frac{\mu}{\rho}} \ . \tag{1.17}$$

In the case of fast diffusion we have $R_M \ll 1$ and the magnetic field completely penetrates the metal. On the other hand, $R_M \gg 1$ means that the field is convected by the metal flow. Normally, for centimeter sized liquid metal drops the magnetic Reynolds number is rather small which allows to decouple magnetic and capillary hydrodynamic calculations.

Magnetic Shielding parameter R_ω

Besides fluid flow, repulsion of the magnetic field can also be caused by a quick variation of the field amplitude which is true for steep transients and high frequencies as well. The effect is reasoned by the smallness of the diffusion speed $U_d = 1/(\mu\sigma L)$ compared to the speed of variation which is $U_\omega = \omega L$ for a harmonic variation. The Shielding parameter R_ω is the ratio between U_ω and U_d resulting in

$$R_\omega = \mu\sigma\omega L^2 \ . \tag{1.18}$$

If $R_\omega \simeq 1$ or higher, the field variation can diffuse into the metal only a short distance before its direction reverses. As a consequence, the amplitude of the magnetic field quickly decays as it penetrates. $R_\omega \ll 1$ means full penetration, $R_\omega \gg 1$ means complete shielding. Calculation of the Shielding parameters of drop experiments shows that R_ω varies from very small to very large.

Gravitational Bond number Bo

The gravitational or ordinary Bond number plays a role when surface tension has to balance gravity. It is the relation between a hydrostatic pressure $p_{hs} = \rho g L$ and a surface pressure $p_\gamma = \gamma/L$ with γ being the surface tension. Hence

$$Bo = \frac{\rho g L^2}{\gamma} \ . \tag{1.19}$$

If $Bo \ll 1$ then the shape of drops will be spherical since surface tension is dominant. On the other hand, if $Bo \gg 1$ then surface tension can support only a small height and the drops will be flat on their upper side if not otherwise supported.

Magnetic Bond number Bo_M

A counterpart to the former one is the magnetic Bond number Bo_M. It is defined as the ratio of a magnetic pressure $p_M \approx B^2/\mu$ which is the integral of the Lorentz force between surface and center of mass and the surface pressure p_γ. We find

$$Bo_M = \frac{1}{\mu\gamma} \cdot B^2 L^2 \ . \tag{1.20}$$

Since the Lorentz force can support surface tension, Bo_M tells how strong the surface can be shaped aided by the magnetic field.

Chapter 2

Classification of Liquid Metal Drop - Magnetic Field Problems

This chapter attempts to classify the various problems concerning liquid metal drops in magnetic fields. As representative geometry we choose a circular sessile drop in an axial magnetic field. Two main magnetic field effects on the drop behavior are in the fore front: i) oscillation and ii) shaping. The drop can be

- oscillating either symmetrically or asymmetrically

- shaped either symmetrically or asymmetrically

- a combination of both

Compulsorily, all asymmetries start with an azimuthal deformation that can be considered periodical in the beginning. An understanding of its occurrence is crucial to elucidate the drop behavior. As we will clarify now, a prediction of the drop behavior is possible by regarding the magnetic field frequency ω and the Shielding parameter R_ω.

2.1   Effect of magnetic field frequency and Shielding parameter

Capillary waves.   Experiments as well as theoretical work ([74], [72]) have exposed the significant role of capillary eigenfrequencies on the behavior of liquid metal surfaces in a magnetic field. If the magnetic field oscillates with a frequency that matches one of those eigenfrequencies the drop is very likely to follow it and to execute oscillations with this frequency [1]. The maximum field strength for stable or at least symmetric deformation is then strongly reduced. We shall give here two capillary eigenfrequency relations that are applicable to the azimuthal oscillations of a sessile drop:

$$\text{disc perimeter} \qquad \omega_c^2 = \frac{\gamma}{\rho a^3} \cdot (m^3 - m) \ , \qquad (2.1)$$

$$\text{sphere equator} \qquad \omega_c^2 = \frac{\gamma}{\rho a^3} \cdot m(m-1)(m+2) \ . \qquad (2.2)$$

Hereby, γ denotes the surface tension, ρ the density, a the drop radius and m the integer mode

---

[1]Actually, the Lorentz force triggers these oscillations with double magnetic field frequency, but the drop oscillates with single frequency because the drop shape repeats after a half period, only rotated

number. According to these relations, starting with the smallest possible mode number 2, we will have a set of capillary eigenfrequencies ω_{c2}, ω_{c3}, ω_{c4}, ... and so on. For centimeter-sized liquid metal drops, the capillary eigenfrequencies are in the range of cycles to some hundred cycles per second. Below ω_{c2} on one hand, we would expect forced axisymmetric oscillations because no eigenfrequency of the drop is driven. For $\omega \geq \omega_{c2}$ on the other hand, the drop would experience azimuthal oscillations. The wavelength $\lambda_m = 2\pi a/m$ of these eigenfrequency oscillations becomes smaller as the mode increases. Nonetheless, the Lorentz force per volume of liquid metal remains constant also for short waves. As a consequence, high magnetic field frequencies, say several kilocycles per second, can also excite high modes, as the experiment of Mohring [77] indicates.

Diffusion waves. For higher magnetic field frequencies where the Shielding parameter exceeds unity, the skin effect becomes important. Connected with the magnetic field decay towards the drop core is the ability to exert steady forces on its surface. A sinusoidal magnetic field penetrating from the drop surface into its core has a wavelength of $\lambda_\delta = 2\pi\delta$, conf. Eq. 1.9. Logically, perturbations along the drop perimeter spread with the same wavelength and can superimpose to what we may call a diffusion wave. As a result, frozen azimuthal waves with a mode number $m = a/\delta$ are excited when the drop perimeter $2\pi a \geq \lambda_\delta$ or $a \geq \delta$, respectively ([80], [85]). The modes are related to the Shielding parameter, conf. Eq. 1.18, by $R_\omega = 2m^2$ which gives $R_{\omega 2} = 8$, $R_{\omega 3} = 18$, $R_{\omega 4} = 32$, $R_{\omega 5} = 50$, ... corresponding to the mode numbers. Again, we have a set of frequencies $\omega_{\delta 2}$, $\omega_{\delta 3}$, $\omega_{\delta 4}$, ... where a typical deformation can be expected, obtained by the relation $\omega_n = R_{\omega n}/(\mu\sigma a^2)$.
Sometimes the diffusion waves are oscillating, too ([79]). The reason for this is not yet completely understood but it seems that the coupling between magnetic energy and drop movement is responsible here. In the chapter "Prospective ideas and outlook" we explain this possibility in more detail.

Shielding parameter Although the Shielding parameter for one drop increases direct proportional to the magnetic field frequency, we will use it as an extra parameter. As mentioned in the "Introduction" it tells how strong the drop shields the field from its core. In a diagram displaying magnetic field frequency versus Shielding parameter we then can see all of a sudden the expected behavior of liquid metal drop and magnetic field as well.
Please note that these two descriptive parameters (Magnetic field frequency and Shielding parameter) do neither account for the field strength nor for inhomogeneous distributions but only for the nature of the drop behavior.

2.2 Expected drop behavior

Summarizing the effects of capillary eigenfrequencies and magnetic diffusion, we have the two identities

$$\omega_{\gamma m}^2 = \frac{\gamma}{\rho a^3} \cdot (m^3 - m) \ , \qquad \omega_{\delta m} = \frac{2m^2}{\mu\sigma a^2} \qquad \text{with m=2,3,4,...} \tag{2.3}$$

that describe the expected frequencies for m-lobed patterns. Here, $\omega_{\gamma m}$ represents an oscillation, in this case of a disc-like drop, and $\omega_{\delta m}$ a steady deformation with mode m. We will express our findings now in a diagram whose axes span the magnetic field frequency versus the Shielding parameter. As examples we consider two disc-like mercury drops of laboratory scale with radii

of $a = 1cm$ and $a = 10cm$, respectively, see Figure 2.1. Its material properties are $\mu = 1,256 \cdot 10^{-6} \frac{Vs}{Am}$, $\sigma = 1,0 \cdot 10^6 S/m$, $\rho = 13,5 \cdot 10^3 kg$ and $\gamma = 0.5N/m$.
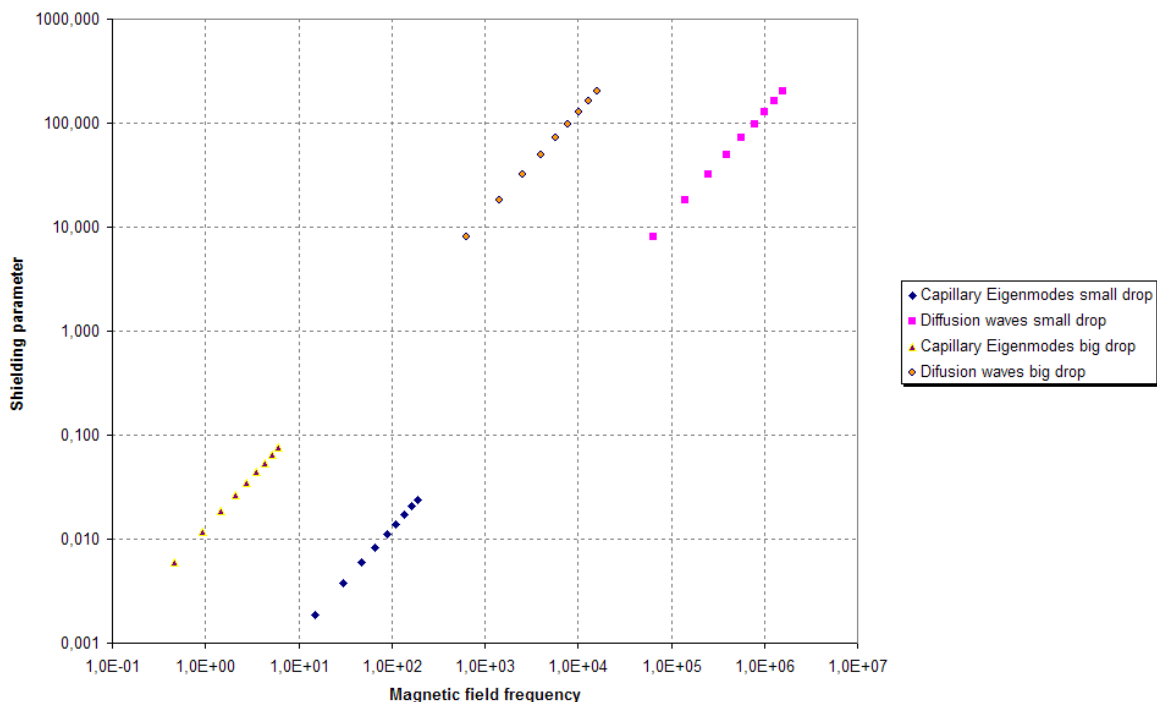
Figure 2.1: Expected capillary oscillations and diffusion wave deformations of a mercury drop of 1cm radius and 10cm radius, respectively. At the same time, the diagram shows the corresponding Shielding parameter.

Figure 2.1 reveals that the deformations due to magnetic diffusion only depend on the Shielding parameter but not on the drop size. A diffusion deformation with mode number two, for example, always occurs at $R_{\omega 2} = 8$ no matter how big the drop is. The capillary eigenfrequencies, in contrast, diminish as the drop size increases. At the same time, the same capillary mode at a bigger drop occurs at a higher Shielding parameter compared to smaller drops. We may also conclude that for symmetric shaping of liquid metal drops a Shielding parameter shortly below $R_{\omega 2} = 8$ is optimal.

2.3 Classification

As Figure 2.1 suggests, the double logarithmic presentation of magnetic field frequency versus Shielding parameter reveals the drop behavior at one glance. From a theoretical point of view it is also useful to distinguish between high, middle and low magnetic field frequency, see Figure 2.2, corresponding to the value of the Shielding parameter. For each of these three frequency regions we must apply different methods to model the magnetic field properly.
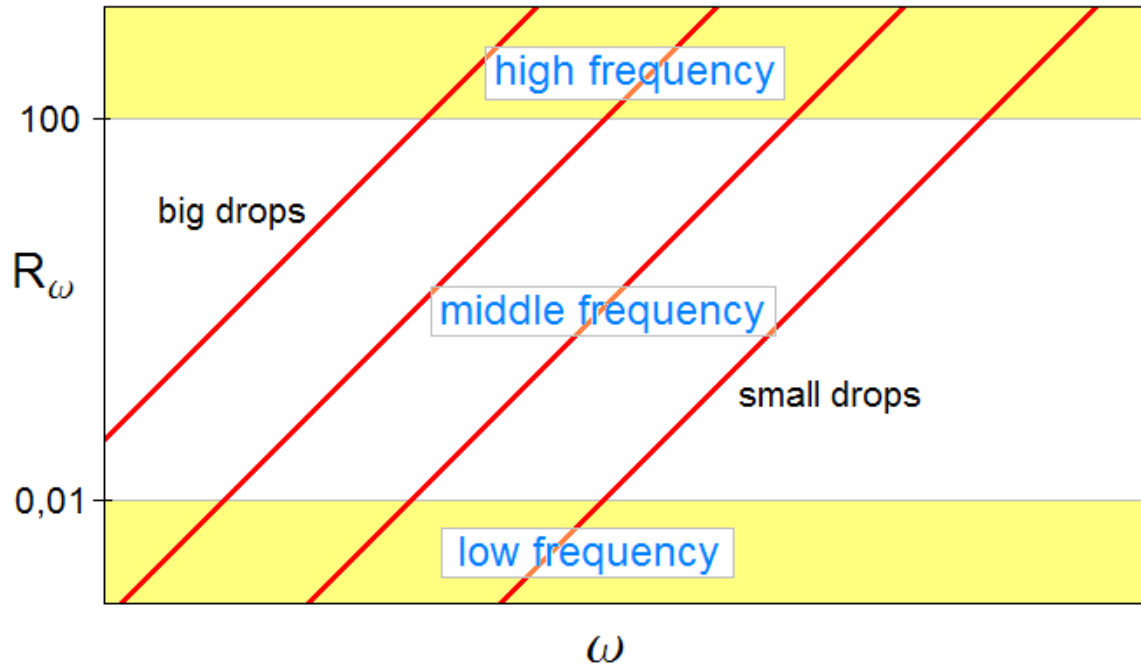
Figure 2.2: Classification of liquid metal drop - magnetic field problems based on magnetic field frequency and Shielding parameter.

Chapter 3

Transient Magnetic Field

If a magnetic field grows in intensity while maintaining its direction, the induced eddy currents and hence the Lorentz force will keep their direction as well. Moreover, by engaging a special time dependence for the magnetic field the Lorentz force becomes static. Although of limited time, transient fields thus offer an interesting viewpoint. Depending on wether the magnetic field grows or falls in an analogous manner, the Lorentz force points constantly into the liquid metal or out of it, i.e. exerts pressure or pull on it.

In this chapter we address two problems. The first is concerned with static dome-shaping. The second deals with the azimuthal modes at the perimeter of a liquid metal disc.

3.1   Problem 1: Mirror-symmetric squeezing

The content of this section is already published in a very similar form [86]. A sessile drop is subjected here to to a transient magnetic field of an inductor that grows in a square-root manner. In that case the Lorentz force remains static and repels the drop from the inductor. The opposite case, attraction between drop and inductor, would eventually comprise the ejection of small drops and their detention at the inductor which would demand a much more sensitive treatment. That is why we restrict ourselves here to the repulsion case and study the static squeezing of liquid metal drops. We analyze the influence of drop volume and Lorentz force strength on the squeezing.

3.1.1   Mathematical model

Fig. 3.1 shows one half of the mirror symmetric arrangement that we analyze. The system consists of a liquid metal drop placed on an electrically insulating substrate at $z = 0$ and an inductor located at $\{x = X, z = Z\}$. Gravity g points downwards. The drop contour is described by the cartesian coordinates $x(s)$ and $z(s)$ with the arc length s as parameter. Arc length and slope angle $\alpha(x, z)$ serve to define the curvature $k(x, z) = \partial\alpha/\partial s$ in each point of the contour. Characteristic points of the drop are the vertex at $\{x = 0, z = a\}$ with $s = 0, k = k_0, \alpha = 0$ and the contact line at $\{x = \pm c, z = 0\}$ with $\alpha_c = \pi$.

Material properties of the drop are the density ρ, the electrical conductivity σ, the magnetic permeability μ_0 and the surface tension γ.

The inductor carries a current I of the form

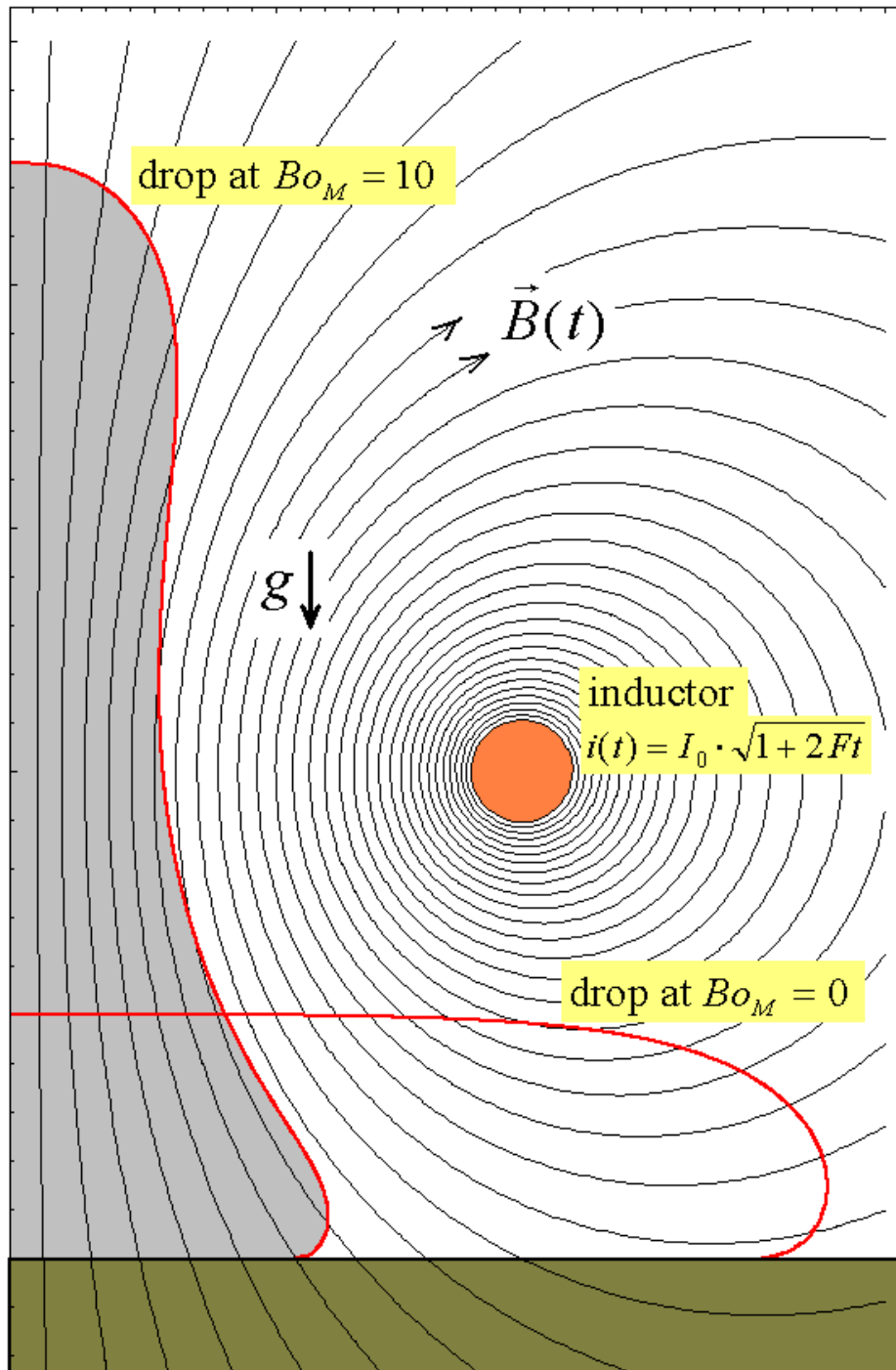$$I = \sqrt{1 + 2Ft} \cdot I_0 \tag{3.1}$$

Figure 3.1: Sketch of the drop - inductor arrangement for the squeezing in the transient field

pointing into the plane at $x = X$ and pointing out of the plane at $x = -X$ (not shown in Fig. 3.1. Here, F is a constant factor assumed to be small compared to the inverse of the magnetic field
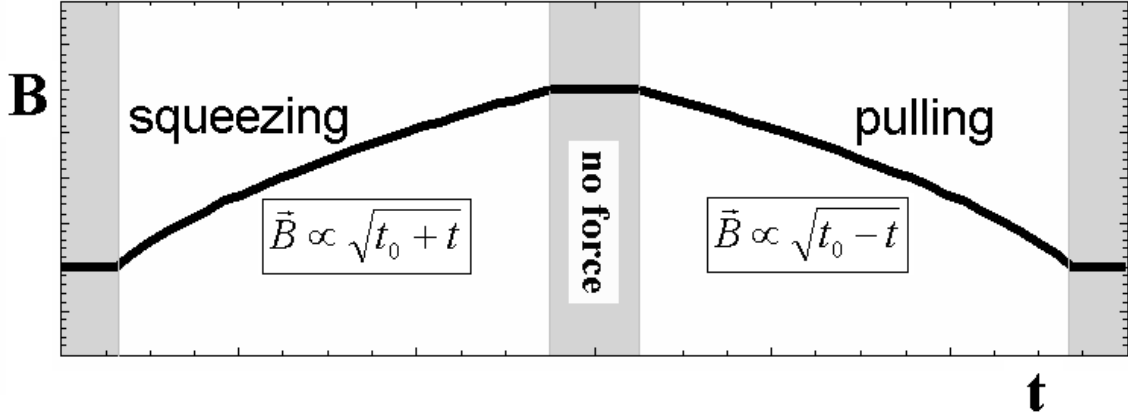
Figure 3.2: Time dependence of the magnetic field to obtain a static Lorentz force

diffusion time $\tau_D \simeq \mu_0 \sigma a^2$. In this case, complete penetration of the magnetic field into the drop is ensured. As a consequence, the curl of the magnetic field vanishes. Thus, for a static drop contour there is no electromagnetically induced fluid-flow inside the drop [53]. The magnetic field reads as

$$\mathbf{B} = \sqrt{1 + 2Ft} \cdot \mathbf{B_0}(x, z) \tag{3.2}$$

as shown in Fig. 3.2. Applying Faraday's law $\nabla \times \mathbf{J} = -\sigma \cdot \partial\mathbf{B}/\partial t$, the induced eddy currents take the form

$$\mathbf{J} = F/\sqrt{1 + 2Ft} \cdot \mathbf{J_0}(x, z) \ , \tag{3.3}$$

pointing in opposite direction as the inductor current. Finally, for the induced Lorentz force $\mathbf{f_L} = \mathbf{J} \times \mathbf{B}$ we obtain

$$\mathbf{f_L} = F \cdot \mathbf{f_{L0}}(x, z) \ . \tag{3.4}$$

It is directed into the liquid metal. In more detail, the spatial function $\mathbf{f_{L0}}(x, z)$ of the Lorentz force writes as

$$\mathbf{f_{L0}} = -C \cdot \ln\left[\frac{(x-X)^2 + (z-Z)^2}{(x+X)^2 + (z-Z)^2}\right] \cdot \left\{ \begin{array}{c} \frac{x-X}{(x-X)^2+(z-Z)^2} - \frac{x+X}{(x+X)^2+(z-Z)^2} \\ \frac{z-Z}{(x-X)^2+(z-Z)^2} - \frac{z-Z}{(x+X)^2+(z-Z)^2} \end{array} \right\} \cdot \left\{ \begin{array}{c} \mathbf{e_x} \\ \mathbf{e_z} \end{array} \right\} \tag{3.5}$$

with $C = \frac{\sigma}{2} \cdot \left(\frac{\mu_0 I_0}{4\pi}\right)^2$. Obviously, in this case the generated Lorentz force is static. The integration of the Lorentz force between $\{x = 0, z = 0\}$ and the drop surface yields the electrostatic pressure distribution. Adding the effect of gravity, we obtain

$$p_{hs}(x, z) = -F \cdot C \cdot \left\{ \ln\left[\frac{(x-X)^2 + (z-Z)^2}{(x+X)^2 + (z-Z)^2}\right] \right\}^2 - \rho g z + p_0 \ . \tag{3.6}$$

Here, p_0 is the bottom pressure at $\{x = 0, z = 0\}$. Once the induced pressure is known, we insert it into the so-called Young-Laplace equation [35] which describes the pressure equilibrium on the drop surface. With the ambient pressure p_∞ this equation reads as

$$p_{hs}(x, z) + \gamma \cdot k(x, z) = p_\infty \ . \tag{3.7}$$

Inserting the boundary condition at $\{x = 0, z = 0\}$, i.e.

$$p_\infty = p_0 - \rho g a + \gamma k_0 \ , \tag{3.8}$$

into the Young-Laplace equation we obtain

$$\gamma k(x, z) = F \cdot C \cdot \left\{ \ln \left[\frac{(x - X)^2 + (z - Z)^2}{(x + X)^2 + (z - Z)^2} \right] \right\}^2 + \rho g(z - a) + \gamma k_0 \ . \tag{3.9}$$

For a further treatment of the problem we introduce dimensionless numbers. We choose the drop height a_0 in absence of the Lorentz force as characteristic length scale. This defines a gravitational Bond number Bo and a magnetic Bond number Bo_M as follows:

$$Bo = \frac{\rho g a_0^2}{\gamma}, \qquad Bo_M = F \cdot C \cdot \frac{a_0}{\gamma} \ . \tag{3.10}$$

These parameters relate the hydrostatic pressure and the magnetically induced pressure to surface tension pressure, respectively. Due to the limited ability of the surface tension to compensate hydrostatic pressure the drop height a_0 and therefore the gravitational Bond number Bo is limited. The limit value $Bo_{max} = 4$ results from the analytical solution that exists for the $Bo_M = 0$ case, ref. [34]. The normalized Young-Laplace equation now reads as

$$k(x, z) = Bo_M \cdot f_M(x, z) + Bo \cdot (z - 1) + k_0 \tag{3.11}$$

where $f_M(x, z) = \left\{ \ln \left[\frac{(x-X)^2+(z-Z)^2}{(x+X)^2+(z-Z)^2} \right] \right\}^2$.

3.1.2 Numerical method

Since the surface curvature is a nonlinear function of the drop contour, Eq. (3.11) cannot be solved analytically. Therefore, we apply a shooting technique based on an improved Euler method [87]. This method basically represents a numerically aided geometrical construction of the drop contour. Starting from the drop vertex at $\{x = 0, z = a\}$ with the slope angle $\alpha = 0$, we choose an arbitrary initial curvature k_0 to calculate the contour at discrete points. The shooting procedure is stopped as soon as the contact angle $\alpha_c = \pi$ is attained. As we do not know the correct initial curvature beforehand, we have to adjust this parameter until the final height for the point at $\alpha_c = \pi$ becomes zero, i.e. $z_c = 0$.

Studying the squeezing phenomena demands also the conservation of the drop volume. In the present case this reduces to the conservation of the cross section A_0 of the drop. As a consequence, we have to adjust another parameter, namely the drop height a. The fixed value A_0 is given by the initial contour without magnetic field, i.e. $Bo_M = 0$. It is calculated by

applying the 'sector formula' of Leibnitz [88]. Once A_0 is known, the initial drop height can be iteratively adapted for each case with $Bo_M \neq 0$.

To test the accuracy of our method we compared the results of our shooting method with the analytical solution that exists for the $Bo_M = 0$ case [34]. The coincidence is excellent as long as the curvature of the drop is rather strong. On the other hand, for large drops that show a flat surface on the upside, the deviation increases with the drop size, i.e. as the gravitational Bond number approaches its theoretical limit of $Bo = 4$. However, we may conclude that the error of the presented results is less than one percent.

3.1.3 Results

In the following we present results on static electromagnetic drop squeezing by evaluating the governing Eq. (3.11) numerically as described in section 2. We discuss the effect of drop volume by fixing the gravitational Bond number at three particular values corresponding to three particular values of the contact line $x = c_0$ at $Bo_M = 0$ while varying the magnetic Bond number within the range $0 \leq Bo_M \leq 10$. The vertical position of the inductor is fixed at $Z = 0$ to prevent downwards directed Lorentz forces. Moreover, in order to obtain similar force distributions, the horizontal position of the inductor is fixed at $X = \frac{5}{3}c_0$.

Fig. 3.1.3 shows the results for a drop that originally spreads to $c_0 = 3$. The $Bo_M = 0$ contour extends six times more wide than high. Clearly, gravity predominates and causes the drop to be almost flat on its upper side. Located at $\{X, Z\} = \{5, 0\}$, the inductor is fed by a current to squeeze the drop statically. The squeezed contours correspond to an increase of the static Lorentz force in equidistant steps, i.e. $Bo_M = 0, 1, .., 10$. At $Bo_M = 10$ for example, the lateral drop meniscus has strongly steepened as the contact position has been declined by a factor of three and the height of the drop vertex has nearly tripled in comparison with the $Bo_M = 0$ case. Fig. 3.1.3 reveals the effect of volume reduction. At first glance, the $Bo_M = 0$ contour looks very similar to that one of the drop in Fig. 3.1.3. Nevertheless, the ratio between drop surface and cross section has increased. Therefore, the role of surface tension is now more important. The inductor at $\{X, Z\} = \{10/3, 0\}$ exerts a Lorentz force on the drop which is similar to that in Fig. 3.1.3. Like there, the magnetic Bond number has assigned values ranging from $Bo_M = 0, 1, .., 10$. However, since surface tension supports the Lorentz force in counteracting gravity, the squeezing effect is stronger. As a result, the lateral drop meniscus has now a vertical slope at $Bo_M = 10$. Finally, Fig. 3.1.3 deals with a smaller drop compared to the ones shown in Figs. 3.1.3 and 3.1.3. Here, the surface tension is able to match gravity and contracts the drop. The width of the $Bo_M = 0$ contour equals two times its height and the initial curvature is obviously not zero. The inductor is now located at $\{X, Z\} = \{5/3, 0\}$. When a field corresponding to $Bo_M = 10$ is applied, the lateral drop meniscus even hangs over. The contact position is shifted to a fifth of the initial value and further increase of the Lorentz force is likely to lift the drop completely. The vertex height, on the other hand, has grown only by a factor of about 2.5. This means that the whole body of the drop is strongly supported.

Overall, the squeezing effect in a sense of shifting the contact line is more pronounced for large drop volumes. Small volumes, on the other hand, tend to surface contraction which allows to lift the whole blob.

3.1.4 Concerning application

To demonstrate the feasibility of the proposed squeezing method we present a numerical example. We consider an aluminum drop at $700°C$ showing the following material properties [4, 89]: $\sigma = 4.1 \cdot 10^6 \ S/m$, $\rho = 2400 \ kg/m^3$, $\gamma \approx 0.9 \ N/m$. We address two questions: i) what are
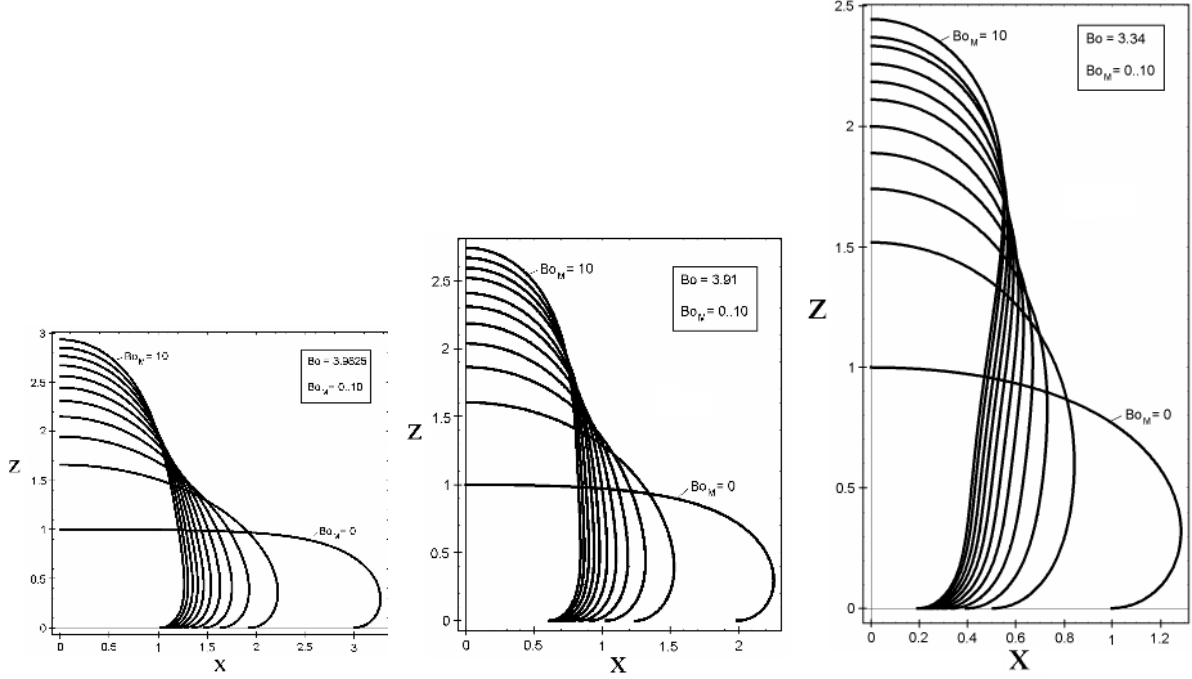
Figure 3.3: Squeezing of drops with three different contact lines or volumes, respectively, in the transient field. The electromagnetic Bond number $Bo_m = 0, 1, .., 10$. The vertical inductor position is $Z = 0$, the horizontal one is $5/3$ times of the initial contact position $x = 3$, $x = 2$ and $x = 1$, respectively.

realistic drop and inductor dimensions? ii) how long is the magnetic field maintainable?

Ad (i), Eq.(3.6) implicates that the squeezing pressure decreases towards the center where it is zero. Therefore, it would be inefficient to squeeze the drop when it is too far off the inductor. For simplicity we assume that the unsqueezed drop has a rectangular cross section $A \approx 2a_{0max}X$ while the squeezed drop has a semicircular shape, i.e. $A \approx \frac{\pi}{2}R^2$. Here, a_{0max} is an averaged drop height for which we take the maximum possible value defined by $Bo_{max} = 4$ and $a_{0max} = \sqrt{Bo_{max}\frac{\gamma}{\rho g}}$, cf. Eq.(3.10). For the given material properties we find $a_{0max} = 12.36mm$. Conservation of cross section yields $R = \sqrt{\frac{4a_{0max}X}{\pi}}$. For an application range of $0.3 \leq R/X \leq 0.9$, the corresponding range of inductor dimension is $19.4mm \leq X \leq 175mm$. Using the results shown in Fig. 3.1.3, for the given Bond number we find $a_0 = 12.34mm$ and so $X = 61.5mm$.

Ad (ii), the possible duration t_{max} of the static force field is determined by the maximum inductor current I_{max} as well as the highest sustainable voltage U_{max} applied to the inductor. The current limit determines the magnetic field $\mathbf{B}_{max}(x,z)$ at the end of the duration while the voltage limit corresponds to the magnetic field rise at the beginning of the duration, i.e. $t = 0$. Modeling the inductor as an R-L-circuit as shown at the left side of Fig. 3.4 we obtain the voltage $u(t) = R \cdot i(t) + L \cdot \partial i(t)/\partial t$. Here, the current $i(t)$ is given by Eq. (3.1) resulting in

$$u(t) = I_0 \cdot \left(R \cdot \sqrt{1 + 2Ft} + \frac{2FL}{\sqrt{1 + 2Ft}} \right). \tag{3.12}$$

Both $i(t)$ and $u(t)$ are qualitatively plotted on the right side of Fig. 3.4. We find that t_{max}
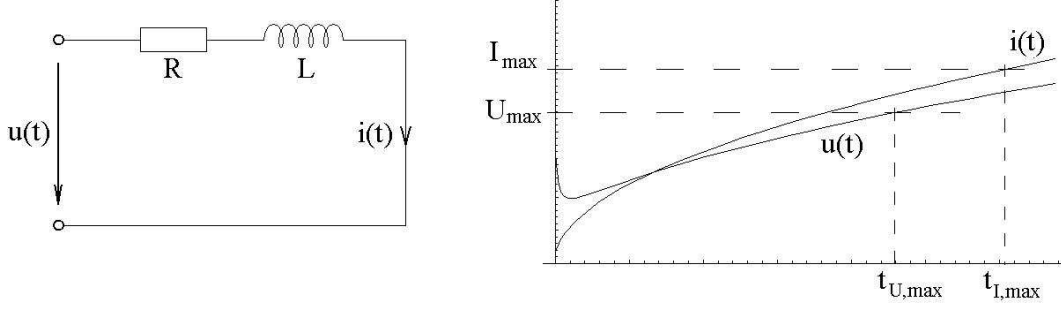
Figure 3.4: Inductor circuit and time dependence of current and voltage to attain a static Lorentz force

can equal $t_{I,max}$ or $t_{U,max}$, depending on whether the current limit or the voltage limit is reached first. Using Eqs. (3.1) and (3.12) we obtain the following limiting values

$$i(t = 0) = I_0 \ , \tag{3.13}$$

$$i(t = t_{I,max}) = I_{max} = I_0 \cdot \sqrt{1 + 2Ft_{I,max}} \ , \tag{3.14}$$

$$u(t = 0) = U_{max} = I_0 \cdot (R + 2FL) \ , \tag{3.15}$$

$$u(t = t_{U,max}) = I_0 \cdot \left(R \cdot \sqrt{1 + 2Ft_{U,max}} + \frac{2FL}{\sqrt{1 + 2Ft_{U,max}}} \right) \ . \tag{3.16}$$

From these values it is straightforward to derive

$$F = \frac{(U_{max}/I_0) - R}{2L} \ , \tag{3.17}$$

$$t_{I,max} = \frac{(I_{max}/I_0)^2 - 1}{2F} \ , \tag{3.18}$$

$$t_{U,max} = 2F \frac{L^2}{R^2} - \frac{1}{2F} \ . \tag{3.19}$$

Finally, to calculate the resistance R and inductance L of our bifilar lead we use the relations $R = s/(\sigma A)$ and $L = s(\mu_0/(4\pi))(1 + 4 \ln 2X/r)$, cf. [90]. Here, s, A and r are length, cross section and radius of the wire, respectively. For example, $s = 1m$ gives approximately $R \approx 10^{-2}\Omega$ and $L \approx 10^{-6}H$. Moreover, the initial current I_0 is determined by the magnetic Bond number Bo_M. Balancing equations Eqs. (3.10) and (3.17), we obtain

$$I_0 = \frac{U_{max}}{2R} - \sqrt{\frac{U_{max}^2}{4R^2} - \frac{2LBo_M}{RC^*}} \tag{3.20}$$

where $C^* = \frac{\sigma a_0}{2\gamma} \cdot \left(\frac{\mu_0}{4\pi} \right)^2$ reflects the drops material parameters and its dimension. Setting $U_{max} = 100V$, $I_{max} = 10000A$ and $Bo_M = 1$, cf. Fig. 3.1.3, we find that $C^* = 2.8 \cdot 10^{-}10 \ s/A^2$, $I_0 = 72 \ A$, $t_{I,max} = 0.014 \ s$ and $t_{U,max} = 0.0138 \ s$, respectively. It may be instructive to relate the inductor current I_{max} to the magnetic field in the center. From the relation $B_{max} = \frac{\mu_0}{\pi X} \cdot I_{max}$

29
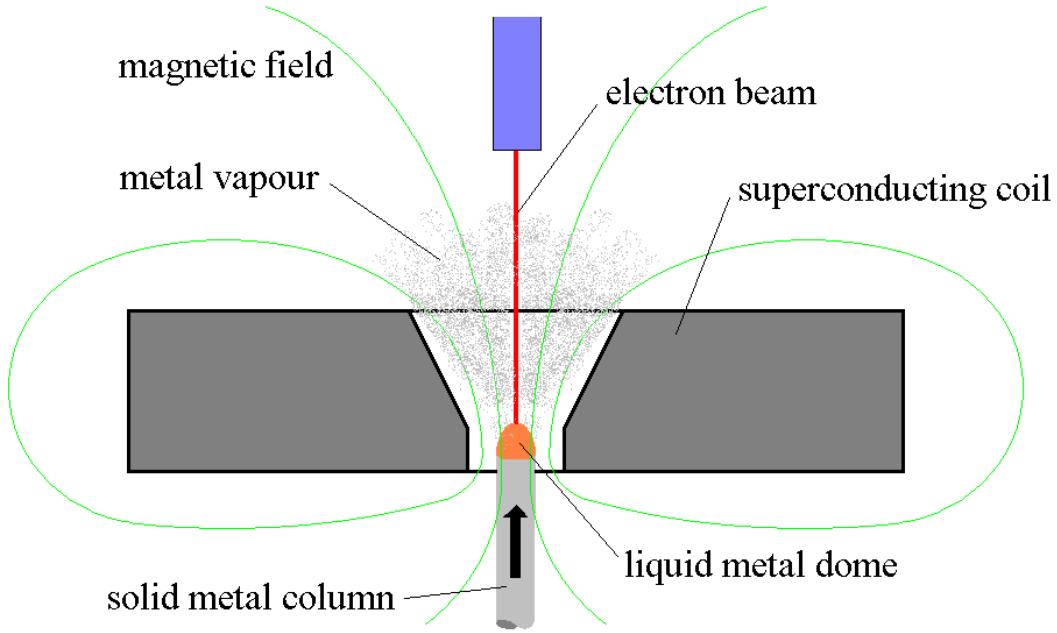
Figure 3.5: Continuous movement of a liquid metal drop along a field gradient. The example shows a possible future way to produce metal vapor. By matching evaporation and feed speed, a liquid metal drop would hold its position while being statically squeezed.

we obtain $B_{max} = 65mT$ and finally

$$t_{max}(B_{max} = 65mT) = 0.0138 \ s \ . \tag{3.21}$$

This value is too small for applications.

However, a transient magnetic field would also be established if the drop moves into an inhomogeneous direct magnetic field. Therefore, at least qualitatively, the results apply also to this case. Fig. 3.5 shows an example for such an application. Much higher field amplitudes are available here with superconducting coils and the maximum squeezing time depends only on $t_{I,max}$. For example, we find that

$$t_{max}(B_{max} = 1T) = 3.31 \ s \ , \tag{3.22}$$

$$t_{max}(B_{max} = 5T) = 82.7 \ s \ . \tag{3.23}$$

These duration times are of much more practical interest.

3.1.5   Summary and conclusion

We have theoretically investigated the static electromagnetic squeezing of a liquid metal drop. We suppose mirror symmetry and a special time-dependence of the magnetic field to achieve a static Lorentz force. The resulting Young-Laplace equation that describes the drop surface

is normalized and solved by a shooting method. We examine the influences of drop volume and Lorentz force strength on the scale of the squeezing. According to our results, this kind of magnetic field seems highly suitable for electromagnetic shaping purposes. The meniscus of large drops that are normally flat on the upside can be pushed to almost three times of its original height. While large drops are lifted especially near the symmetry plane, small drops facilitate a lift of their whole body due to the stronger surface contraction. Regarding practical application, it seems much more promising to move the drop into a strong static field instead of using an inductor.

3.2 Problem 2: Azimuthal deformations at a liquid metal disc

If a thin liquid metal drop is squeezed and locked up between two horizontal planes it forms a liquid metal disc as shown in Fig. 3.6. The free surface is now restricted to the disc perimeter and only two-dimensional flow is possible. This geometry is advantageous for theoretical studies due to its simplicity. Nevertheless, it can easily be established in validation experiments.

In the present section we will discuss the behavior of infinitesimal and periodic deformations of the disc perimeter.
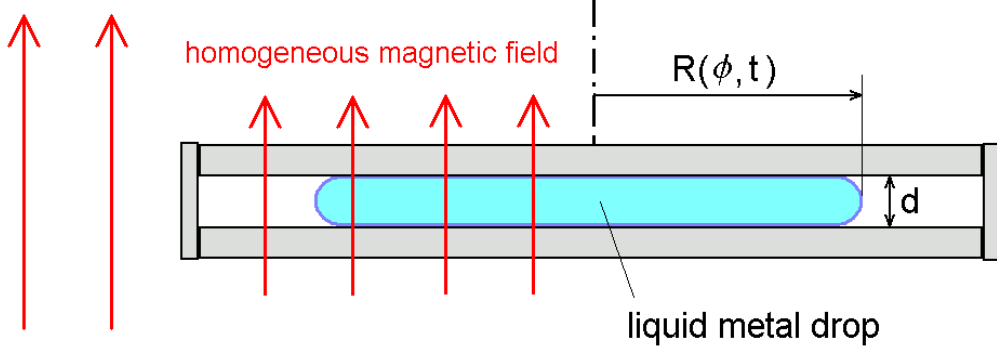
Figure 3.6: Liquid metal disc originating in a squeezed and locked up drop

3.2.1 Governing equations

Following the classical procedure of the Rayleigh-Plateau instability (see for example Drazin[91]) we assume an incompressible fluid with zero viscosity. The azimuthal deformations under consideration are of infinitesimal amplitude. The liquid metal disc is placed in a transient growing or falling homogeneous magnetic field of axial orientation to the disc. The two-dimensional motion in the bulk of the drop is described by the incompressible continuity equation

$$\nabla \cdot \mathbf{u} = 0 \tag{3.24}$$

as well as the magnetohydrodynamic Navier-Stokes equation for an ideal fluid

$$\frac{\partial \mathbf{u}}{\partial t} + (\mathbf{u} \cdot \nabla)\mathbf{u} = -\frac{\nabla p}{\rho} + \frac{\mathbf{f}_L}{\rho} \quad . \tag{3.25}$$

At the free perimeter $\zeta(\phi)$ of the disc the Young-Laplace equation

$$p_0 + \int_0^\zeta \mathbf{f}_L(\mathbf{s}) \cdot d\mathbf{s} = \gamma \nabla \cdot \mathbf{n} = \gamma \cdot \left(\frac{1}{\zeta} - \frac{\partial^2 \zeta}{\zeta^2 \partial \phi^2} \right) \tag{3.26}$$

holds where $\mathbf{s}$ is the path along which the Lorentz force acts and $\mathbf{n}$ is the unity normal vector on the free surface. The last term (in brackets) is an approximation that only accounts for the linear terms of the very small amplitude. In addition to the above equations we have a kinematic boundary condition at the free surface, describing the radial component of the flow velocity as

$$u_r(r = \zeta) = \frac{d\zeta}{dt} \quad . \tag{3.27}$$

Usually, to calculate the magnetic field, the magnetic diffusion equation had to be solved. Here, we will restrict this analysis to the full penetration case, i.e. a Shielding parameter $R_\omega \ll 1$. In this case, we can assume the magnetic field to be always undistorted by the disc shape, homogeneous and in axial direction. We set

$$\mathbf{B}_0 = (B_0 + \Gamma t) \cdot \mathbf{e}_z \tag{3.28}$$

where Γ denotes a constant growth rate of the magnetic field. The eddy currents $\mathbf{J}$ induced in the disc are calculated by

$$\nabla \times \mathbf{J} = -\sigma \cdot \frac{\partial \mathbf{B}_0}{\partial t} \tag{3.29}$$

and produce a magnetic field of their own that we may call $\mathbf{b}_{self}$. It is

$$\nabla \times \mathbf{b}_{self} = \mu \cdot \mathbf{J} \quad . \tag{3.30}$$

Since we demanded full penetration it is $\mathbf{b}_{self} \ll \mathbf{B}_0$, otherwise Eq. 3.29 was not correct. We find the Lorentz force to be

$$\mathbf{f}_L = \mathbf{J} \times (\mathbf{B}_0 + \mathbf{b}_{self}) \quad . \tag{3.31}$$

Although the value of $\mathbf{J} \times \mathbf{B}_0$ is much higher than that of $\mathbf{J} \times \mathbf{b}_{self}$, the small term becomes important for the deformed disc as we will see later on.

3.2.2 Basic state

In the undisturbed basic state the disc is at rest and in circular shape. Flow and meniscus are described by

$$u_0(r, \phi, t) = 0 \qquad , \qquad \zeta_0(\phi, t) = a \tag{3.32}$$

which leads to a purely radial distribution of eddy currents, Lorentz force and pressure inside the disc. From the Navier-Stokes equation, see Eq. 3.25, we find

$$\frac{\partial p}{\partial r} = \mathbf{f}_L(r) \qquad \Rightarrow \qquad p(r) = p_c + \int_0^r \mathbf{f}_L(r) dr \tag{3.33}$$

where p_c is the pressure in the center of the drop. From the Young-Laplace equation, see Eq. 3.26, we obtain

$$p_c = \frac{\gamma}{a} - \int_0^a \mathbf{f}_L(r)dr \quad . \tag{3.34}$$

Substituting Eq. 3.34 into Eq. 3.33 yields the pressure distribution in the basic state

$$p_0(r) = \frac{\gamma}{a} - \int_r^a \mathbf{f}_L(r)dr \quad . \tag{3.35}$$

3.2.3 Perturbed state

What happens when the shape of the disc slightly deviates from circular? Since every deformation can, aided by a Fourier transformation, be decomposed into a sum of azimuthal modes we will focus on single-mode deformations as illustrated in Fig. 3.7 but in contrast to the picture with infinitesimal amplitude.
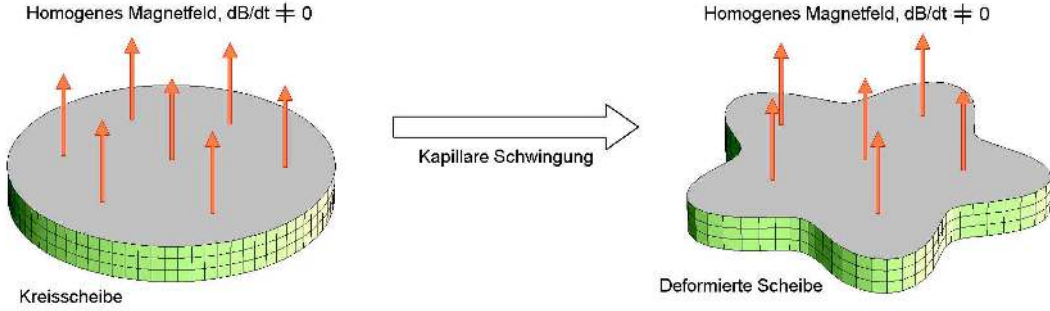
Figure 3.7: Azimuthal deformations of the disc

Lorentz force   First, to assess the effect of Lorentz force on the circular and the deformed disc as well we need to calculate the induced eddy currents $\mathbf{J}$ therein. The procedure is presented in *Appendix A*, an example of the resulting distribution is shown in Fig. 3.8. The main Lorentz force $\mathbf{f}_{main} = \mathbf{J} \times \mathbf{B}_0$ is always orthogonally directed to the eddy current lines and points into or out of the disc depending on whether the magnetic field grows or falls. It is obvious on one hand, that the disc deformation affects the distribution of $\mathbf{f}_{main}$. But its integration between the disc center at $r = 0$ and the free surface at $r = \zeta$ results in an isobar distribution looking exactly like that of the eddy currents, refer to Fig. 3.8, with constant pressure at the free surface. We may therefore conclude on the other hand, that $\mathbf{f}_{main}$ does not promote azimuthal deformations.
Not so the tiny self-excited Lorentz force $\mathbf{f}_{self} = \mathbf{J} \times \mathbf{b}_{self}$. The exact analytical calculation of $\mathbf{b}_{self}$ is rather complicated due to the oblate spheroidal geometry that would apply here. Nevertheless, it is a consequence of the Gauss relation

$$\int_A \mathbf{J}dA = \frac{1}{\mu} \cdot \oint_l \mathbf{b}_{self}dl \tag{3.36}$$
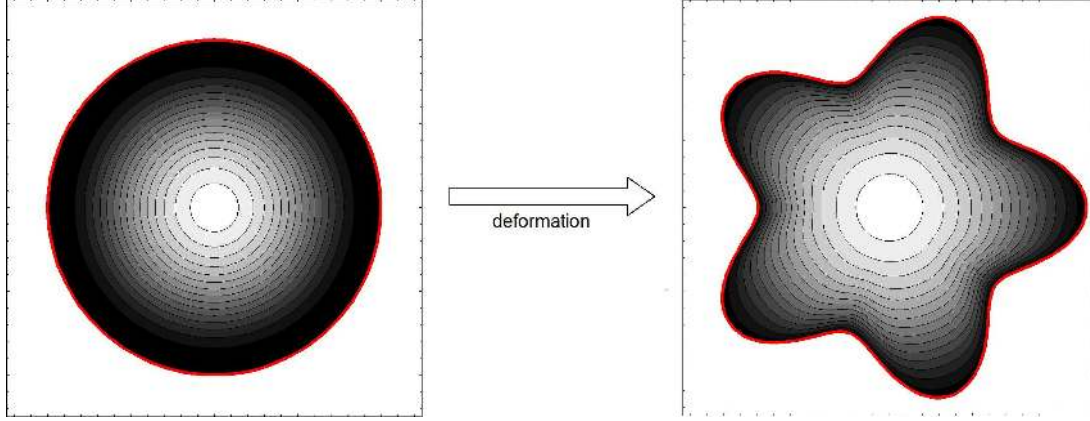
Figure 3.8: Eddy current distribution in the circular and deformed disc.

that $\mathbf{f}_{self}$ will promote any constriction of the cross section for the eddy currents.

Perturbation equations   In general, the perturbed state $\Upsilon = \{\zeta, \mathbf{u}, p, \mathbf{f}_L\}$ can be thought as the basic state Υ_0 plus a deviation $\hat{\Upsilon}$ which leads to

$$
\begin{aligned}
\zeta &= \zeta_0 + \hat{\zeta} \\
\mathbf{u} &= \mathbf{u}_0 + \hat{\mathbf{u}} \\
p &= p_0 + \hat{p} \\
\mathbf{f}_L &= \mathbf{f}_{L0} + \hat{\mathbf{f}_L}
\end{aligned}
\quad \Rightarrow \quad
\begin{aligned}
\zeta &= a + \hat{\zeta} \\
\mathbf{u} &= \hat{\mathbf{u}} \\
p &= \tfrac{\gamma}{a} - \int\limits_r^a \mathbf{f}_L \partial r + \hat{p}
\end{aligned}
\quad . \tag{3.37}
$$

The Navier-Stokes equation, see Eq. 3.25, transforms to

$$
\rho \frac{\partial \hat{\mathbf{u}}}{\partial t} = \hat{\mathbf{f}} - \nabla \hat{p} \quad . \tag{3.38}
$$

Due to the incompressibility of the drop fluid, the Nabla operator applied to this equation results in

$$
\triangle \hat{p} = \nabla \cdot \hat{\mathbf{f}} \tag{3.39}
$$

Inserting the perturbed state into the Young-Laplace equation, see Eq. 3.26, yields

$$
\hat{p}|_\zeta + \int\limits_0^\zeta \hat{\mathbf{f}} dr = -\frac{\gamma}{a^2} \cdot \left(\hat{\zeta} + \frac{\partial^2 \hat{\zeta}}{\partial \phi^2} \right) \tag{3.40}
$$

while the kinematic boundary condition, see Eq. 3.27, becomes

$$
\hat{u}(r = \zeta) = \frac{d\hat{\zeta}}{dt} \quad . \tag{3.41}
$$

35

3.2.4 Intrinsic relation for the disc deformations

We assume the perturbations in the form of normal modes, more precisely as standing wave deformations that can grow or decay exponentially since $s = \sigma + i\omega$.

$$\left\{ \begin{array}{c} \hat{\zeta} \\ \hat{p} \\ \hat{\mathbf{u}} \\ \hat{\mathbf{f}}_{self} \end{array} \right\} = \left\{ \begin{array}{c} \tilde{\zeta} \\ \tilde{p}(r) \\ \tilde{\mathbf{u}}(r) \\ \tilde{f}_{self}(r) \end{array} \right\} \cdot \exp[st + im\phi] \tag{3.42}$$

We start with Eq. 3.39. Written out the terms are

$$\triangle p = \frac{\partial p}{r \partial r} + \frac{\partial^2 p}{\partial r^2} + \frac{\partial^2 p}{r^2 \partial \phi^2} \quad , \qquad \nabla \cdot \hat{\mathbf{f}} = \frac{1}{r}\frac{\partial}{\partial r}(r\hat{f}_r) \tag{3.43}$$

and lead with Eq. B.19 from the *Appendix B* to

$$\tilde{p}'' + \frac{1}{r}\tilde{p}' - \frac{m^2}{r^2}\tilde{p} = -\frac{\mu\sigma^2\Gamma^2}{2} \cdot \frac{\tilde{\zeta}}{a} \cdot (a^2 - 2r^2) \quad . \tag{3.44}$$

Supposing that $\tilde{p}(r)$ does not diverge at $r = 0$, the solution is

$$\tilde{p}(r) = C_1 r^m - \frac{\mu\sigma^2\Gamma^2}{2(4 - m^2)} \cdot \tilde{\zeta}ar^2 + \frac{\mu\sigma^2\Gamma^2}{a(16 - m^2)} \cdot \tilde{\zeta}r^4 \tag{3.45}$$

with C_1 being an unknown constant. The Navier-Stokes equation 3.38 becomes

$$\rho s\tilde{u} = -C_1 mr^{m-1} - \mu\sigma^2\Gamma^2\tilde{\zeta} \cdot \frac{r}{a} \cdot \left(\frac{a^2 - r^2}{4} - \frac{a^2}{4 - m^2} + \frac{4r^2}{16 - m^2} \right) \tag{3.46}$$

and with its help we obtain from the kinematic boundary condition in Eq. 3.41

$$\tilde{u}|_\zeta = -C_1 \frac{ma^{m-1}}{\rho s} + \frac{\mu\sigma^2\Gamma^2}{\rho s}\tilde{\zeta} \cdot \frac{3a^2 m^2}{(4 - m)(16 - m^2)} = s\tilde{\zeta} \quad . \tag{3.47}$$

The last one of the perturbation equation quartet, the Young-Laplace equation 3.40, contains the terms

$$\tilde{p}(r = \zeta) = C_1 a^m - \frac{\mu\sigma^2\Gamma^2}{2}\tilde{\zeta}a^3 \cdot \frac{8 + m^2}{(4 - m^2)(16 - m^2)} \quad , \tag{3.48}$$

$$\int_0^\zeta \hat{f}dr = -\frac{\mu\sigma^2\Gamma^2}{16} \cdot a^3\hat{\zeta} \tag{3.49}$$

and hence becomes

$$C_1 a^m - \frac{\mu\sigma^2\Gamma^2}{16}\tilde{\zeta}a^3 \cdot \left[1 + \frac{8(8 + m^2)}{(4 - m^2)(16 - m^2)} \right] = -\frac{\gamma}{a^2}\tilde{\zeta} \cdot (1 - m^2) \quad . \tag{3.50}$$

Finally, we rearrange Eqs. 3.47 and 3.50 for C_1 and equate the two expressions. In this way,

both C_1 and $\tilde{\zeta}$ cancel out and release the intrinsic relation for the transient behavior s of the disc deformations.

$$s^2 = \frac{\gamma}{\rho a^3} \cdot m(1 - m^2) - \frac{\mu \sigma^2 \Gamma^2 a^2}{16\rho} \cdot \left[m + \frac{8m(8 + m^2) - 3m^2}{(4 - m^2)(16 - m^2)} \right] \quad . \tag{3.51}$$

Hereby, the first term represents purely capillary oscillations of the disc while the second accounts for the influence of the magnetic field. Figure 3.9 shows the mode dependence of the two terms. Looking at the amplitudes of the two terms in Eq. 3.51, we find that

$$s^2 \simeq O(a^{-3}) \cdot m(1 - m^2) - O(a^2) \cdot \left[m + \frac{8m(8 + m^2) - 3m^2}{(4 - m^2)(16 - m^2)} \right] \tag{3.52}$$

which means that the capillary term dominates for small drops whereas big drops are dominated by the magnetic field. Since $s = \sigma + i\omega$ and $s^2 = \sigma^2 + 2i\sigma\omega - \omega^2$, respectively, we may conclude that if s^2 is negative and non complex, Eq. 3.51 describes oscillations.
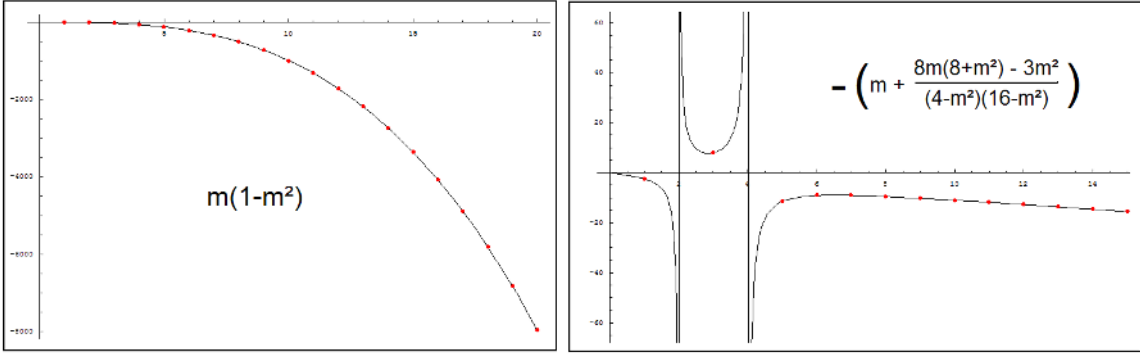
Figure 3.9: Mode dependence of the two terms in the intrinsic relation for the deformed liquid metal disc. Left) Capillary term, right) Lorentz force term

According to Eq. 3.51, at mode number $m = 1$ the surface tension is without effect but the magnetic field allows an oscillation. For the modes $m = 2$ and $m = 4$, respectively, the relation is not defined and allows no statement about the behavior. A possible reason is that there are two counteracting effects that could cancel out here. On one hand, each solenoidal current repels itself which generates an outwardly directed force. But the constriction of the cross section for the current promotes further constriction on the other hand. For all modes $m > 4$ both terms in Eq. 3.51 are negative. Here, the magnetic field just alters the capillary frequency. A special case is mode $m = 3$ because the second term becomes positive here. If the drop is big enough, the magnetic field will overpower the surface tension and drive an $m = 3$ deformation.

Chapter 4

High Frequency Magnetic Fields

If the Shielding parameter of a liquid metal drop in an alternating magnetic field is far beyond unity, i.e. $R_\omega \gg 1$, we speak of high frequency. In this case, magnetic field and Lorentz force are bound to the drop surface. Henceforth, the skin depth approximation may be applied, conf. Eq. 1.12, where the Lorentz force is replaced by a scalar magnetic pressure acting on the drop surface. For centimeter-sized liquid metal drops, the high frequency state starts at several Kilohertz. Since this frequency is far too high to match the capillary eigenfrequencies of the surface, the oscillating part of the magnetic pressure is ejected. As a result, the effect of the magnetic field reduces to a static pressure which allows to shape, to squeeze, to support or even to levitate liquid metal drops. Despite those simplifications it remains difficult to account for the coupling between magnetic field and drop surface shape.

In this chapter we offer two ways to model the coupling. In the first problem we use a weak coupling insofar as we apply a qualitatively similar field where we consider symmetric deformations of the drop. In the second problem we repose the question. Here, we assume an easy geometry and search the magnetic field that best complies with the coupling.

4.1 Problem 1: Symmetric deformation of sessile wetting drops

The content of this chapter is already published in [92].

An analytical model for the electromagnetic shaping of sessile liquid metal drops in high-frequency magnetic fields is presented. We deal with both an infinitely long drop and a circular drop. In each case, the arrangement of drop and inductor is symmetric. Applying the skin depth approximation reduces the Lorentz force induced in the liquid metal drop to a magnetic pressure acting on the drop surface. We neglect the coupling between drop contour and magnetic field distribution. In this case, the magnetic field can be calculated analytically with the mirror image method. Finally, we achieve an analytical solution of the static drop contours with the help of Green's functions. The theory is applied to three problems: (i) squeezing a drop while conserving its volume, (ii) supporting of drops with a fixed contact line and (iii) pumping up of drops. The results demonstrate the suitability of high-frequency magnetic fields for the shaping of liquid metals.

4.1.1 Mathematical model

Fig. 4.1 shows a sketch of the long drop arrangement and Fig. 4.2 the same for the circular drop. While the long drop is described in a cartesian $x - z$ plane, cylindrical coordinates $r - z$ are used for the circular drop. The drop is placed on an electrically conducting substrate at
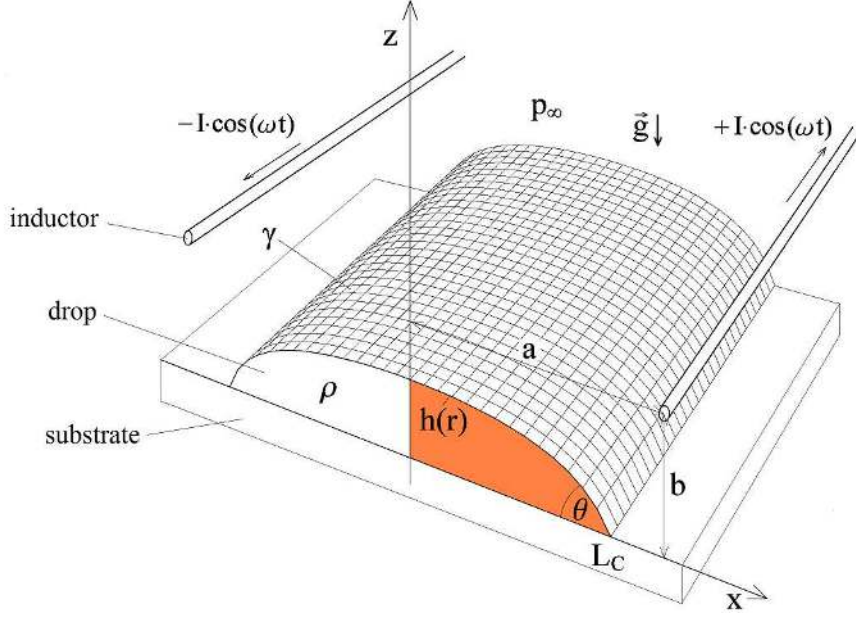
Figure 4.1: Sketch of the long drop arrangement
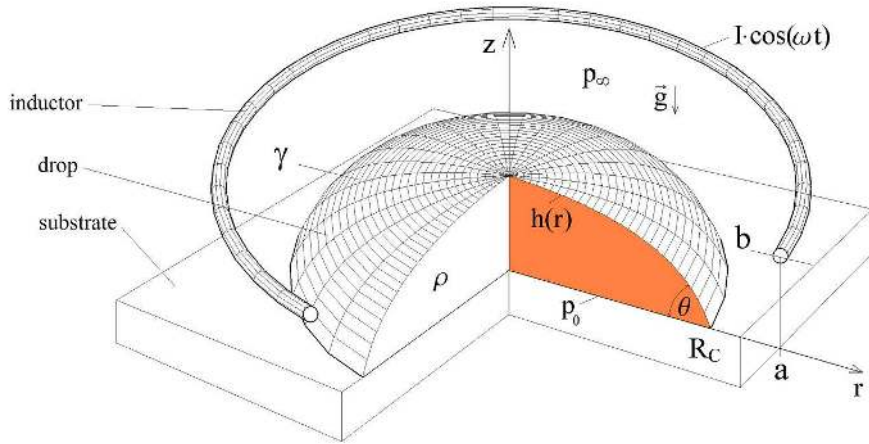
Figure 4.2: Sketch of the circular drop arrangement

$z = 0$. The drop contour is given by $h(x)$ for the long drop and $h(r)$ for the circular drop. The contour intersects the substrate with a contact angle θ. The contact line is located at $x = L_C$ and $r = R_C$, respectively. The constant fluid properties are the density ρ and the surface tension γ. The ambient pressure is p_∞, while the pressure inside the drop on the bottom is p_0. Gravity g acts downward. The magnetic field is generated by an inductor filament symmetrically positioned at height $z = b$ above the plate and at a distance $x = a$ and $r = a$, respectively, to the center of symmetry. The inductor is fed by an alternating electrical current I of frequency ω. We will treat both arrangements simultaneously. Equations related to the long drop will be indicated by an $\mathcal{L}$, while those of the circular drop are indicated by a $\mathcal{C}$. This distinction will be skipped for equations that are valid for both drops.

39

Skin depth approximation Due to the skin effect, the high frequent magnetic field does not penetrate the electrically conducting drop. Instead, the effects are limited to a thin skin layer of thickness δ, conf. Eq. 1.8. Here, the skin depth approximation is equivalent with the limits $\delta/L_C \to 0$ and $\delta/R_C \to 0$, respectively. Within these limits, the Lorentz force can be represented by a time-averaged magnetic pressure

$$p_M = B_s{}^2/(2\mu) \tag{4.1}$$

where B_s is the magnetic field on the drop surface.

Flat drop approximation Furthermore, we restrict the analysis to flat drops. In this case, the slope of the drop contour is assumed to be small, i.e.

$$h' \ll 1 \ . \tag{4.2}$$

This flat drop approximation greatly simplifies the solution of the Young-Laplace equation. To estimate the validity of this approximation we compare the solutions for purely hydrostatic drop contours ($p_M = 0$) of flat drop approximated and exact solution that result from Eqs. 1.13. The approximated solutions show deviations less than 10 percent from the exact solutions up to a contact angle of $\theta = 30°$. In the present analysis we assume that θ is fixed.

Magnetic field modeling We suppose an electrically conducting substrate that extends to infinity. Within the limit of the skin depth approximation, the magnetic field will neither penetrate the substrate nor the drop. If the drop is absent, the magnetic field can be calculated analytically using the mirror image method [93]. We assume that the flat drop merely affects the magnetic field distribution of Figs. 4.1 and 4.2. This assumption is justified in the limit $h(0) \ll b$. By this weak coupling we apply the magnetic field calculated at z = 0 on the drop surface at z = h. In doing so we find an analytical expression for the magnetic pressure, conf. Eq. 4.1.

Young-Laplace equation of the free surface Along the free surface we have a pressure jump due to surface tension and curvature that balances hydrostatic and magnetic pressure. The equilibrium reads as

$$\begin{aligned} p_0 - \rho g h(x) - p_\infty &= \quad \gamma k_1 + p_M \qquad &\mathcal{L} \\ p_0 - \rho g h(r) - p_\infty &= \gamma(k_1 + k_2) + p_M \qquad &\mathcal{C} \end{aligned} \ . \tag{4.3}$$

Hereby, the k_i denote the curvature of the surface. It is

$$\begin{aligned} k_1 &= \quad h''(1+h'^2)^{-\frac{3}{2}} \qquad &\mathcal{L} \\ k_1 + k_2 &= h''(1+h'^2)^{-\frac{3}{2}} + h'\left[r(1+h'^2)^{\frac{1}{2}}\right]^{-1} \qquad &\mathcal{C} \end{aligned} \ . \tag{4.4}$$

The prime denotes derivation with respect to x and to r, respectively. Substituting Eq. 4.4 into Eq. 4.3, we obtain the Young-Laplace equation

$$\begin{aligned} \frac{h''}{(1+h'^2)^{\frac{3}{2}}} - \frac{\rho g}{\gamma}h &= \frac{p_\infty - p_0}{\gamma} + \frac{p_M(x)}{\gamma} \qquad &\mathcal{L} \\ \frac{h''}{(1+h'^2)^{\frac{3}{2}}} + \frac{h'}{r(1+h'^2)^{\frac{1}{2}}} - \frac{\rho g}{\gamma}h &= \frac{p_\infty - p_0}{\gamma} + \frac{p_M(r)}{\gamma} \qquad &\mathcal{C} \end{aligned} \ . \tag{4.5}$$

Even when $p_M = 0$, i.e. in absence of the magnetic field, only Eq. 4.5$\mathcal{L}$ has an analytical solution. That is why we focus on flat drops where $h' \ll 1$. Applying the flat drop approximation, Eq. 4.5 simplifies to

$$
\begin{aligned}
h'' - \frac{\rho g}{\gamma} h &= \frac{p_\infty - p_0}{\gamma} + \frac{p_M(x)}{\gamma} \qquad &\mathcal{L} \\
h'' + \frac{1}{r} h' - \frac{\rho g}{\gamma} h &= \frac{p_\infty - p_0}{\gamma} + \frac{p_M(r)}{\gamma} \qquad &\mathcal{C}
\end{aligned}
\tag{4.6}
$$

which is a linear and ordinary differential equation. We now wish to nondimensionalize Eq. 4.6. To this end we choose the contact position in absence of the magnetic field, L_{C0} and R_{C0}, respectively, as a characteristic length scale and the magnetic field B_0 in the center of the inductor. We define three dimensionless parameters, namely a Bond number Bo, an electromagnetic Bond number Bo_M and a third pressure ratio κ that will cancel out later on:

$$
\begin{aligned}
Bo &= \frac{\rho g L_{C0}{}^2}{\gamma} \qquad &\mathcal{L} \\
Bo &= \frac{\rho g R_{C0}{}^2}{\gamma} \qquad &\mathcal{C}
\end{aligned}
\quad ,
\tag{4.7}
$$

$$
\begin{aligned}
Bo_M &= \frac{B_0{}^2 L_{C0}}{2\mu\gamma} \qquad &\mathcal{L} \\
Bo_M &= \frac{B_0{}^2 R_{C0}}{2\mu\gamma} \qquad &\mathcal{C}
\end{aligned}
\quad ,
\tag{4.8}
$$

$$
\begin{aligned}
\kappa &= \frac{(p_\infty - p_0) L_{C0}}{\gamma} \qquad &\mathcal{L} \\
\kappa &= \frac{(p_\infty - p_0) R_{C0}}{\gamma} \qquad &\mathcal{C}
\end{aligned}
\quad .
\tag{4.9}
$$

Using these parameters, Eq. 4.6 transforms to

$$
\begin{aligned}
h'' - Bo\,h &= \kappa + Bo_M f_1(x) \qquad &\mathcal{L} \\
h'' + \frac{1}{r} h' - Bo\,h &= \kappa + Bo_M f_1(r) \qquad &\mathcal{C}
\end{aligned}
\tag{4.10}
$$

where f_1 accounts for the spatial distribution of the magnetic field. The boundary conditions to this equation are

$$
\begin{aligned}
h(x = 1) = 0 \qquad h'(x = 0) = 0 \qquad h'(x = 1) = -\tan\theta \qquad &\mathcal{L} \\
h(r = 1) = 0 \qquad h'(r = 0) = 0 \qquad h'(r = 1) = -\tan\theta \qquad &\mathcal{C}
\end{aligned}
\quad .
\tag{4.11}
$$

Magnetic pressure on the drop surface   To close the problem given by Eq. 4.10 it is necessary to derive an analytical expression for the distribution of the magnetic pressure. As mentioned before, in the double limit $\delta/L_{C0} \to 0$ and $h(0)/b \ll 1$, the mirror image method can be applied. Figure 4.3 illustrates this method for the Cartesian case. The two inductor filaments at $z = b$ are supplemented by their images at $z = -b$ whose current is of same amplitude ut opposite direction. As we expected due to the shielding, there is only a tangential magnetic field component on the interface leading to a magnetic pressure. The axisymmetric analogy is given by the circular current loop at $z = b$ and their image at $z = -b$, conf. [90]. After some straightforward analysis we obtain for the magnetic field at the interface
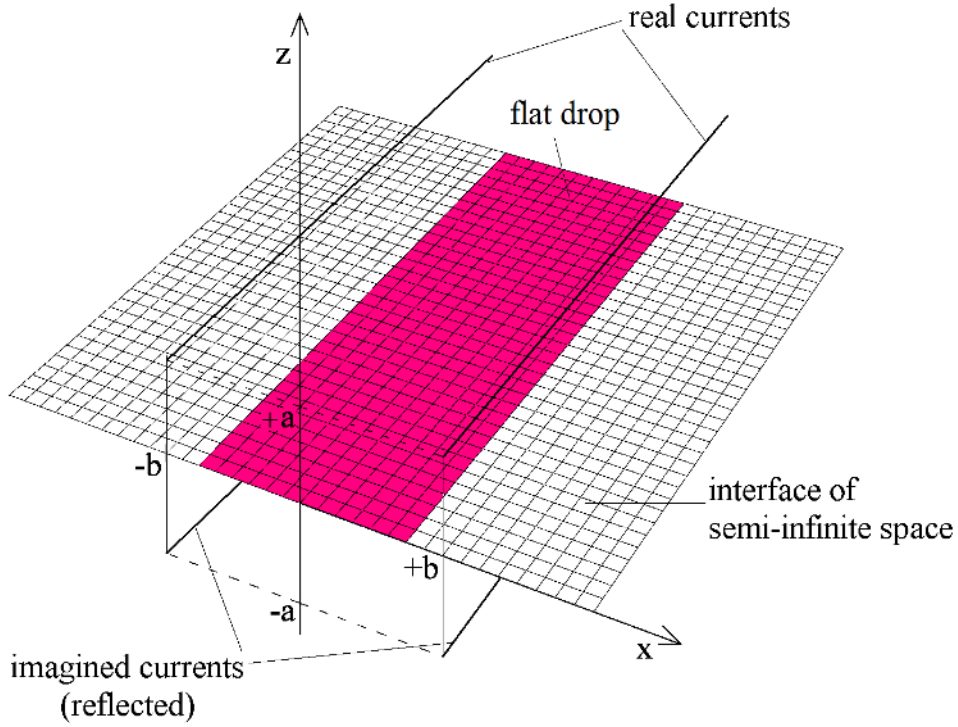
Figure 4.3: Superposition of real and image currents to deduce the magnetic field on the interface

$$B_x(z=0) = 2B_0 \left[\frac{b/a}{(b/a)^2+(x/a+1)^2} - \frac{b/a}{(b/a)^2+(x/a-1)^2} \right] \qquad \mathcal{L}$$

$$B_r(z=0) = B_0 \frac{b\sqrt{a}}{2r\sqrt{r}} k \left[\frac{2+k^2}{2} K(k^2) - \frac{1}{1-k^2} E(k^2) \right] \qquad \mathcal{C}$$

$$(4.12)$$

where in Eq. 4.12C K and E represent the complete elliptic integrals of the first and second kind, respectively. The parameter k is defined as $k^2 = 4ra\left[(r+a)^2+b^2\right]^{-1}$, furthermore is $B_0 = \mu I/(2\pi a L_{C0})$ and $B_0 = \mu I/(2\pi a R_{C0})$, respectively. According to Eqs. 4.1 and 4.10, the distribution of the magnetic pressure on the surface becomes

$$f_1(x) = 4 \left[\frac{b/a}{(b/a)^2+(x/a+1)^2} - \frac{b/a}{(b/a)^2+(x/a-1)^2} \right]^2 \qquad \mathcal{L}$$

$$f_1(r) = \frac{4b^2}{r^2[(r+a)^2+b^2]} \left[\frac{2+k^2}{2} K(k^2) - \frac{1}{1-k^2} E(k^2) \right]^2 \qquad \mathcal{C}$$

$$(4.13)$$

Drop shape in absence of the magnetic field Inserting Eq. 4.13 into 4.10 yields an expression that cannot be solved by direct integration. We will therefore apply Green's function theory. To do so, we first look at the $Bo_M = 0$ case, i.e. absent magnetic field, to find the needed functions. The flat drop approximated and dimensionless Young-Laplace equation without magnetic pressure is

$$h'' - Bo\,h \quad\;\; = \kappa \qquad \mathcal{L}$$
$$h'' + \tfrac{1}{r}h' - Bo\,h = \kappa \qquad \mathcal{C} \tag{4.14}$$

It is convenient to express the solution of Eq. 4.14 as the superposition of the general homogeneous solution h_H and the particular solution h_P, i.e.

$$h(x) = h_H(x) + h_P(x) \qquad \mathcal{L}$$
$$h(r) = h_H(r) + h_P(r) \qquad \mathcal{C} \tag{4.15}$$

We find that

$$h_H(x) = C_1 \cosh\left(\sqrt{Bo}x\right) + C_2 \sinh\left(\sqrt{Bo}x\right) \qquad \mathcal{L}$$
$$h_H(r) = \;\; C_1 I_0\left(\sqrt{Bo}r\right) + C_2 K_0\left(\sqrt{Bo}r\right) \qquad \mathcal{C} \tag{4.16}$$

$$h_P = C_3 = -\frac{\kappa}{Bo} \tag{4.17}$$

Substituting the boundary conditions given by Eq. 4.11 into Eq. 4.15, the constants become

$$C_1 = -\frac{\tan\theta}{\sqrt{Bo}\cdot\sinh\left(\sqrt{Bo}\right)} \qquad C_2 = 0 \qquad C_3 = \frac{\tan\theta}{\sqrt{Bo}\cdot\tanh\left(\sqrt{Bo}\right)} \qquad \mathcal{L}$$

$$C_1 = -\frac{\tan\theta}{\sqrt{Bo}\cdot I_1\left(\sqrt{Bo}\right)} \qquad C_2 = 0 \qquad C_3 = \frac{\tan\theta\cdot I_0\left(\sqrt{Bo}\right)}{\sqrt{Bo}\cdot I_1\left(\sqrt{Bo}\right)} \qquad \mathcal{C} \tag{4.18}$$

Hence for the drop contour in absence of the magnetic field we obtain

$$h(x) = \frac{\tan\theta}{\sqrt{Bo}\cdot\sinh\left(\sqrt{Bo}\right)}\left[\cosh\left(\sqrt{Bo}\right) - \cosh\left(\sqrt{Bo}\cdot x\right)\right] \qquad \mathcal{L}$$

$$h(r) = \;\; \frac{\tan\theta}{\sqrt{Bo}\cdot I_1\left(\sqrt{Bo}\right)}\left[I_0\left(\sqrt{Bo}\right) - I_0\left(\sqrt{Bo}\cdot r\right)\right] \qquad \mathcal{C} \tag{4.19}$$

As obvious from Eqs. 4.9 and 4.18, the parameters κ, Bo and θ are interrelated according to

$$\kappa = \;\; -\frac{\sqrt{Bo}\cdot\tan\theta}{\tanh\left(\sqrt{Bo}\right)} \qquad \mathcal{L}$$

$$\kappa = -\frac{\sqrt{Bo}\cdot\tan\theta\cdot I_0\left(\sqrt{Bo}\right)}{I_1\left(\sqrt{Bo}\right)} \qquad \mathcal{C} \tag{4.20}$$

Green functions of the drop In general, a Green function $G(x,\xi)$ or $G(r,\xi)$ describes the effect of a point disturbance at ξ on a differentially connected system [94]. Outside this singular point the homogeneous solution of the problem holds. Hence, the Green function meets the equation

$$G'' - Bo\cdot G \quad\;\; = \delta(x-\xi) \qquad \mathcal{L}$$
$$G'' + \tfrac{1}{r}\cdot G' - Bo\cdot G = \delta(r-\xi) \qquad \mathcal{C} \tag{4.21}$$

The Green function is monotone over the whole interval $x = [0, L_C]$ and $r = [0, R_C]$, respectively, except for the position ξ of the point disturbance. Because of this singular behavior in ξ, we

divide the function in a left part G_L and a right part G_R, see Fig. 4.4. The functions must satisfy the conditions
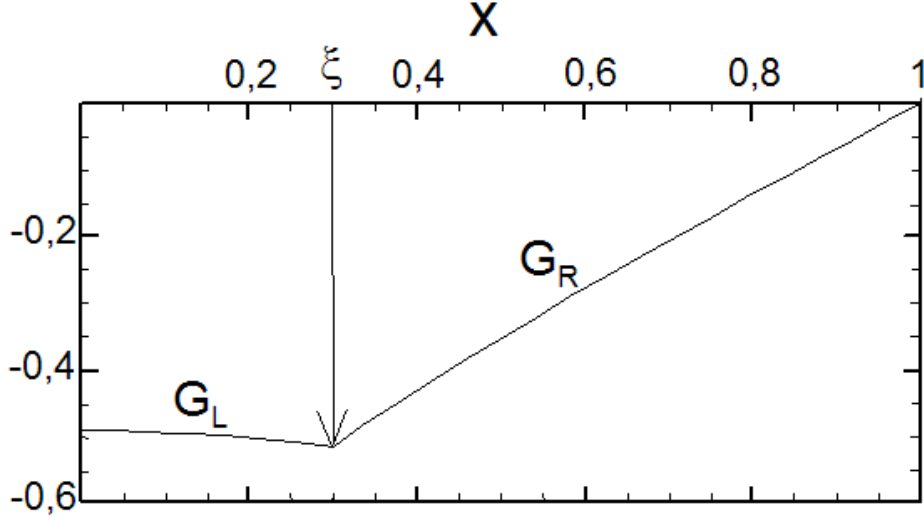

Figure 4.4: The Green function corrsponding to a disturbation in Superposition of real and image currents to deduce the magnetic field on the interface

$$G_L(x = \xi) = G_R(x = \xi) \qquad G_R(x = L_C) = 0 \qquad G_L'(x = \xi) = G_R'(x = \xi) \qquad \mathcal{L}$$
$$. \quad (4.22)$$
$$G_L(r = \xi) = G_R(r = \xi) \qquad G_R(r = R_C) = 0 \qquad G_L'(r = \xi) = G_R'(r = \xi) \qquad \mathcal{C}$$

While the two first boundary conditions are obvious, the last one results from an integration of Eq. 4.21. The problem defined Eqs. 4.21 and 4.22 yields the solutions

$$G_L(x, \xi) = \frac{\cosh\left(\sqrt{Bo} \cdot x\right) \cdot \cosh\left(\sqrt{Bo} \cdot \xi\right)}{\sqrt{Bo}} \left[\tanh\left(\sqrt{Bo} \cdot \xi\right) - \tanh\left(\sqrt{Bo} \cdot L_C\right)\right]$$
$$\mathcal{L} \quad , \quad (4.23)$$
$$G_R(x, \xi) = \frac{\cosh\left(\sqrt{Bo} \cdot \xi\right)}{\sqrt{Bo}} \left[\sinh\left(\sqrt{Bo} \cdot x\right) - \tanh\left(\sqrt{Bo} \cdot L_C\right) \cdot \cosh\left(\sqrt{Bo} \cdot x\right)\right]$$

$$G_L(r, \xi) = \xi I_0\left(\sqrt{Bo} \cdot r\right) \cdot \left[\frac{K_0\left(\sqrt{Bo} \cdot R_C\right)}{I_0\left(\sqrt{Bo} \cdot R_C\right)} \cdot I_0\left(\sqrt{Bo} \cdot \xi\right) - K_0\left(\sqrt{Bo} \cdot \xi\right)\right]$$
$$\mathcal{C} \quad . \quad (4.24)$$
$$G_R(r, \xi) = \xi I_0\left(\sqrt{Bo} \cdot \xi\right) \cdot \left[\frac{K_0\left(\sqrt{Bo} \cdot R_C\right)}{I_0\left(\sqrt{Bo} \cdot R_C\right)} \cdot I_0\left(\sqrt{Bo} \cdot r\right) - K_0\left(\sqrt{Bo} \cdot r\right)\right]$$

Drop shape in the presence of a magnetic field   Using the Green functions defined above, the drop contour can be represented as an integral sum of point disturbances,

$$h(x) = \int\limits_0^x G_R(x,\xi) \cdot [\kappa + Bo_M \cdot f_M(\xi)] \, d\xi + \int\limits_x^{L_C} G_L(x,\xi) \cdot [\kappa + Bo_M \cdot f_M(\xi)] \, d\xi \qquad \mathcal{L}$$

$$h(r) = \int\limits_0^r G_R(r,\xi) \cdot [\kappa + Bo_M \cdot f_M(\xi)] \, d\xi + \int\limits_r^{R_C} G_L(r,\xi) \cdot [\kappa + Bo_M \cdot f_M(\xi)] \, d\xi \qquad \mathcal{C}$$

(4.25)

As we shall see next, it is also necessary to determine the slope of the drop contour. It is given by the relation

$$h'(x) = \int\limits_0^x G'_R(x,\xi) \cdot [\kappa + Bo_M \cdot f_M(\xi)] \, d\xi + \int\limits_x^{L_C} G'_L(x,\xi) \cdot [\kappa + Bo_M \cdot f_M(\xi)] \, d\xi \qquad \mathcal{L}$$

(4.26)

$$h'(r) = \int\limits_0^r G'_R(r,\xi) \cdot [\kappa + Bo_M \cdot f_M(\xi)] \, d\xi + \int\limits_r^{R_C} G'_L(r,\xi) \cdot [\kappa + Bo_M \cdot f_M(\xi)] \, d\xi \qquad \mathcal{C}$$

where

$$G'_L(x,\xi) = \sinh\left(\sqrt{Bo} \cdot x\right) \cdot \cosh\left(\sqrt{Bo} \cdot \xi\right) \cdot \left[\tanh\left(\sqrt{Bo} \cdot \xi\right) - \tanh\left(\sqrt{Bo} \cdot L_C\right)\right]$$

$$G'_R(x,\xi) = \cosh\left(\sqrt{Bo} \cdot \xi\right) \cdot \left[\cosh\left(\sqrt{Bo} \cdot x\right) - \tanh\left(\sqrt{Bo} \cdot L_C\right) \cdot \sinh\left(\sqrt{Bo} \cdot x\right)\right]$$

$$\mathcal{L}$$

(4.27)

and

$$G'_L(r,\xi) = \xi\sqrt{Bo} \cdot I_1\left(\sqrt{Bo} \cdot r\right) \cdot \left[\frac{K_0\left(\sqrt{Bo} \cdot R_C\right)}{I_0\left(\sqrt{Bo} \cdot R_C\right)} \cdot I_0\left(\sqrt{Bo} \cdot \xi\right) - K_0\left(\sqrt{Bo} \cdot \xi\right)\right]$$

$$G'_R(r,\xi) = \xi\sqrt{Bo} \cdot I_0\left(\sqrt{Bo} \cdot \xi\right) \cdot \left[\frac{K_0\left(\sqrt{Bo} \cdot R_C\right)}{I_0\left(\sqrt{Bo} \cdot R_C\right)} \cdot I_1\left(\sqrt{Bo} \cdot r\right) - K_1\left(\sqrt{Bo} \cdot r\right)\right]$$

$$\mathcal{C}$$

(4.28)

In the present case the inhomogeneity at the right-hand side of Eq. 4.10 consists of two parts. The first part κ is constant (cf. Eq. 4.9). As discussed before, for a constant Bond number Bo, the parameter κ determines the contact angle θ which is fixed in the present analysis. However, the second part, $Bo_M \cdot f_M(x)$ and $Bo_M \cdot f_M(r)$, respectively, which is related to the magnetic pressure, alters the contact angle. The value of this alteration is given by

$$\tanh\theta_M(x = L_C) = \int\limits_0^{L_C} G'_R(x = L_C, \xi) \cdot Bo_M \cdot f_M(\xi) d\xi \qquad \mathcal{L}$$

(4.29)

$$\tanh\theta_M(r = R_C) = \int\limits_0^{R_C} G'_R(r = R_C, \xi) \cdot Bo_M \cdot f_M(\xi) d\xi \qquad \mathcal{C}$$

Therefore, to reinstate the fixed contact angle we have to correct our analysis by exactly this value. Finally, we calculate the drop contour by evaluating the relation

$$
\begin{aligned}
h(x) \;=\;\; & \int\limits_{0}^{x} G_R(x,\xi)\cdot\left[\frac{\sqrt{Bo}}{\tanh(\sqrt{Bo})}\cdot(\tan\theta_M-\tan\theta)+Bo_M\cdot f_M(\xi)\right]d\xi \\
+\;\; & \int\limits_{x}^{L_C} G_L(x,\xi)\cdot\left[\frac{\sqrt{Bo}}{\tanh(\sqrt{Bo})}\cdot(\tan\theta_M-\tan\theta)+Bo_M\cdot f_M(\xi)\right]d\xi \;\;,\qquad \mathcal{L}
\end{aligned}
\tag{4.30}
$$

$$
\begin{aligned}
h(r) \;=\;\; & \int\limits_{0}^{r} G_R(r,\xi)\cdot\left[\frac{\sqrt{Bo}\cdot I_0(\sqrt{Bo})}{I_1(\sqrt{Bo})}\cdot(\tan\theta_M-\tan\theta)+Bo_M\cdot f_M(\xi)\right]d\xi \\
+\;\; & \int\limits_{r}^{R_C} G_L(r,\xi)\cdot\left[\frac{\sqrt{Bo}\cdot I_0(\sqrt{Bo})}{I_1(\sqrt{Bo})}\cdot(\tan\theta_M-\tan\theta)+Bo_M\cdot f_M(\xi)\right]d\xi \;\;.\qquad \mathcal{C}
\end{aligned}
\tag{4.31}
$$

The drop volume can be calculated using the relation

$$
\begin{aligned}
V \;=\;\; & \int\limits_{0}^{L_C} h(x)dx \qquad\qquad \mathcal{L} \\
\\
V \;=\;\; & 2\pi\cdot\int\limits_{0}^{R_C} r\cdot h(r)dr \qquad \mathcal{C}
\end{aligned}
\tag{4.32}
$$

Summarizing our theoretical model, we use the flat drop approximation to simplify the governing Young-Laplace equation. The skin depth approximation enables us to include the magnetic pressure into this equation. The effect of the magnetic field is represented by an integral sum of point disturbances. The drop contours are then obtained analytically by applying the Green's function theory. A correction is made to restore the fixed contact angle. The integration of these corrected contours determines the drop volume.

4.1.2 Squeezing, supporting and pumping up of drops

When solving Eqs. 4.30 and 4.31, there are three main questions we want to address. First, assuming conserved volume, how will the drop be squeezed when submitted to a magnetic field? Second, which amount of fluid can be supported within the inductor dimensions at different magnetic field intensities? And third, how is the drop shaped when pumped up in a given magnetic field? In the following we show results of drop contours for a fixed contact angle of $\theta=30°$. The inductor is located at $b=1$ for the squeezing and supporting case but at $b=0.5$ for the pumping up case. Nevertheless, the results are discussed for varying Bond number, magnetic Bond number and vertical inductor positions as well.

Squeezing In this section we consider the case when a drop of fixed volume is squeezed in a high-frequency magnetic field. This case is important in applications concerning the electromagnetic shaping of a liquid metal dome. During the squeezing process, we increase the magnetic Bond number Bo_M while inductor position a,b and Bond number Bo remain unchanged. The drop volume is calculated in the case $Bo_M=0$ when the magnetic field is absent and the contact is at $L_{C0}=1$ and $R_{C0}=1$, respectively. For $Bo_M\neq 0$ we first use Eq. 4.32 to determine the changed contact positions L_C and R_C at the given volume. Inserting these new contact positions into Eqs. 4.30 and 4.31 leads to the desired drop contours. The left picture in Fig. 4.5 shows the resulting shapes of a long drop when magnetically squeezed from $Bo_M=0$ to $Bo_M=10$ in equidistant steps. The induced magnetic pressure is highest at the contact line and decreases to zero at the center. Therefore, when the magnetic field is intensified, the growing pressure near
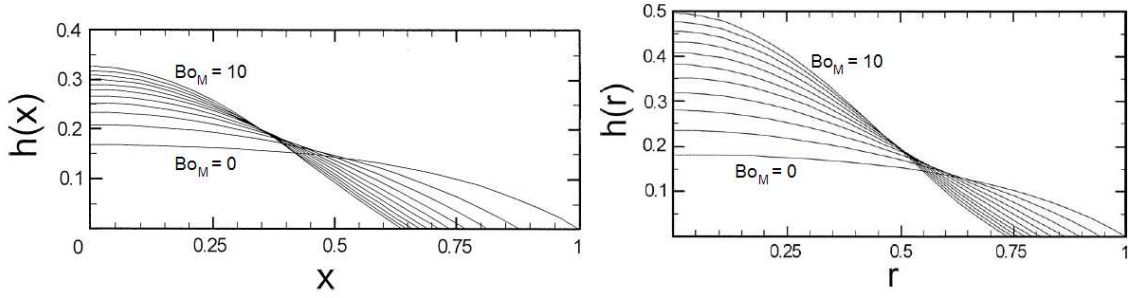
Figure 4.5: Squeezing of a liquid metal drop in a high frequency magnetic field. $Bo = 10$, $b = 1$. Left) long drop, right) circular drop

the contact line is balanced by an elevation of the drop in the center. Because of the volume conservation, the position of the contact line moves toward the center. The drop is squeezed. For instance, when $Bo_M = 10$, the original contact length is diminished by about one third while the drop height in the center is doubled. However, due to the squeezing, the inductor loses its effectiveness as its distance to the contact line increases. In Fig. 4.5 this can be seen by the slowing down of the squeezing at higher values of Bo_M.

Considering the squeezing of a circular drop, see the right picture of Fig. 4.5, we observe a definite difference. Here, at $Bo_M = 10$, the drop mounts up to almost three times the original height. This contrast arises from the geometrical differences. In the circular geometry we have a concentric distribution of the magnetic isolines. Hence, the pressure on the drop border has more surface to act on and causes a higher elevation of the fluid in the center.

According to Eq. 4.7, at constant material properties, a decrease of the Bond number corresponds to a decrease of the drop volume. It therefore equals the pumping up problem. For smaller Bond numbers the drop shape resembles more a circle section. This can be explained by the fact that for smaller drops the surface tension is dominant. However, the relative squeezing effect of the magnetic field on the drop is nearly independent of the Bond number. For a given value of the magnetic Bond number Bo_M, the position of contact does not change upon decreasing Bo. We conclude that this result is due to the assumption of a fixed contact angle favouring geometrically similar shapes.

Supporting We discuss next the case of drops with a fixed contact position at $L_C = 1$ and $R_C = 1$, respectively. In application, the contact position may be pinned by the solid material below. Consequently, to meet this condition, for a different value of the parameter Bo_M each contour confines a different volume that can be supported by the magnetic field. In this case we can calculate the contours directly using Eqs. 4.30 and 4.31. Results are shown in Fig. 4.6 for the long and the circular drop as well. Upon increasing Bo_M we see a clear increase of the drop volume that can be supported by the magnetic field. For instance, at a magnetic Bond number $Bo_M = 10$, the supported drop volume increases by a factor two or more compared to the case when the magnetic field is absent, i.e. $Bo_M = 0$. Obviously, a special property of the resulting deformation is that in the case of a fixed contact position an increase of Bo_M results in a corresponding increase of the drop height in the center. This is due to the fact that the induced effective magnetic pressure is not weakened by a movement of the contact line. Thus, the magnetic pressure can balance completely the hydrostatic pressure rise.
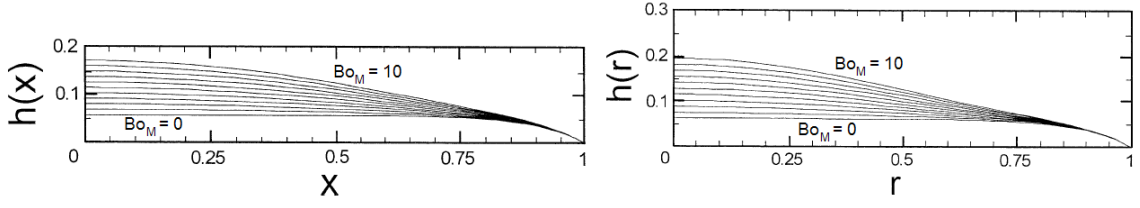
Figure 4.6: Supporting of a liquid metal drop in a high frequency magnetic field. $Bo = 100$, $b = 1$. Left) long drop, right) circular drop
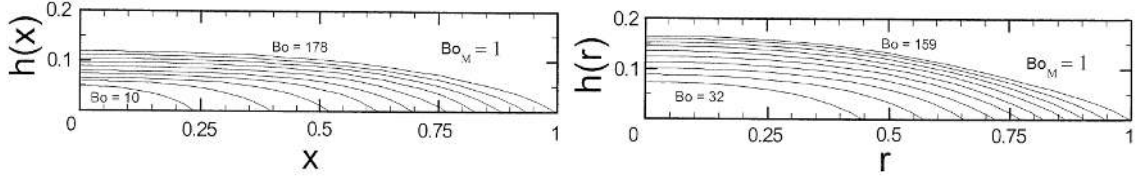

Figure 4.7: Pumping up of a liquid metal drop in a high frequency magnetic field. $Bo_M = 1$, $b = 0.5$. Left) long drop, right) circular drop

Pumping up   Finally, we calculate the static shape of drops of different Bond numbers in a given magnetic field, i.e. $Bo_M = 1$ being constant, while the contact position is free to move. According to Eq. 4.7, at constant material properties, an increase of the Bond number corresponds to an increase of the drop volume. Thus, the present case corresponds to a pumping up. Using Eq. 4.32 we first calculate the volume V_1 of a drop with contact position at $L_{C1} = 1$ and $R_{C1} = 1$ for a given Bond number Bo_1 and $Bo_M = 1$. We divide this volume in ten portions and determine the corresponding contact positions. Inserting these contact positions into Eqs. 4.30 and 4.31, respectively, leads to the contours shown in Fig. 4.7. Mathematically, this calculation method corresponds to a rescaling of the coordinates according to $x, h(x) \propto L_{C1}$ and $r, h(r) \propto R_{C1}$, respectively. Fig. 4.7 shows the result when the inductor is arranged at $b = 0.5$. We find that for small Bond numbers the drop shape resembles more a circle section. This can be explained by the fact that smaller drops are more dominated by surface tension. As the drop volume and thus the Bond number increases the drop spreads towards the inductor. Hence, the support by the magnetic field increases. By that the drop height in the center likewise increases.

4.2 Problem 2: Longitudinal levitation of a liquid cylinder

Electromagnetic levitation of liquid metal is not only a fascinating metallurgical tool but still a challenge. One promising approach to lift volumes clearly beyond a cubic centimeter is a torus-shaped liquid metal drop lifted by two circular current loops acting as inductor. This was already suggested 1982 by Sneyd and Moffatt [67]. As the drop radius is much smaller compared to the torus radius we can treat it as a cylinder.

In this section we reverse the question: Instead of calculating the drop shape in a given magnetic field we are interested in the appropriate magnetic field to support a given drop shape, in this case a cylinder.

4.2.1 Mathematical model

Calculation of the magnetic field with mirror images We apply the skin depth approximation $R_\omega \gg 1$ which means that the cylinder completely shields the magnetic field. There exists no normal field component at the surface which makes it coincide with a field line. Moreover, the vector potential A on the surface is constant. Hence, to calculate the magnetic field between inductor filament and cylinder we can make use of the mirror image method as illustrated in Fig. 4.8 together with a sketch of the arrangement.
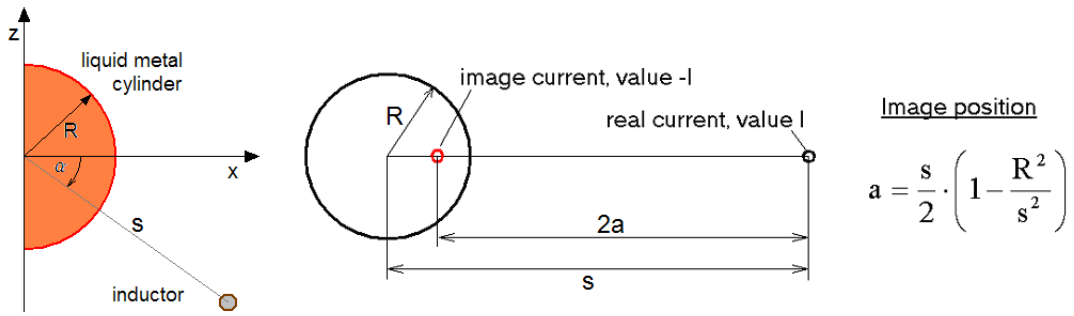

Figure 4.8: Sketch of the arrangement and correct position of the image current to make the cylinder surface a field line.

Altogether, the magnetic fields of four filaments have to be superimposed to obtain the magnetic field of the whole arrangement. This superposition can be done for the vector components of the magnetic field $\mathbf{B}$ or for the vector potentials of all filaments. The vector potential field A of one filament is generally given by

$$A(r, r_0) = \frac{\mu I}{4\pi} \ln \frac{r}{r_0} \tag{4.33}$$

where r is the distance from the filament and $A(r = r_0) = 0$. If the center of the cylinder marks the origin of our cartesian coordinate system and the inductor is located at $x = \pm x_0$, $z = -z_0$ then the image currents are located at $x_1 = \pm R^2/s^2 \cdot x_0$, $z_1 = -R^2/s^2 \cdot z_0$ with $s^2 = x_0{}^2 + z_0{}^2$. Principally, the inductor currents of the two filaments can be of same or opposite direction. Therefore, for the complete expression of the vector potential we find

$$A(x,z) = \frac{\mu I}{4\pi} \left[\ln \sqrt{\frac{(x-x_0)^2 + (z+z_0)^2}{(x-x_1)^2 + (z+z_1)^2}} \pm \ln \sqrt{\frac{(x+x_0)^2 + (z+z_0)^2}{(x+x_1)^2 + (z+z_1)^2}} \right] \qquad (4.34)$$

which represents the two possible magnetic fields plotted in Fig. 4.9.
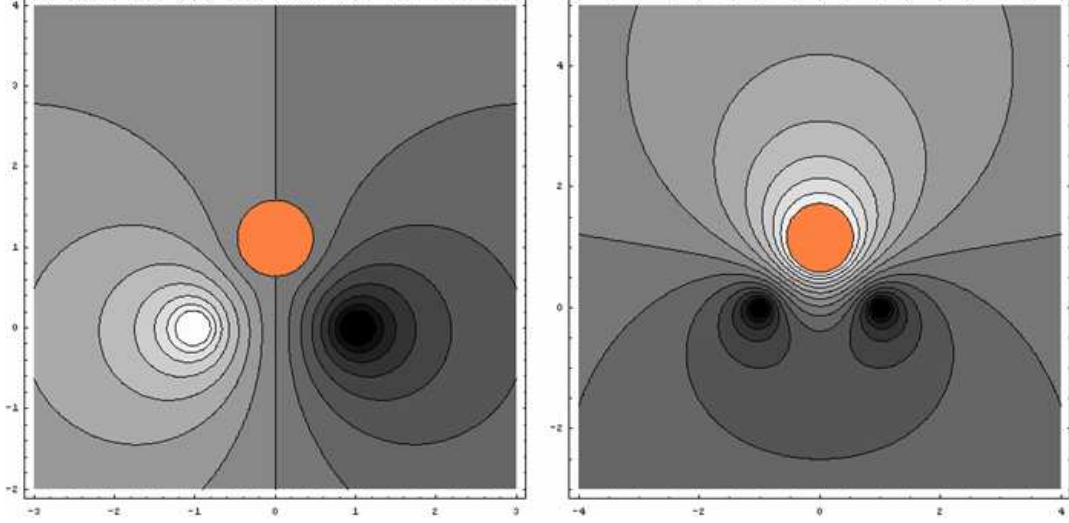

Figure 4.9: The two possible magnetic fields in a longitudinal inductor arrangement. Left: Opposite inductor currents cause a separation point and thus a magnetic hole at the bottom. Right: Inductor currents of same direction generate a closed magnetic vessel.

For our purpose, especially the field on the right-hand side is of importance because the closed field line along the surface exerts a magnetic pressure

$$p_{mag} = \frac{B_s{}^2}{2\mu} \qquad (4.35)$$

on it without zero points, i.e. without a magnetic hole. As Eq. 4.35 suggest, we need the components of the magnetic field $\mathbf{B}_s$ on the cylinder surface. One filament generates a magnetic field

$$B = \frac{\mu I}{2\pi r} \quad . \qquad (4.36)$$

For each filament, we have to split the value of the $\mathbf{B}_s$ vector found by Eq. 4.36 into its components aided by angular functions. Afterwards, the B_x-components of all four filaments are superimposed to find the complete expression for $B_x(x,z)$ and analogously $B_z(x,z)$ is found. We obtain

$$
\begin{aligned}
B_x &= \frac{\mu I}{2\pi} \cdot \left[\frac{x-x_0)}{(x-x_0)^2+(z+z_0)^2} - \frac{x-x_1)}{(x-x_1)^2+(z+z_1)^2} + \frac{x+x_0)}{(x+x_0)^2+(z+z_0)^2} - \frac{x+x_1)}{(x+x_1)^2+(z+z_1)^2} \right] \ , \\
B_z &= \frac{\mu I}{2\pi} \cdot \left[-\frac{z+z_0)}{(x-x_0)^2+(z+z_0)^2} + \frac{z+z_1)}{(x-x_1)^2+(z+z_1)^2} - \frac{z+z_0)}{(x+x_0)^2+(z+z_0)^2} + \frac{z+z_1)}{(x+x_1)^2+(z+z_z)^2} \right] \ .
\end{aligned}
\qquad (4.37)
$$

We are now able to determine the magnetic pressure on the cylinder surface Γ in dependence from the height, $p_{mag}(z)$. To this end, we replace the x in Eq. 4.37 by $x = \sqrt{R^2 - z^2}$ which is the $x - z$-relation for the cylinder surface and evaluate

$$p_{mag\Gamma}(z) = \frac{1}{2\mu} \cdot (B_{x\Gamma}{}^2 + B_{z\Gamma}{}^2) \quad . \tag{4.38}$$

Necessary condition for the levitation of a liquid cylinder The pressure equilibrium on the cylinder surface Γ that has to be established for a successful levitation is shown in Fig. 4.10. Three compartments are involved here: i) the surface tension that contracts the surface with an inward pointing pressure that is constant due to the constant curvature, ii) the hydrostatic pressure due to gravity that linearly increases with the fluid height and iii) the magnetic pressure which could, in theory, balance the hydrostatic pressure and thus prevent a deformation.

$$p_\gamma = \gamma \cdot K \qquad p_{hs} = \rho \cdot g \cdot (2R - z) \qquad p_{mag} = B^2(z)/(2\mu)$$

constant surface pressure + hydrostatic pressure + magnetic pressure = (another) constant surface pressure
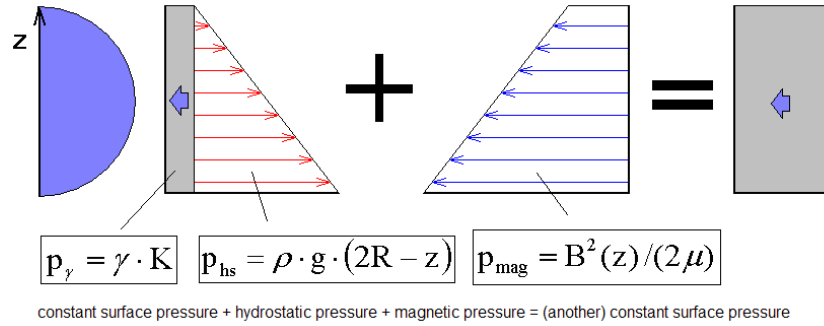
Figure 4.10: Necessary equilibrium between hydrostatic and magnetic pressure on the surface of a levitated liquid metal cylinder.

The consequent condition for a successful compensation of the hydrostatic pressure is

$$\frac{\partial p_{mag\Gamma}}{\partial z} = \rho g \quad , \tag{4.39}$$

or adequately and more fundamental

$$\frac{\partial}{\partial z}(B_{\Gamma x}{}^2 + B_{\Gamma z}{}^2) = constant \quad . \tag{4.40}$$

4.2.2 Optimal inductor

Magnetic pressure distribution depending on the inductor parameters Next, we will evaluate the magnetic pressure on the cylinder surface in dependence of inductor distance s and inclination α using Eq. 4.38. A result is presented in Fig. 4.11 for a fixed inductor distance, i.e. $s = 3$. It can be seen that the magnetic pressure varies almost linearly in height for an inclination $\alpha \approx 40..50°$.

To judge the linearity of $p_{mag\Gamma}(z)$ we relate it to a linear course $L(z)$ constructed with the values at top and bottom
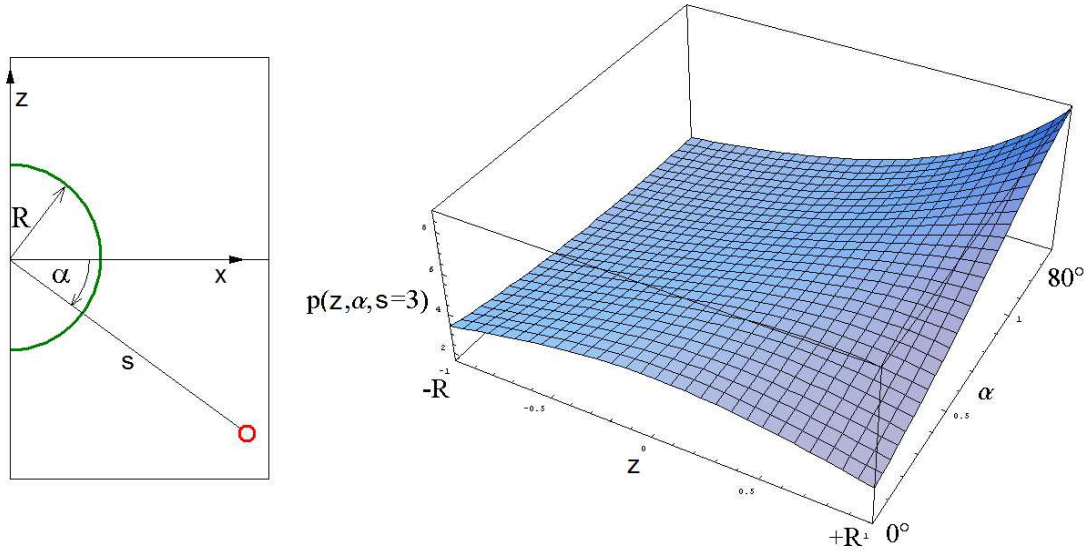
Figure 4.11: Exemplary 3d-Plot of the magnetic pressure along the cylinder surface in dependence of the vertical coordinate. The inductor distance is kept at $s = 3$.

$$L(z) = p_{M\Gamma}(z = -R) + \frac{p_{M\Gamma}(z = +R) - p_{M\Gamma}(z = -R)}{2R} \cdot (z + R) \quad . \tag{4.41}$$

With its help we define an absolute effective deviation from the linear course

$$\tilde{D}(\alpha, s) = \sqrt{\int_{-R}^{+R} [p_{M\Gamma}(z) - L(z)]^2 dz} \quad . \tag{4.42}$$

This parameter is supplemented by the total magnetic force exerted on the cylinder surface

$$\tilde{F} = \int_{-R}^{+R} p_{M\Gamma} dz \tag{4.43}$$

that allows to point out the relative deviation from the linear course

$$D(\alpha, s) = \frac{\tilde{D}}{\tilde{F}} \quad . \tag{4.44}$$

The corresponding result shows Fig. 4.12. It reveals that the magnetic pressure goes more linear on the cylinder surface as the inductor distance increases. Moreover, it seems that an inclination $\alpha = \pi/4$ guarantees the most linear course. It was indeed found that for $\alpha = \pi/4$ and $s \to \infty$ the magnetic pressure variation becomes completely linear.

It is reserved to future analysis to deepen the understanding about the feasibility of this levitation approach.
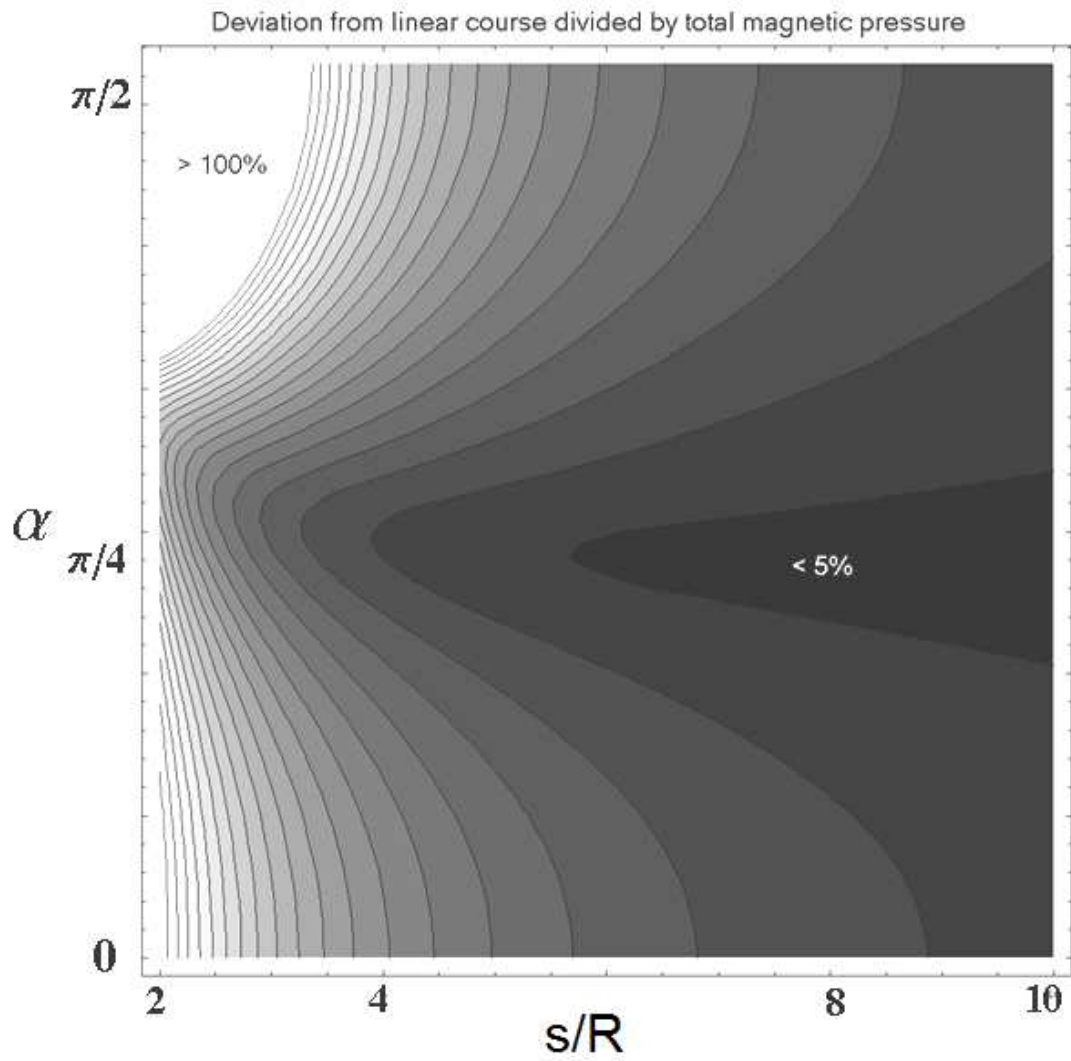
Figure 4.12: Percentage deviation $D(\alpha, s)$ for a wide range of inductor properties.

53

Chapter 5

Middle frequency magnetic fields

5.1 Behavior of a liquid metal disc

In this chapter we present experimental results for the two-dimensional deformation of a liquid metal drop submitted to a middle frequency magnetic field. These results were gained in the frame of the Studienarbeit of Francesco Ivaldi [95] that was supervised by the author. The basic idea behind the experiment is illustrated by Fig. 5.1.
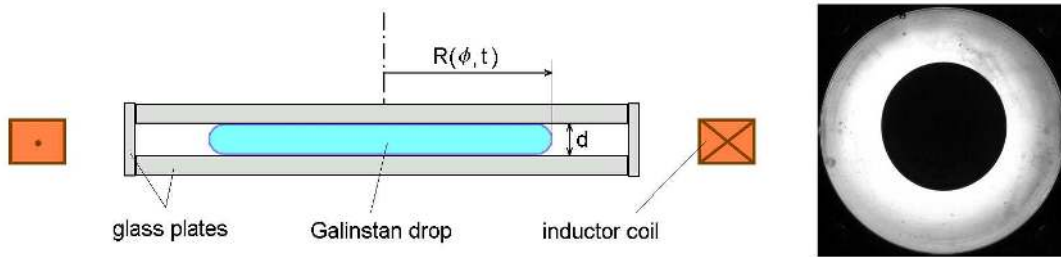

Figure 5.1: Left) Drop suspended between two horizontal glass planes with the inductor coil around, Right) Camera view from above on the liquid metal drop in absence of deformation

5.1.1 Experimental setup

In our experiment we use a liquid metal drop at room temperature. The metal is Galinstan, an alloy of gallium, indium and thin. To prevent corrosion it is covered with a 6 percent hydrochloric acid. The drop is locked up between two plane horizontal glass plates which allow observation by a camera system from above. Moreover, the plates exclude gravitational effects and restrict the liquid metal motion to 2D. The maximum drop diameter is about $65mm$, the height is fixed at $3mm$. Hence, it can be regarded as a liquid metal disk. A water cooled inductor coil with ten windings surrounds the drop at equal height. The inductor is fed by an electric current which can be varied up to 300 *Ampere* and a frequency in the range 5..50 kHz. Due to the induction losses the drop will rapidly heat up. To remove the joule heat the lower glass plate is water-cooled and in the core of the drop container a copper cylinder of $10mm$ diameter acts as heat bridge to the cold water reservoir. To observe the drop, a high-speed camera is installed above while from below the apparatus the drop is elucidated by halogen lights. Due to the heat production, the measurements in magnetic field were restricted to about three seconds for worst

case conditions, i.e. maximum drop diameter, maximum frequency and maximum current. Less extreme conditions often allowed thermal steadiness. In any case, inductor current and frequency were adjusted beforehand and then instantly jumped from zero to its final value. As a result, the drop experienced a switch-on-shock. Before every new "shot", the current was switched off again.

5.1.2 Experimental results

Overview experiments   In a first approach, the parameters inductor current, frequency and drop volume were varied in a wide range. The measurements were less accurate and mainly served to explore the phenomenons to expect. As one can see in the Figures 5.2, 5.3 and 5.4, the observed deformations of the liquid metal disk cover very interesting shapes. All those shapes did not move once they were in place. No oscillations were observed disregarded a slight trembling of the surface that could indicate internal flow or capillary oscillations as well. That the deformation patterns are frozen is in contrast to the experiments of Kocourek et al. [78] that were carried out with the same inductor and in agreement with the experiments of Perrier et al. [80]. The core cylinder obviously causes a center effect. Below a critical current the disk remains circular as is shown on the right-hand side of Fig. 5.1. Beyond the critical current a single nose ejects in a random direction and retains this shape without further movement. It seems that this is a new equilibrium shape. As the current increases further the number of noses becomes two, three and four, see the other picture of Fig. 5.2. Also in these cases, the direction of the noses is randomly. Therefore, three noses can for example form a Latin E or even more strange shapes as is illustrated by Fig. 5.3. Even separation of smaller drops was observed during these overview experiments, see Figure 5.4.
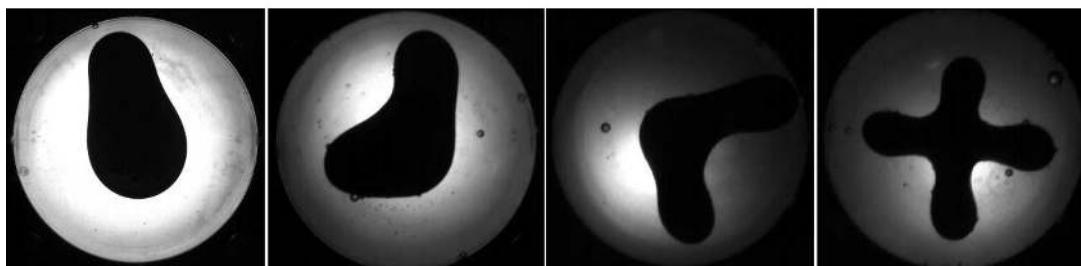

Figure 5.2: Simple deformations observed in the experiments

Getting into detail   After getting a first impression of the involved effects and disc deformations, the disc volume was fixed. Then the inductor current and frequency were successively modified to track the parameter spaces in which the different deformations occurred. Thus, a stability diagram for all states of the liquid metal disk was obtained which is shown in Fig 5.5. In order to cover the whole parameter range, the stability curves in the diagram could not be recorded at maximum precision.

An exemplary stability curve at the precision limit is recorded for the occurrence of the first nose as shown in Fig 5.6. Since this first stability threshold is assumably the most accessible one for theoretical predictions we chose this one. There is a difference between this curve in Fig. 5.5 and Fig. 5.6 which results from the wider mesh of measurement points in Fig. 5.5. The scattering of the measurement points even at highest precision is due to some practical problems in
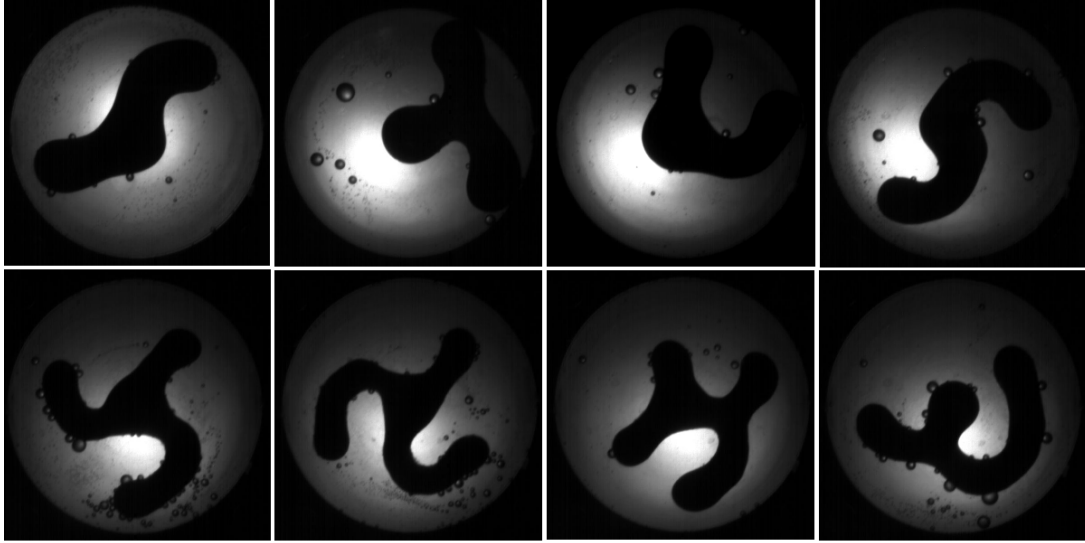
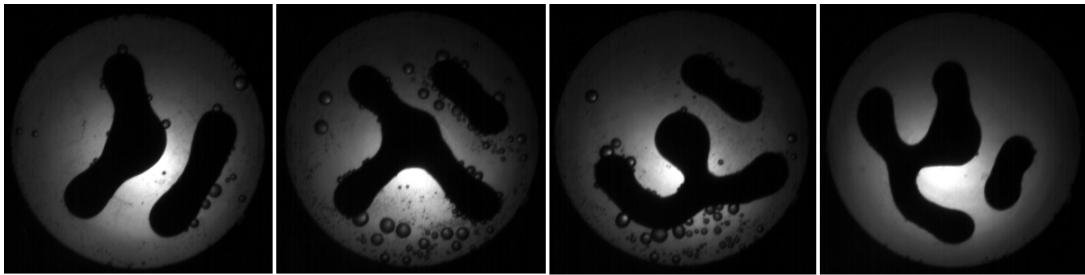Figure 5.3: More complex deformations observed in the experiments

Figure 5.4: Deformations with separation observed in the experiments

the experiment. Those include non-constant wetting properties between glass plates and liquid metal, gas bubbles sticking to the liquid metal surface, partial oxidation as well as sensitivity to the initial disc shape and symmetry. However, the trend line in Figure 5.6 shows a dependency of the critical current I_c from the magnetic field frequency f that goes as

$$I_c \propto f^{-0,2235} \quad . \tag{5.1}$$

5.1.3   Summary and conclusion

We have presented experimental results on the behavior of a liquid metal disc in the field of a circular current loop. The two main parameters in the experiment were inductor current and frequency. The perimeter of the disk was subject to strong but frozen deformations that can be described as nose-shaped or fingering. After those shapes had formed, oscillations never occurred. We have presented a stability diagram for the whole measurable parameter space and one most precisely measured stability curve for the onset of the first nose. The course of this one
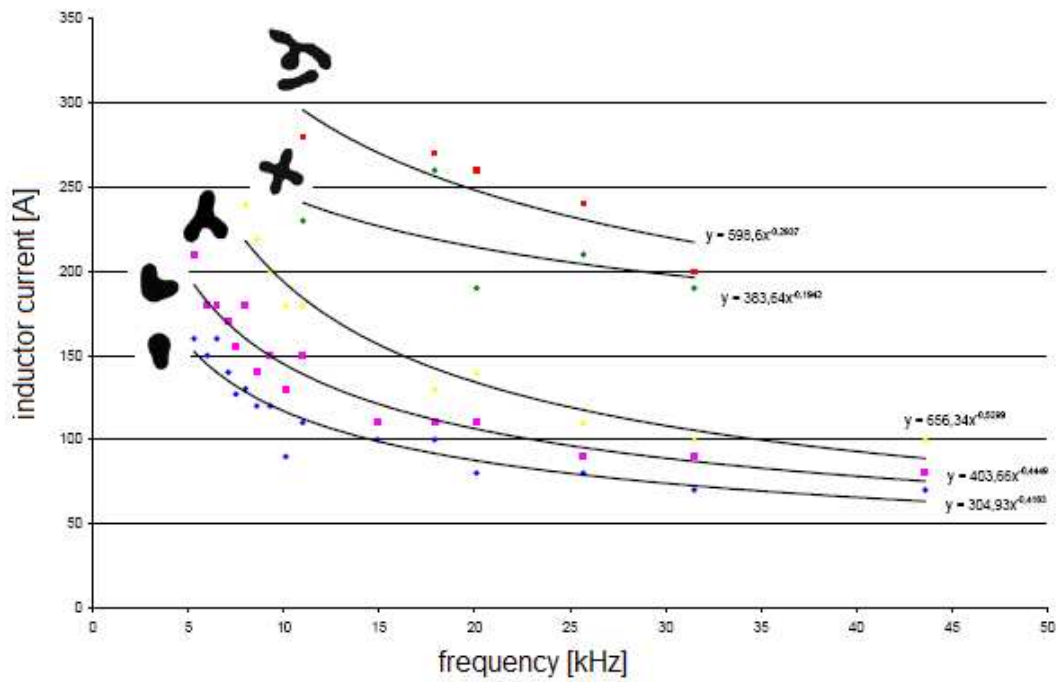
Figure 5.5: Stability diagram of the disc deformations
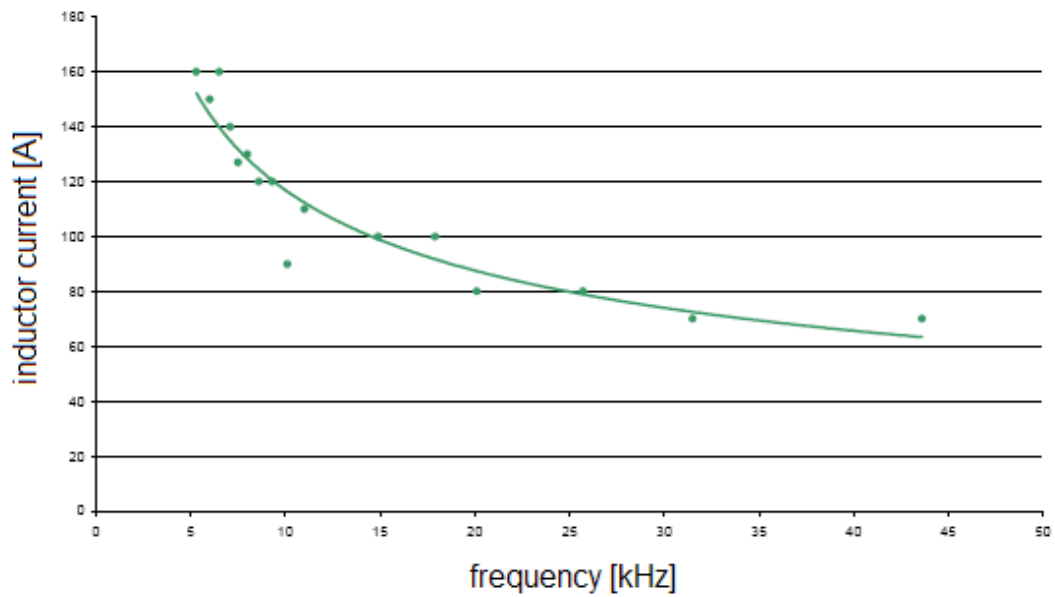

Figure 5.6: Stability curve for the occurrence of the first nose, recorded at maximum precision.

curve revealed an exponent of $-0,2235$, conf. Eq. 5.1. Here, we see a remarkable resemblance to a prediction of a model of Karcher and Mohring [76]. Their model is based on Hele-Shaw as well as skin-depth approximation and predicts a dependency $I_c \propto f^{-0,25}$. Unfortunately, the

Cartesian geometry of their model does not match to our experiment. Therefore, a properly adapted model would be helpful in future.

It has shown that the heat bridge cylinder in the center of the liquid metal disc widens the possible duration of measurements, sometimes even steady measurements are possible. Disadvantageous is the strong centering effect and its impact on the magnetic field, on the other hand. We therefore believe that the construction of a more sophisticated experiment without this core cylinder but isothermal conditions would be desirable.

Chapter 6

Prospective Ideas

6.1 Self-excitation of drop oscillations in middle-frequent magnetic fields

Here, we will try to elucidate why the liquid metal drop in the middle frequency experiment of Kocourek [79] oscillates - in contrast to the similar experiment of Perrier [80].

The generator Our consideration starts with the generator that feeds the inductor to which the liquid metal drop is submitted. In the Kocourek-experiment this is the middle-frequency generator $MFG15$ of the enterprise "eldec". Nevertheless, the following explanations qualitatively apply also to other middle frequency experiments. Figure 6.1 displays the essential parts of such a generator, in this case a power electronic resonant converter.

1 - Three-phase rectifier
2 - Resonant converter (bridge circuit)
3 - Transformer to adapt the load
4 - Capacitances to adjust the frequency
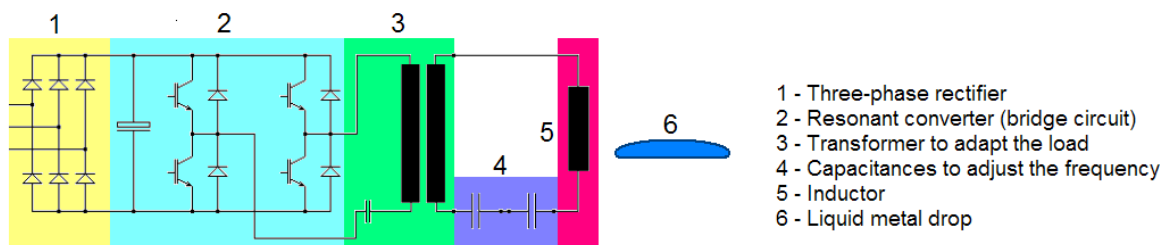5 - Inductor
6 - Liquid metal drop

Figure 6.1: Electrical circuit of the generator that feeds the inductor with the drop as ingot

As usually, there is a three-phase electric power supply to strain the net evenly. The three-phasic power is rectified by a diode bridge that yields a direct voltage of about 540 Volts. This supplies the two half-bridges, each consisting of two power electronic switches (here: IGBT transistors). To prevent a shortcut, the sensible electronics that controls the switches (not shown in the figure) ensures that only one switch of a half-bridge conducts and the other is blocked. Put together, the two half-bridges thus allow to reverse the current direction in the load between them. The inductor which actually is the load is connected to the half-bridges aided by a transformer to get low voltage and high current. Figure 6.2 shows the load circuit simplified.
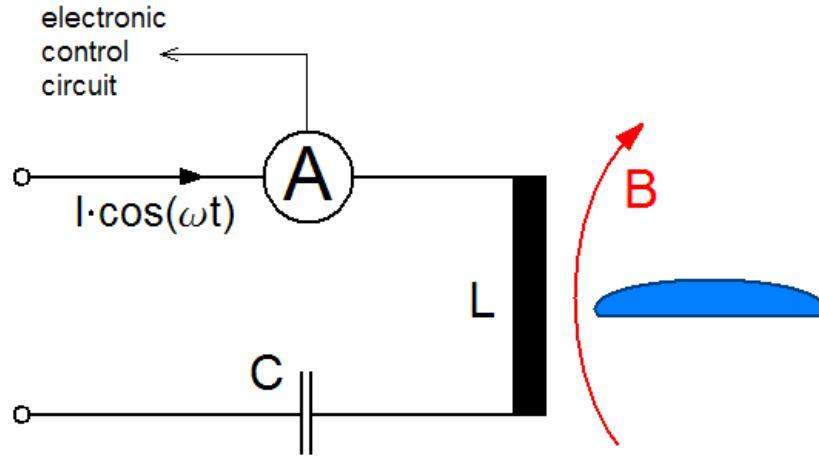
Figure 6.2: Simplified load circuit with the drop that is magnetically coupled to the inductor

An Ampere meter in the load circuit monitors the current and its reversals. Each time the current crosses the zero line, the electronic switch control blocks all transistors for a short safe time and then applies the voltage in the reversed direction to the load. So basically, the inductor current is supplied to oscillate exactly with the loads electrical resonance frequency which is $\omega = 1/\sqrt{LC}$.

Magnetic coupling between drop and inductor   The inductance L of the load circuit in Figure 6.2 does not only origin in the magnetic flux produced by the inductor. Instead, the additional magnetic flux from the liquid metal drop must be taken into account, too. Consequently, the total magnetic flux through the inductor becomes

$$\Psi_I = L_I I_I + M I_D \tag{6.1}$$

where L_I, M denote the self-inductance of the inductor and the mutual inductance between drop and inductor, respectively. The corresponding inductance L of the load circuit is therefore

$$L = \frac{\Psi_I}{I_I} = L_I + M \cdot \frac{I_D}{I_I} \quad . \tag{6.2}$$

Frequency modulation and self-excitation mechanism   Hereby, the mutual inductance depends on the drop shape, say the mode m and amplitude η of deformation yielding $M = M(m, \eta)$ or

$$L = L(m, \eta) \quad . \tag{6.3}$$

For the resonance frequency of the load circuit that means

$$\omega = \omega(m, \eta) = \frac{1}{\sqrt{L(m, \eta)C}} \quad . \tag{6.4}$$

60

In other words is the drop deformation linked to a frequency modulation of the inductor current. That, in turn, leads to a modulation of the skin depth $\delta = 2/\sqrt{\mu\sigma\omega}$ and the Lorentz force distribution as well. The Shielding parameters for modes two, three and four, for instance are 8, 18, 32 which means that the field is not yet completely shielded from the drop center. Hence, varying the skin depth means varying the magnetic pressure on the drop surface. This is a self-excitation mechanism that can lead to oscillations.

The more inhomogeneous the inductor field is, the more pronounced is the variation $M(m,\eta)$. Besides, in the Kocourek experiment the substrate has a slope. Hence, potential energy also varies deformation-dependent and supports oscillations.

Preventing middle-frequency oscillations   Concluding from the above considerations, there are two ways to get rid of such oscillations: i) minimize potential energy variations and ii) control the frequency of the inductor current. While the first possibility has already been successfully applied for the experimental middle frequency study presented in this work, the second possibility would demand some more effort. For this, an electronic control circuit had to be designed to extinguish frequency shifts.

Chapter 7

Summary

Introduction

We have introduced the subject of this work in a rather extended manner, presenting it in its historical context. Hopefully, that will make it easier for the interested reader to draw insights from related subjects because the present one is merely 50 years old.

Classification

We have suggested to classify a liquid metal drop - magnetic field problem by the frequency of the magnetic field and the shielding parameter of the metal drop in this field. Such a scheme seems sufficient for theoretical considerations where second order effects are not considered. Of course, this scheme could be supplemented by a third parameter, for example the Interaction parameter, to account also for the field strength.

Transient magnetic fields

In principle, transient fields can be everything. All other field types can be decomposed in transient intervals. Knowledge of the drop behavior in transient fields can therefore be applied to other fields. We have presented two analytical studies to expound the possibilities of transient fields.

In the first study, a square-root time dependence of the magnetic field induces time-independent static Lorentz forces that are used to support a static squeezing of the drop. The problem is simplified by the assumption of a very low Shielding parameter. A solution is found aided by a shooting method. The results show that also extreme deformations can be modeled under these conditions. Furthermore, we make clear that such a field for practical applications or experiments could also achieved by movement into a high Tesla static magnet.

In the second study we consider a liquid metal disc in a transient magnetic field. We present a linear stability analysis of the azimuthal deformations. Again, we simplify the problem by the low-shielding assumption. We show that the Lorentz force in the disc consist of a strong part due to the ambient magnetic field and a weak part due to the self-excited magnetic field. We find that the strong part has no effect on azimuthal disc deformations, only the weak one. Therefore, we assume a linear time dependence of the ambient magnetic field which leads to a time-independent self-excited Lorentz force in the disc. In the end, we obtain an intrinsic relation for the azimuthal deformations suggesting that i) for the modes $m = 1$ and $m > 4$ the frequency of capillary oscillations is affected by the magnetic field, ii) for modes $m = 2$ and $m = 4$ no

statement is possible and iii) for mode $m = 3$ and large drops infinitesimal perturbations of the disc perimeter will grow.

High frequency magnetic fields

Within this work, high frequency means a Shielding parameter $R_\omega \gg 100$. That chapter contains also two studies.

The first study is devoted to the electromagnetic shaping of liquid metal drops in a given magnetic field. Herby, we engage skin-depth approximation, flat-drop approximation and mirror image method to obtain an equation that is solved aided by Green functions. The cases of symmetric i) squeezing, ii) supporting and iii) pumping up of liquid metal drops in high-frequent magnetic fields are considered.

The second study tackles the problem of longitudinal levitation. It asks about the optimal inductor to generate a closed magnetic vessel around a levitated liquid metal cylinder. Hereby, the magnetic pressure variation on the cylinder surface in height must be linear to compensate the hydrostatic pressure. It is found that the inductor bars should be 45 degrees below with respect to the cylinder axis to achieve the best distribution.

Middle frequency magnetic fields

Within this work, middle frequency means a shielding parameter between $R_\omega = 0.01$ and $R_\omega = 100$ which is the usual case.

We present here an experimental study on the behavior of a liquid metal disc in the field of an inhomogeneous inductor field. Variation of drop volume, inductor current and frequency yields a lot of interesting shapes, mostly irregular and sometimes even separated. All shapes seem to represent a new equilibrium state because they do not move once they are in place. The switch-on shock and the center cylinder to enhance the heat transfer are surely two factors that should be improved in future.

Prospective ideas

This chapter contains no real model. It is more a collection of ideas to explain the observations in the Kocourek experiment. To this end, we develop a causal chain resulting in a possible mechanism for self-excited drop oscillations.

Chapter 8

Conclusions

Regarding the subject of the present work, the disc geometry turned out to be promising for a fusion of analytical prediction and experiment. It is rather easy to model and to build as well. It allows two-dimensional studies which is less complicated of course. From the analytical point of view it would be desirable to solve the magnetic diffusion equation in oblate spherical coordinates which should, in principle, be possible even with a circular current loop as inductor. That would be a good base to develop more powerful models in future. From the experimental point of view, it would be desirable to design a liquid metal disc experiment that is isothermal, without adhesion to the glass plates and continuous variation of magnetic field strength and frequency.

Overall, it seems safe to say that the investigation of liquid metal drops in magnetic fields remains an interesting and challenging research topic. Many experiments and theoretical studies are still to be done to answer a lot of open questions. Among these open question are thermal effects, equilibrium states due to magnetic energy, bulk flow due to Lorentz shear force, stability of deformations also for finite amplitudes and the occurrence and behavior of extreme deformations like a pinch. Last but not least we are looking for ways to avoid or control unwelcome behavior - after we understood it.

Acknowledgement

Appendix A

Eddy currents in a deformed disc

The current density is related to the electric field strength by $\mathbf{J} = \sigma\mathbf{E}$. Since we intend to calculate the induced eddy currents we apply Faradays law

$$\nabla \times \mathbf{E} = -\frac{\partial \mathbf{B}}{\partial t} = \Gamma \tag{A.1}$$

in cylindrical coordinates. Due to the independence of $\mathbf{E}$ from the z-direction, Eq. A.1 leads to

$$\frac{E_\phi}{r} + \frac{\partial E_\phi}{\partial r} - \frac{\partial E_r}{r\partial \phi} = \Gamma \quad . \tag{A.2}$$

An important property of the induced electric field strength and the corresponding eddy currents as well is the solenoidy constraint

$$\nabla \cdot \mathbf{E} = 0 \tag{A.3}$$

which becomes in written out form

$$\frac{\partial}{\partial r}(rE_r) + \frac{\partial E_\phi}{\partial \phi} = 0 \quad . \tag{A.4}$$

Now, the two vector components of $\mathbf{E}$ can be relied to one scalar function by introducing a stream function Ψ and defining

$$E_r = \frac{\partial \Psi}{r\partial \phi} \qquad \text{and} \qquad E_\phi = -\frac{\partial \Psi}{\partial r} \quad . \tag{A.5}$$

With this definition Eq. A.3 is met and Eq. A.2 transforms to

$$r^2\frac{\partial^2 \Psi}{\partial r^2} + r\frac{\partial \Psi}{\partial r} + \frac{\partial^2 \Psi}{\partial \phi^2} = -r^2\Gamma \tag{A.6}$$

with a general solution in the form

$$\Psi(r,\phi) = \Psi_h + \Psi_p \quad . \tag{A.7}$$

66

Hereby, h and p indicate the homogeneous and the particular compartment, respectively, of the solution. Setting $\Psi_p \sim r^2$ we quickly find the particular solution to be

$$\Psi_p = -\frac{\Gamma}{4}r^2 \quad . \tag{A.8}$$

The homogeneous solution Ψ_h is found by setting

$$r^2\frac{\partial^2\Psi_h}{\partial r^2} + r\frac{\partial\Psi_h}{\partial r} + \frac{\partial^2\Psi_h}{\partial\phi^2} = 0 \tag{A.9}$$

and choosing the separation of variables approach

$$\Psi_h(r,\phi) = R(r)\cdot\Phi(\phi) \quad . \tag{A.10}$$

As we insert Eq. A.10 into Eq. A.9 we get

$$r^2R''\Phi + rR'\Phi + R\Phi'' = 0 \tag{A.11}$$

which can be rearranged and separated, aided by an unknown variable m, to obtain the two ordinary differential equations for R and Φ

$$r^2\frac{R''}{R} + r\frac{R'}{R} = m^2$$

$$\frac{\Phi''}{\Phi} = -m^2 \tag{A.12}$$

that have the solutions

$$R(r) = C_1r^m + C_2r^{-m}$$

$$\Phi(\phi) = C_3\cos m\phi + C_4\sin m\phi \tag{A.13}$$

Now we can assemble the complete solution. But we must pay attention to the fact that m is unknown. It is also clear that the waves around the disc can only superimpose when m has discrete values. Therefore the general solution for the stream function has the form

$$\Psi(r,\phi) = -\frac{\Gamma}{4}r^2 + \sum_{m=0}^{\infty}R_m(r)\Phi_m(\phi) \tag{A.14}$$

and the complete expression is

$$\Psi(r,\phi) = -\frac{\Gamma}{4}r^2 + \sum_{m=0}^{\infty}[C_{1m}r^m + C_{2m}r^{-m}]\cdot[C_{3m}\cos m\phi + C_{4m}\sin m\phi] \quad . \tag{A.15}$$

The special solution of Ψ is determined by the following boundary conditions

1. Focus on single mode deformations $\rightarrow$ no sum of modes but only one m

2. Phase orientation of the deformation is unimportant $\rightarrow$ no Sinus terms (chosen at will)

3. Stream function starts in the middle with the value $\Psi = 0$

Applying these conditions to Eq. A.15 we obtain

$$\Psi(r, \phi) = -\frac{\Gamma}{4}r^2 + C_m \cdot r^m \cos m\phi \quad . \tag{A.16}$$

A last boundary condition is needed to rule out C_m. This is the conservation of the magnetic flux. Please note that the flux is only conserved because we have a homogeneous and fully penetrating magnetic field through a disc with constant projection area. Naming the amplitude of the deformation with $\zeta(\phi)$, we can say that $A_\zeta = A_0$ and therefore $\Gamma A_\zeta = \Gamma A_0$ or

$$\Psi(r, \phi) = \Psi_0 \tag{A.17}$$

Here, Ψ_0 corresponds to no deformation, i.e. $m = 0$ and $\zeta_0 = a$. Since on the perimeter of the deformed disc $\Psi_\zeta = constant$ we may write

$$\Psi_0 = \Psi_\zeta = -\frac{\Gamma}{4} \cdot a^2 = -\frac{\Gamma}{4} \cdot \zeta^2 + C_m \cdot \zeta^m \cos m\phi \tag{A.18}$$

yielding

$$C_m = \frac{\Gamma(\zeta^2 - a^2)}{4\zeta^m \cos m\phi} \quad . \tag{A.19}$$

Finally, the stream function for the eddy current distribution in the disc becomes

$$\Psi(r, \phi) = \frac{\Gamma}{4} \cdot \left[(\zeta^2 - a^2) \cdot \left(\frac{r}{\zeta}\right)^m - r^2 \right] \quad . \tag{A.20}$$

From the stream function Ψ, applying Eq. A.5, the vector components of the induced electric field strength are found and with $\mathbf{J} = \sigma\mathbf{E}$

$$J_r(r, \phi) = \frac{\sigma\Gamma}{4} \cdot \left(\frac{r}{\zeta}\right)^{m-1} \cdot \frac{\partial\zeta}{\partial\phi} \cdot \left[2 + m\left(\frac{a^2}{\zeta^2} - 1\right) \right] \quad , \tag{A.21}$$

$$J_\phi(r, \phi) = \frac{\sigma\Gamma}{4} \cdot \left[2r - m\frac{\zeta^2 - a^2}{\zeta^m} \cdot r^{m-1} \right] \quad . \tag{A.22}$$

Among the possible values for the factor Γ representing the time dependence of the eddy currents are three of special interest:

1. Low-frequency oscillation, $\mathbf{B} = B_0 \sin \omega t$, which leads to $\Gamma = B_0 \omega \cos \omega t$

2. Continuous increase, $\mathbf{B}(t) = B_0 + mt$, which leads to $\Gamma = m$ and thus constant eddy currents as well as a constant Lorentz force compartment that promotes the azimuthal deformation

3. Increase in a square-root manner, $\mathbf{B} = B_0\sqrt{1 + 2Ft}$, which leads to $\Gamma = 2FB_0(1 + 2Ft)^{-\frac{1}{2}}$ and for which the axisymmetric squeezing force remains constant

Appendix B

Lorentz force in a deformed disc

The Lorentz force generated by a low-shielded magnetic field consists of two parts, say $\mathbf{f}_L = \mathbf{f}_0 + \mathbf{f}_{self}$.

First part of the Lorentz force The first part originates in the interaction of the induced eddy currents $\mathbf{J}$ with the inducing magnetic field $\mathbf{B}_0$ and is

$$\mathbf{f}_0 = \mathbf{J} \times \mathbf{B}_0 = (J_\phi B_z) \cdot \mathbf{e}_r - (J_r B_z) \cdot \mathbf{e}_\phi \quad . \tag{B.1}$$

Since $\mathbf{B}_0 = B(t) \cdot \mathbf{e}_z$ is a precondition and $\mathbf{J}$ is given by Eqs. A.21 and A.22 we find at once that

$$f_{0r}(r,\phi) = \frac{\sigma}{4} \cdot B(t) \frac{\partial B}{\partial t} \cdot \left[2r - m \frac{\zeta^2 - a^2}{\zeta^m} \cdot r^{m-1} \right] \quad , \tag{B.2}$$

$$f_{0\phi}(r,\phi) = \frac{\sigma}{4} \cdot B(t) \frac{\partial B}{\partial t} \cdot \left(\frac{r}{\zeta} \right)^{m-1} \cdot \frac{\partial \zeta}{\partial \phi} \cdot \left[2 + m \left(\frac{a^2}{\zeta^2} - 1 \right) \right] \quad . \tag{B.3}$$

The pressure p_{L0} in the disc which is built up by $\mathbf{f}_0$ follows from the relation $\mathbf{f}_0 = \nabla p_{L0}$. Relating the eddy currents to the stream function again, conf. Eq. A.5, we see that

$$\frac{\partial p_{L0}}{\partial r} = -\sigma B(t) \cdot \frac{\partial \Psi}{\partial r} \qquad \text{and} \qquad \frac{\partial p_{L0}}{\partial \phi} = -\sigma B(t) \cdot \frac{\partial \Psi}{r \partial \phi} \tag{B.4}$$

where Ψ is the known expression from Eq. A.20. After stepwise integration with respect to r and ϕ we obtain for the pressure distribution

$$p_{L0}(r,\phi) = -\sigma B(t) \Psi(r,\phi) + p(r=0) \quad . \tag{B.5}$$

According to this result, the disc perimeter is always an isobar of p_{L0} which means that $\mathbf{f}_0$ does not promote azimuthal deformations. It would squeeze the whole disc, if possible, but would not cause asymmetry.

Second part of the Lorentz force The other part of the Lorentz force is much weaker, i.e. $\mathbf{f}_{self} \ll \mathbf{f}_0$, it is nevertheless reason for azimuthal disc deformations. It emerges from the interaction of induced eddy currents $\mathbf{J}$ and the self-generated magnetic field $\mathbf{b}_{self}$ driven by $\mathbf{J}$ according to $\nabla \times \mathbf{b}_{self} = \mu \mathbf{J}$. Figure B.1 shows a geometry where the calculation of $\mathbf{b}_{self}$ is
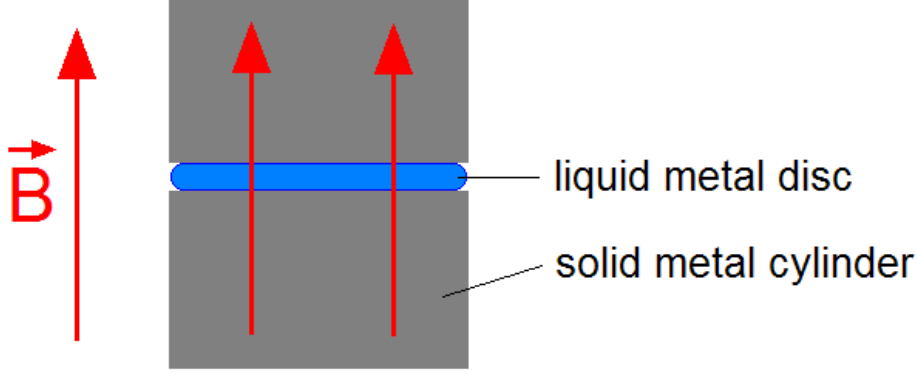
rather simple.

Figure B.1: Liquid metal disc between solid metal cylinders of equal diameter

Starting with the circular disc we find with $m = 0$ and Eq. A.22 that the eddy current distribution is

$$\mathbf{J} = J_\phi(r) = \frac{\sigma\Gamma}{2}r \quad , \tag{B.6}$$

and $\mathbf{b}_{self}$ is found by

$$\mu\mathbf{J} = \nabla \times \mathbf{b}_{self} \qquad \rightarrow \qquad -\frac{\partial b_z}{\partial r} = \mu J_\phi \tag{B.7}$$

which leads to

$$b_z = b_c - \mu\sigma\frac{\Gamma}{4}r^2 \quad . \tag{B.8}$$

Hereby, b_c denotes the magnetic field in the disc center, i.e. $r = 0$. Right there on the symmetry axis the generated magnetic field of all eddy current solenoids from $r = 0$ to $r = a$ superimposes why b_c and $b_z(r)$ become

$$b_c = \mu\sigma\frac{\Gamma}{4}a^2 \quad , \tag{B.9}$$

$$b_z(r) = \mu\sigma\frac{\Gamma}{4}(a^2 - r^2) \quad . \tag{B.10}$$

We can now put the terms together to obtain $\mathbf{f}_{self} = \mathbf{J} \times \mathbf{b}_{self} = J_\phi b_z \cdot \mathbf{e}_r$ which reads as

$$f_{self0}(r) = \frac{\mu\sigma^2\Gamma^2}{8}r(a^2 - r^2) \quad . \tag{B.11}$$

Inside the disc it is always directed outwards.
Next, we will consider the effect of azimuthal disc deformations on the self-generated force.

For infinitesimal amplitude deformations from circular disc shape, $\zeta(\phi) = a + \hat{\zeta}(\phi)$, we can assume that the total induced current

$$I_{eddy} = H \int_0^\zeta J_\phi dr \tag{B.12}$$

is conserved with H being the disc height. As a consequence, the new eddy current distribution in the disc becomes

$$J_{\phi\zeta} = \frac{\sigma\Gamma}{2} \cdot \frac{a^2}{\zeta^2} \cdot r \tag{B.13}$$

and at the surface at $r = \zeta$ it is

$$J_{\phi\zeta}|_{r=\zeta} = \frac{\sigma\Gamma}{2} \cdot \frac{a^2}{\zeta} = J_{\phi 0}|_{r=a} \cdot \frac{a}{\zeta} \quad . \tag{B.14}$$

Since we consider infinitesimal deformations we can simplify the problem in the way that we assume a purely radial force whose amplitude varies along the azimuth. We can map the variations on the circular disc so that

$$J_\phi = \frac{\sigma\Gamma}{2} \cdot \frac{a}{\zeta} \cdot r \tag{B.15}$$

The corresponding magnetic field will then be $b_{z\zeta} = b_{z0} \cdot a/\zeta$ and becomes

$$b_{z\zeta} = \frac{\mu\sigma\Gamma}{4} \cdot \frac{a}{\zeta} \cdot [a^2 - r^2]. \tag{B.16}$$

The resulting Lorentz force is

$$f_{r\zeta} = f_{r0} \cdot \frac{a^2}{\zeta^2} = \frac{\mu\sigma^2\Gamma^2}{8} \cdot \frac{a^2}{\zeta^2} \cdot r \cdot (a^2 - r^2) \tag{B.17}$$

As a last step, we consider the force difference between the perturbed and basic state, $\hat{f}_r = f_{r\zeta} - f_{r0}$, and find that

$$\hat{f}_r = f_{r0} \cdot \left(\frac{a^2}{\zeta^2} - 1 \right) \tag{B.18}$$

which gives, taking into account only linear terms, i.e. $a^2 - \zeta^2 \simeq -2a\hat{\zeta}$, and $\hat{\zeta} \ll a$

$$\hat{f}_r = -\frac{\mu\sigma^2\Gamma^2}{4} \cdot \frac{\hat{\zeta}}{a} \cdot r \cdot (a^2 - r^2) \quad . \tag{B.19}$$

Bibliography

[1] G. Barraclough (editor). *Knaurs historischer Weltatlas.* 6th edition. Droemer Knaur, München, 2002.

[2] A. Neuburger. *Die Technik des Altertums.* Voigtländer Verlag, Leipzig, 1919.

[3] K. Seubert. *Das natürliche System der chemischen Elemente. Abhandlungen von L. Meyer(1864-69) und D.I. Mendelejew (1869-71).* Leipzig, Engelmann, 1895.

[4] P.A. Davidson. *An Introduction to Magnetohydrodynamics.* Cambridge University Press, 2001.

[5] K. Simonyi. *Kulturgeschichte der Physik.* 2nd edition, translated from the hungarian original. Verlag Harri Deutsch, Frankfurt(Main), 1995.

[6] G. Bakker. *Handbuch der Experimentalphysik. Band 6 - Kapillarität und Oberflächenspannung.* Akademische Verlags GmbH, Leipzig, 1928.

[7] J.H. Zedler and J.P. Ludewig. *Grosses vollständiges Universal-Lexicon Aller Wissenschafften und Künste (volume 5 of 60).* published in Halle-Leipzig by J.H. Zedler, 1733. (online available at http://www.zedler-lexikon.de).

[8] B. Taylor. Concerning the ascent of water between two glass planes. *Philosophical Transactions of the Royal Society of London*, 27:538, 1712.

[9] F. Hauksbee. An experiment touching the ascent of water between two glas planes in an hyperbolick figure. *Philosophical Transactions of the Royal Society of London*, 27:539–540, 1712.

[10] J.A. Segner. De figuris superficierum fluidarum. *Commentarii Societatis Regiae Scientiarum Gottingensis*, 1:301–372, 1751.

[11] T. Young. An essay on the cohesion of fluids. *Philosophical Transactions of the Royal Society of London*, 94:65–87, 1805.

[12] P.S. de Laplace. *Traité de Mécanique Céleste. 4th volume, 1st section (théorie de l'action capillaire) of the supplement to book 10 (sur divers points relatifs au systéme du monde).* Chez Courier, Paris, 1805.

[13] S.D. Poisson. *Nouvelle theorie de l'action capillaire.* Bachelier, Paris, 1831.

[14] C.E. Delauney. Sur la surface de revolution dont la courbourc moyenne est constante. *Journal de mathematiques pures et appliquees*, 6:309–315, 1841.

[15] J. Plateau. *Statique experimentale et theoretique des liquides soumis aux seules forces moleculaires. 2 Volumes.* Gauthier-Villars, Paris, 1873.

[16] Lord J.W. Rayleigh. On the instability of jets. *Proceedings of the London Mathematical Society*, 10:4–13, 1879.

[17] J. Eggers. Nonlinear dynamics and breakup of free-surface flows. *Reviews of Modern Physics*, 69,3:865–929, 1997.

[18] Lord Kelvin (alias W. Thomson). *Popular Lectures and addresses, Volume 1 of 3.* Macmillan, London, 1891.

[19] F. Bashforth and J.C. Adams. *An Attempt to Test the Theories of Capillary Action by Comparing the Theoretical and Measured Forms of Drops of Fluid.* Cambridge University Press, 1883.

[20] F.P. Buff. The theory of capillarity. In *Handbuch der Physik, Volume 10.* 1960.

[21] J.F. Padday. The profiles of axially symmetric menisci. *Philosophical Transactions of the Royal Society of London, A*, 269:265–293, 1971.

[22] Lord Kelvin (alias W. Thomson). Dynamical problems regarding elastic spheroidal shells and spheroids of incompressible liquid. *Philosophical Transactions of the Royal Society of London*, 153:583–616, 1863.

[23] J.A. Tsamopoulos and R.A. Brown. Nonlinear oscillations of inviscid drops and bubbles. *Journal of fluid Mechanics*, 127:519–537, 1983.

[24] H. Azuma and S. Yoshihara. Threedimensional large-amplitude drop oscillations: experiments and theoretical analysis. *Journal of Fluid Mechanics*, 393:309–332, 1999.

[25] J. Kern. Zur hydrodynamik der rinnsale. *Verfahrenstechnik*, 3,10:425–430, 1969.

[26] J. Kern. Stabilitätsprobleme der rinnsalströmung. *Verfahrenstechnik*, 5,7:289–294, 1971.

[27] R.F. Allen and C.M. Biggin. Longitudinal flow of a lenticular filament down an inclined plane. *Physics of Fluids*, 17,2:287–291, 1974.

[28] S.H. Davis. Moving contact lines and rivulet instabilities. part 1 - the static rivulet. *Journal of Fluid Mechanics*, 98:225–242, 1980.

[29] T. Nakagawa and J.C. Scott. Stream meanders on a smooth hydrophobic surface. *Journal of Fluid Mechanics*, 149:89–99, 1984.

[30] H.Y. Kim, J.H. Kim, and B.H. Kang. Meandering stability of a rivulet. *Journal of Fluid Mechanics*, 498:245–256, 2004.

[31] C.A. Perazzo and J. Gratton. Navier-stokes solutions for parallel flow in rivulets on an inclined plane. *Journal of Fluid Mechanics*, 507:367–379, 2004.

[32] P. Ehrhard and S. Davis. Non-isothermal spreading of liquid drops on horizontal plates. *Journal of Fluid Mechanics*, 229:365–388, 1991.

[33] P.G. de Gennes. Wetting: statics and dynamics. *Reviews of Modern Physics*, 57,3:827–863, 1985.

[34] A.D. Myshkis, V.G. Babskii, N.D. Kopachevskii, L.A. Slobozhanin, and A.D. Tyuptsov. *Low-Gravity Fluid Mechanics.* translated from the russian original(1976), Springer Verlag Berlin, 1987.

[35] D. Langbein. *Capillary surfaces. Shape - stability - dynamics, in particular under weightlessness.* Springer, Berlin, 2002.

[36] A. Volta. *On the electricity excited by the mere contact of conducting substances of different kinds. (Letter to Sir Joseph Banks of the 20th of March 1800).* Pavia : Univ. degli studi, 1999.

[37] G. Dettmar. *Die Entwicklung der Starkstromtechnik in Deutschland. Teil 1: Die Anfänge bis etwa 1890.* ETZ-Verlag, Berlin, 1940.

[38] M. Faraday. *Experimental researches in electricity. Series 1-30.* Taylor, London, 1832-56.

[39] J.C. Maxwell. A dynamical theory of the electromagnetic field. *Philosophical Transactions of the Royal Society of London*, 155:459–512, 1865.

[40] J.C. Maxwell. *An elementary treatise on electricity.* Clarendon Press, Oxford, 1881.

[41] O. Mahr. *Die Entstehung der Dynamomaschine.* ETZ-Verlag, Berlin, 1941.

[42] C. Hering. A practical limitation of resistance furnaces: The pinch phenomenon. In *11th general meeting of the American Electrochemical Society, Philadelphia*. 1907.

[43] E.R. Laithwaite. Electromagnetic levitation. *Proceedings of the IEE*, 112,2:2361–2375, 1965.

[44] J. Hartmann. Hg-dynamics i. theory of the laminar flow of an electrically conductive liquid in a homogeneous magnetic field. *Det Kgl. Danske Videnskabernes Selskab, Mathmatisk-fysiske Meddelelser*, XV(6):1–27, 1937.

[45] C.D. Dodd and Deeds. W.E. Analytical solutions to eddy-current probe-coil problems. *Journal of Applied Physics*, 39,6:2829–2838, 1968.

[46] L.S. Piggott and G.F. Nix. Electromagnetic levitation of a conducting cylinder. *Proceedings of the IEE*, 113,7:1229–1235, 1966.

[47] J.W. Luquire, W.E. Deeds, and C.V. Dodds. Axially symmetric eddy currents in a spherical conductor. *Journal of Applied Physics*, 41,10:3976–3982, 1970.

[48] L. Hannakam and G. Mrozynski. Transienter skineffekt in der kugel bei beliebiger form der erregenden leiterschleife. *Archiv fr Elektrotechnik*, 55:299–309, 1973.

[49] A.B. Kapusta and I.B. Nosovitskaya. Forces in a liquid metal in a rotationally symmetric field. *Magnetohydrodynamics*, 9,2:142–145, 1973.

[50] U.B. Sathuvalli and Y. Bayazitoglu. The lorentz forces on an electrically conducting sphere in an alternating magnetic field. *IEEE Transactions on Magnetics*, 32,2:386–399, 1996.

[51] T.P. Theodoulidis, N.V. Kantartzis, T.D. Tsiboukis, and E.E. Kriezis. Analytical and numerical solution of the eddy-current problem in spherical coordinates based on the second-order vector potential formulation. *IEEE Transactions on Magnetics*, 33,4:2461–2472, 1997.

[52] J.A. Tegopoulos and E.E. Kriezis. *Eddy currents in linear conducting media.* Elsevier, 1985.

[53] R. Moreau. *Magnetohydrodynamics*. Kluwer Academic Publishers, 1990.

[54] A.P. Zambran. Small oscillations of a viscous liquid metal drop in the presence of a magnetic field. *Magnetohydrodynamics*, 2,2:54–56, 1966.

[55] A. Gailitis. Oscillations of a conducting drop in a magnetic field. *Magnetohydrodynamics*, 2,2:47–53, 1966.

[56] I.M Kirko, E.I. Dobychin, and V.I. Popov. Experimental investigation of the dynamics of liquid metal drops in an electromagnetic field under reduced gravity conditions. *Magnetohydrodynamics*, 6,3:368–371, 1970.

[57] E.I. Dobychin. Effect of crossed electric and magnetic fields on the oscillations of liquid metal drops. *Magnetohydrodynamics*, 9,1:128–131, 1973.

[58] A. Podoltsev. Motion of a molten metal drop in a pulse magnetic field. *Magnetohydrodynamics*, 32,2:221–226, 1996.

[59] H. Knoeppel. *Pulsed high magnetic fields*. North-Holland Publishing Company, Amsterdam, 1970.

[60] J. Priede and G. Gerbeth. Spin-up instability of electromagnetically levitated spherical bodies. *IEEE Transactions on Magnetics*, 36,1:349–353, 2000.

[61] S.P. Song and B.Q. Li. Oscillation of melt drops in magnetic fields. *Magnetohydrodynamics*, 37,1:62–70, 2001.

[62] V. Shatrov, V. Galindo, and G. Gerbeth. Stability analysis of the flow inside an electromagnetically levitated drop. *Magnetohydrodynamics*, 37,1:45–54, 2001.

[63] V. Shatrov, J. Priede, and G. Gerbeth. 3d linear stability analysis of the flow in a liquid spherical droplet driven by an alternating magnetic field. *Physics of Fluids*, 15,3:668–678, 2003.

[64] J. Priede and G. Gerbeth. Oscillatory instability of electromagnetically levitated spherical bodies. *IEEE Transactions on Magnetics*, 36,1:354–357, 2000.

[65] H. Yasuda, I. Ohnaka, and Y. Ninomiya. Levitation of metallic melt by using the simultaneous imposition of the alternating and the static magnetic fields. *Journal of Crystal Growth*, 260:475–485, 2004.

[66] D.L. Cummings and D. Blackburn. Oscillations of magnetically levitated aspherical droplets. *Journal of Fluid Mechanics*, 224:395–416, 1991.

[67] A.D. Sneyd and H.K. Moffatt. Fluid dynamical aspects of the levitation-melting process. *Journal of Fluid Mechanics*, 117:45–70, 1982.

[68] D.N. Riahi and J.S. Walker. Float zone shape and stability with the electromagnetic body force due to a radio-frequency induction coil. *Journal of Crystal Growth*, 94:635–642, 1989.

[69] K. ed. by Ehrke and W. Schneider. *Continuous Casting*. based on the International Congress on Continuous Casting held from 13-15 November 2000 in FrankfurtMain, Wiley-VCV, 2000.

[70] F. Durand. The electromagnetic cold crucible as a tool for melt preparation and continuous casting. *International Journal of Cast Metals Research*, 18,2:93–107, 2005.

[71] M.J. Schaffer. Hydromagnetic surface waves with alternating magnetic fields. *Journal of Fluid Mechanics*, 33,2:337–351, 1968.

[72] Y. Fautrelle and A.D. Sneyd. Instability of a plane conducting free surface submitted to an alternating magnetic field. *Journal of Fluid Mechanics*, 375:65–83, 1998.

[73] D. Perrier, Y. Fautrelle, and J. Etay. Experimental and theoretical studies of the motion generated by a two-frequency magnetic field at the free surface of a gallium pool. *Metallurgical and Materials Transactions B*, 34B:669–678, 2003.

[74] Y. Fautrelle, J. Etay, and S. Daugan. Free-surface horizontal waves generated by low-frequency alternating magnetic fields. *Journal of Fluid Mechanics*, 527:285–301, 2005.

[75] A. Sneyd, J. Etay, and Y. Fautrelle. The starfish experiment: some theoretical considerations. In *Proceedings of 5th International pamir Conference in Ramatuelle (France)*. 2002.

[76] C. Karcher and J.U. Mohring. Stability of a liquid metal interface affected by a high-frequency magnetic field. *Magnetohydrodynamics*, 39,3:267–276, 2003.

[77] J.U. Mohring, C. Karcher, and D. Schulze.

[78] Kocourek V., M. Conrath, and C. Karcher. Shaping of a liquid metal drop using high-frequency magnetic fields. In *Proceedings of the 5th International pamir Conference in Ramatuelle (France)*. 2002.

[79] V. Kocourek, C. Karcher, M. Conrath, and D. Schulze. Stability of liquid metal drops affected by a high-frequency magnetic field. *Physical Review E*, 74:026303, 2006.

[80] D. Perrier, Y. Fautrelle, and J. Etay. Free surface deformations of a liquid metal drop submitted to a middle-frequency ac magnetic field. In *Proceedings of the 4th International Conference on Electromagnetic Processing of Materials in Lyon (France)*. 2003.

[81] Y. Fautrelle, D. Perrier, and J. Etay. Free surface controlled by magnetic fields. *ISIJ International*, 43,6:801–806, 2003.

[82] B. Bardet, J. Priede, and J. Etay. A metal droplet levitated in the amplitude-modulated ac magnetic field. In *Proceedings of the 6th International pamir Conference in Riga Jurmala (Latvia)*. 2005.

[83] M. Hinaje, G. Vinsard, and F. Dufour. A computation and a use of the magnetic energy in a thin liquid metal submitted to an ac magnetic field. *IEEE Transactions on Magnetics*, 42,4:1059–1062, 2006.

[84] M. Hinaje, G. Vinsard, and S. Dufour. Analytical modelling of a thin liquid metal layer submitted to an ac magnetic field. *Journal of Applied Physics D*, 39,13:2641–2646, 2006.

[85] M. Conrath, V. Kocourek, and C. Karcher. Behavior of a liquid metal disk in the magnetic field of a circular current loop. In *Proceedings of the 5th International Conference on Electromagnetic Processing of Materials in Sendai(Japan)*. 2006 (in press).

[86] M. Conrath and Ch. Karcher. Static electromagnetic shaping of liquid metal drops in transient magnetic fields. *Magnetohydrodynamics*, 42,1:21–30, 2006.

[87] W.H. Press, S.A. Teukolsky, W.T. Vetterling, and B.P. Flannery. *Numerical recipes in Fortran 77, 2nd edition*. Cambridge University Press, 1992.

[88] I.N. Bronstein and K.A. Semendjajew. *Handbook of Mathematics, 20th edition*. Van Nostrand Reinhold, 1991.

[89] T. Iida and R.I.L. Guthrie. *The Physical Properties of Liquid Metals*. Oxford University Press, 1988.

[90] W.R. Smythe. *Static and dynamic electricity, 3rd edition*. Taylor and Francis, 1989.

[91] P.G. Drazin. *Introduction to hydrodynamic stability*. Cambridge University Press, 2002.

[92] M. Conrath and C. Karcher. Shaping of sessile liquid metal drops using high-frequency magnetic fields. *European Journal of Mechanics/B-Fluids*, 24:149–165, 2005.

[93] J.D. Jackson. *Classical Electrodynamics, 3rd edition*. Wiley and Sons, 1999.

[94] G.D Duffy. *Green's functions with applications*. Chapman and Hall/CRC, 2001.

[95] F. Ivaldi. *Experimentelle Untersuchungen einer Flüssigmetallscheibe im Magnetfeld, Studienarbeit*. Private communication, 2006.